People's Democratic Republic of Algeria
Ministry of Higher Education and Scientific Research
University of Ahmed Draia - Adrar
Faculty of Science and Technology
Department of Electrical Engineering

جامعة أحمد دراية ـ أدرار

Thesis for obtaining the LMD doctorate in electrical engineering

Option: Electrical Engineering

Presented by: Mr. ABBAS FADLALLA GESMALLA MOHMMEDALI

Thème

Power system stability analysis and losses evaluation of grid-connected solar PV system

---

Presented in: 8/6/2023,

In front the jury composed of:

Pr. MAKHLOUFI Salim	University of Adrar	Professor	Chairman
Pr. HAMOUDA Messaoud	University of Adrar	Professor	Supervisor
Dr. GHAITAOUI Touhami	University of Adrar	MCA	Co-Supervisor
Pr. HARROUZ Abdeldkader	University of Adrar	Professor	Examiner
Dr. NECAIBIA Ammar	URERMS- Adrar	MRA	Examiner
Dr. BOURAIOU Ahmed	URERMS- Adrar	MRA	Examiner

2022/2023

Dedication

This thesis is dedicated to my father, my mother, my sisters, and my brothers

Acknowledgement

First, I want to thank God for providing me with the confidence and fortitude to finish my thesis.

I would like to thank my supervisors, Professor Messaoud Hamouda, Director of the Development Laboratory Sustainable and IT (LDDI), and Dr. Touhami Ghaitaoui, for all the help, support, and guidance they have given me during every step of my PhD studies.

I also want to express my gratitude to my family for their support and kindness.

I would like to thank all the staff of Adrar University, College of Science and Technology (LDDI). Also, many thanks to my colleagues in Development Laboratory Sustainable and IT (LDDI) for their help.

Abstract

The network stability of the power system is at risk because more electricity is being used and moved between utilities. Due to worldwide load demand, power systems must operate securely. Thus, renewable energy-based generation is increasing rapidly to supply electrical demand and address fossil fuel-related environmental challenges. This generation can improve or degrade power system stability. the objective of this thesis is to study how solar power integration affects grid stability. In the integration process, different types of power stability were studied and analysed using three different software. In transient stability analysis, ETAP power system simulation software was used to model PV plant and Zaouiet Kounta medium voltage network (Wilaya Adrar) which is locate in southwest Algeria. Three transient situations were examined. The main bus voltage, frequency, and generator relative rotor angle were examined for each of the three circumstances. On the other hand, the effect of PV power inclusion on the power system's voltage stability utilizing static methodologies was analyzed and discussed. Four analytical methods were used to improve efficacy and accuracy, comprehend voltage stability, and detect instability reasons. Modal, sensitivity, PV, and QV curve analysis are methods. NEPLAN software analyses IEEE 14-bus voltage stability as well as static analysis. In addition, utilizing the IEEE 14 node system, an investigation into the influence of solar PV power generation system on the small signal stability of the power system was carried out. In order to study the impact that the solar PV power generation unit has on the stability of the system's small signal, the solar PV power was connected at several locations. The simulations are carried out with the assistance of PSAT simulation toolbox.

When a traditional power plant is utilized to supply a network without control units, transient stability analyses demonstrated that the inclusion of PV plant has a negative impact on network behaviour. But it has a positive impact when the traditional power generation operates with control units. Furthermore, when a grid source is utilized to supply the network, it has little influence on the voltage at the main bus. The voltage stability analysis simulations demonstrated that incorporating a PV power system that is based on renewable energy resources into the test system improved the stability degree, bus sensitivity, system MW loading, voltage profile, and reactive power margin. In addition, the inclusion of PV power showed improvement in the small signal stability of the test power system. In steady state analysis, addition PV system improved voltage level and reduced system losses.

Keywords: power system; PV generation system integration, steady state analysis, transient stability; voltage stability, small signal stability

Résumé

La stabilité du réseau du système électrique est en danger car davantage d'électricité is used and moved between public services. En raison de la demande de charge mondiale, les systèmes électriques doivent fonctionner en toute sécurité. Ainsi, la production basée sur les énergies renouvelables augmente rapidement pour répondre à la demande d'électricité et relever les défis environnementaux liés aux combustibles fossiles. Cette génération peut améliorer ou dégrader la stabilité du système électrique. The objective of this thesis is to study how the integration of solar energy affects the stability of the network. Dans le processus d'intégration, différents types de stabilité de puissance ont été étudiés et analysed à l'aide de trois logiciels différents. Dans l'analyse de stabilité transitoire, le logiciel de simulation de système électrique ETAP a été utilisé pour modéliser la centrale photovoltaque et le réseau moyenne tension de Zaouiet Kounta (Wilaya Adrar), qui est situé dans le sud-ouest de l'Algérie. Three transitory situations have been examined. La tension du bus principal, la fréquence, et l'angle du rotor du générateur ont été examinés pour chacune des trois circonstances. D'autre part, l'effet de l'inclusion de la puissance PV sur la stabilité de la tension du système électrique en utilisant des méthodologies statiques a été analysed and discussed. Quatre méthodes analytiques sont utilisées pour améliorer l'efficacité et la précision, comprendre la stabilité de la tension, et détecter les raisons de l'instabilité. L'analyse des courbes modales, de sensibilité, PV, and QV are methods. Le logiciel NEPLAN analyse la stabilité de la tension du bus IEEE 14 ainsi que l'analyse statique. De plus, en utilisant le système IEEE 14 nuds, une enquête sur l'influence du système de production d'énergie solaire PV sur la stabilité du petit signal du système d'alimentation a été réalisée. Afin d'étudier l'impact de l'unité de production d'énergie solaire PV sur la stabilité du petit signal du système, l'énergie solaire PV est connectée à plusieurs endroits. Les simulations sont réalisées à l'aide de la boîte aux outils de simulation PSAT.

Lorsqu'une centrale électrique traditionnelle est utilisée pour alimenter un réseau sans unités de contrôle, les analyses de stabilité transitoire ont démontré que l'inclusion d'une centrale photovoltaque a un impact négatif sur le comportement du réseau. Mais cela a un impact positif lorsque la production d'électricité traditionnelle fonctionne avec des unités de contrôle. De plus, lorsqu'une source de réseau est utilisée pour alimenter le réseau, elle a peu d'influence sur la tension au niveau du bus principal. Les simulations d'analyse de la stabilité de la tension ont démontré que l'incorporation d'un système d'alimentation photovoltaque basé sur des ressources d'énergie renouvelables dans le système de test améliorait le degré de stabilité, la sensibilité du bus, la charge en MW du système, le profil de tension, et la marge de puissance réactive. De

plus, l'inclusion de la puissance PV a montré une amélioration de la stabilité des petits signaux du système d'alimentation de test. L'interconnexion du système d'énergie solaire a amélioré le niveau de tension et réduit les pertes du système.

Mots clés : système électrique, Intégration du système de génération PV, analyse en régime permanent ; stabilité transitoire, stabilité de la tension, petite stabilité du signal

المستخلص

ان الاستعمال المفرط للقدرة الكهربائية ونقلها بين المرافق أصبح يشكل خطرا على استقرار شبكة نظام القدرة. كما انه يتسبب في حدوث معدلات عالية في التكاليف والتلوث البيئي والأمن الطاقوي. فبتوليد الطاقة المتجددة وربطها على الشبكات قد يساهم من جهة في الحد من هذه الظاهرة والتصدي للتحديات البيئية المتعلقة بالوقود الأحفوري. ومن جهة أخري قد يؤثر على استقرار نظام القدرة. تهدف دراستنا هاته الى دراسة تأثير ربط الطاقة الشمسية الكهروضوئية بالشبكة الكهربائية على استقرار الشبكة. في هذه الدراسة تمت دراسة وتحليل أنواع مختلفة من استقرار نظام القدرة باستخدام ثلاثة برامج مختلفة . ففي تحليل استقرار الحالة العابرة، تم استخدام برنامج ETAP لنمذجة محطة الطاقة الشمسة وشبكة توزيع الجهد المتوسط لزاوية كونتا (ولاية أدرار) والتي تقع جنوب غرب الجزائر. تمت دراسة ثلاث حالات عابرة لتحليل تأثير ربط محطة الطاقة الشمسية على الشبكة. ولكل من الحالات الثلاثة تم توضيح التأثير على الجهد والتردد في قضيب التوصيل الرئيسي للشبكة بالإضافة إلى زاوية الدوار النسبية للمولد. من جهة أخرى، تمت دراسة تأثير ربط الطاقة الشمسية الكهروضوئية على استقرار جهد نظام القدرة باستخدام عدد من طرق التحليل وذلك بغرض تحسين الدقة والكفاءة واعطاء فهم أعمق لمشكلة استقرار الجهد. طرق التحليل شملت: تحليل الحساسية، منحني القدرة- الجهد، منحني القدرة الغير فعالة – الجهد، والتحليل الشكلي. وهذا التحليل تم على شبكة IEEE 14 نقطة حمل باستخدام برنامج NEPLAN. ايضا فان دمج نظام الطاقة الشمسية الكهروضوئية على استقرار التغيرات الصغيرة لنظام القدرة تمت دراسته باستخدام اداءة المحاكاة PSAT.

أظهرت نتائج دراسة استقرار الحالة العابرة ان ربط محطة الطاقة الشمسة على الشبكة لها تأثير سلبي عند تغذية الشبكة من محطة التوليد التقليدية عند عملها من غير وحدات تحكم. ولكن له تأثير ايجابي عند عملها بوحدات تحكم. أظهرت النتائج أيضا ان دمج نظام الطاقة الشمسية أدي الى تحسن واضح في درجة استقرار النظام، نسبة التحميل، التقليل في حساسية نقاط احمال نظام القدرة، بالإضافة الي التحسن في مستوي الجهد الحرج وهامش القدرة الغير فعالة. اضافة الى ذلك، فان دمج نظام الطاقة الشمسية الكهروضوئية أدى الى تحسن في استقرار نظام القدرة للتغيرات الصغيرة. في تحليل الحالة المستقرة، أدى تربط نظام الطاقة الشمسية إلى تحسين مستوى الجهد وتقليل خسائر النظام.

الكلمات المفتاحية :نظام القدرة، دمج نظام توليد الطاقة الكهروضوئية، تحليل الحالة المستقرة، استقرار الحالة العابرة , استقرار الجهد ,استقرار التغيرات الصغيرة

TABLE OF CONTENTS

Chapter III: Power System Stability Concept

Chapter IV: Simulation and Results Analysis

LIST OF FIGURES

Chapter I: Solar Photovoltaic Power Generation Systems

(Characteristics and integration impacts)

Chapter II: Power System

(Modelling, Power Flow Analysis, and Losses Review)

Chapter III: Power System Stability Concept

Chapter IV: Simulation and Results Analysis

LIST OF TABLES

General Introduction

General Introduction

As a result of reasons such as increasing load, declining fossil fuel resources, and pollution brought on by traditional generators, the requirement for renewable energy sources is significantly increasing in importance in the modern world [1] . The power that is derived from the sun is an essential component of the renewable energy that is now available. Solar power may be classified as two distinct categories of technology that are both widely used today, and each one is determined by the process by which solar energy is transformed into electrical energy. These are concentrated solar power (CSP) and solar PV power systems. Concentrated solar power is a type of solar power that, in its operational mode, is quite similar to that of thermal power plants. Solar energy is concentrated using mirrors to heat a fluid, which in turn drives a turbine to produce electricity. That's because it uses solar energy in a roundabout way. Using a photovoltaic material, solar PV power directly transforms solar radiation into electricity (semiconductor material). The effects of a CSP system on the grid can be understood in terms of how conventional thermal power plant's function. Since Photovoltaic (PV) solar power systems function differently from traditional generating systems, it is important to fully understand the implications on an existing transmission or distribution system in power system before any significant integration can be implemented [2]. Of the many types of renewable energy, PV systems are the most popular due to their potential benefits of being environmentally benign, non-polluting, and low-maintenance. A global assessment predicts that solar energy will meet 28% of the world's energy needs by 2040 [3].

There are primarily two distinct kinds of applications for photovoltaic (PV) power systems, which are grid linked and off-grid systems, respectively. Solar photovoltaic systems that are coupled to the grid contribute their generated power to the grid. Solar photovoltaic system that are not integrated to the grid are referred to as "off-grid." In this scenario, the generated power is used locally, for things like water pumps and communication antennae, among other things. When PV plants produce energy on a big scale, the possibility of using grid-connected PV systems becomes more viable. When a solar photovoltaic system is tied to a grid, the working conditions of the grid are altered, and these changes can be either beneficial or detrimental [4] [5] .

Transmission and distribution system operators are facing increased solar PV power worldwide. So, understanding the effects of adding a solar PV system to an existing electricity network is necessary [6].

Solar PV power that are connected to the grid are frequently put into use in order to boost

the voltage profile and reduce the amount of power that is lost along the power system network. Sometimes this isn't the case, however, given that these systems have the potential to have a number of negative consequences on the network, particularly if the amount of their penetration is particularly high. These potentially harmful effects include problems with power and voltage fluctuations, harmonic distortion, faulty protective devices, overloading and underloading of lines, and system stability. Solar PV power generation system effects on the power grid are becoming increasingly important to electric utilities and researchers. Accurate assessment and practical solutions make this topic important [7].

The primary purpose, of the thesis is to examine the influences of incorporating solar PV power systems into power system network. This is done to investigate steady state impacts as well as transient effects of connecting solar PV on power system grid. The power grid with and without solar PV power is modelled using simulation software sus as: ETAP, NEPLAN and PSAT toolbox. NEPLAN software is used to investigate the static impacts of the integration of solar PV systems in terms of power grid losses, voltage profile, and static voltage stability. Besides that, ETAP software is used to examine dynamic effect of integrating solar PV plant into medium voltage grid. Moreover, PSAT toolbox is used to study the impact of incorporation of solar PV power generation on power system small signal stability.

To achieve the aforementioned objectives and facilitate the presentation of the results obtained in this thesis, the thesis is systematized as follows:

In the first chapter, we will begin with overview of solar PV characteristics and its work principle which is represents the main component of solar PV system. Also, the benefits and challenges of grid linked PV systems is reviewed in this chapter. In addition, related work is discussed.

Components of the power system, models of each component, and load flow analysis methods were discussed in the second chapter. These methods are employed in the simulation of the power system using software. In addition to that, the various kinds of power system losses that took place are presented.

In the third chapter, a general review of the concept of the stability power system as well as the several types of power system stability that were investigated is presented.

The outcomes of the modelling of the power system grid that was integrated with the photovoltaic (PV) system are discussed in the fourth chapter. NEPLAN, ETAP, and the PSAT toolbox are the three separate software programs that were utilized in order to discuss and analyze a variety of various scenarios pertaining to a variety of different forms of power system stability.

Chapter I
Solar Photovoltaic Power Generation Systems (Characteristics and integration impacts)

Chapter I Solar Photovoltaic Power Generation Systems (Characteristics and integration impacts)

I.1 Introduction

As there is an abundance of sunlight and a need to minimize carbon-emitting systems, the potential for solar energy has expanded. This has driven interest in the study and development of solar photovoltaic power systems, in which sunlight is immediately converted into energy. A photovoltaic (PV) solar system is a system that is capable of directly converting the energy from the sun into electrical energy. The solar cell, when coupled in groups to make solar modules and arrays, is the primary component of a solar energy system. Solar systems are utilized in order to generate energy, which can then be utilized for the purpose of feeding various electrical loads. Solar cells generate direct current (DC) electrical energy, which can be used to directly energize certain kinds of DC loads; alternatively, this energy can be converted into AC current or DC current to energize other kinds of loads. Solar power installations can be linked together to create larger systems, or they can even be integrated into existing power grids to sell or buy power from such grids [8].

The following are the two primary classifications of solar photovoltaic (PV) systems [9]:

➢ The stand-alone systems (off grid), which are typically installed in rural and remote parts of developing countries where there is no possibility of connectivity to the grid. Nonetheless, the inexpensive cost of manufacture combined with new ideas has led to a wide variety of uses in developed nations as well. Off grid systems are typically supplemented by storage systems (such as batteries) in order to meet the load at times when the solar irradiation is not sufficient for the PV to cover the entire requirement. This is because there are times when the solar irradiation is not sufficient for the PV to cover the full need.

➢ The grid-integrated systems, which are solar PV installations that are connected to the regional power distribution system and provide power to that grid. The connection is made through the use of an inverter, which not only changes the DC current into AC current but also ensures that the voltage and frequency are in sync with the grid. The photovoltaic systems can be connected either directly to the public grid or initially to the grid in the home, where they will meet the household's electricity needs and then transfer any extra power to the public grid. There is no energy storage outside the grid, however some systems incorporate batteries to boost PV self-consumption, system availability, and grid backup. To be more competitive, the systems' benefits should balance the extra investment and maintenance.

Chapter I Solar Photovoltaic Power Generation Systems (Characteristics and integration impacts)

I.2 Advantages of Solar PV Systems

The solar photovoltaic (PV) technology offers a great number of benefits. The paragraphs that follow will focus on each of these points [10].

1. Clean energy: The production of electrical power by the solar photovoltaic modules does not result in the generation of any greenhouse gases (GHG). PV technology assures that there are no emissions produced during the generation of electrical power, so preventing the major environmental damage caused by greenhouse gases (GHGs), such as global warming and climate change.

2. Sustainable energy source: Silicon, which is initiate in sand and is one of the most plentiful elements on the earth, is used in the construction of the modules that are at the heart of photovoltaic, or PV, technology. This allows sunlight to be converted into electricity. We will always have access to reliable sources of electricity so long as the sun continues to shine around the world.

3. Noise-free technology: To minimize noise, most PV systems are designed without the use of any moving parts. Hence, it is a viable renewable resource that may be integrated into urban areas. However, alternative renewable generation systems are unsuitable for local installation due to their size and complexity of operation. ty.

4. Low maintenance technology: Modules that convert sunlight into electricity have a low technical maintenance requirement. The modules need to be cleaned on a regular basis so that trash doesn't accumulate and block the sunshine.

5. Performance guarantee over service life: Typically, manufacturers of PV modules will offer a linear performance guarantee in the product datasheet.
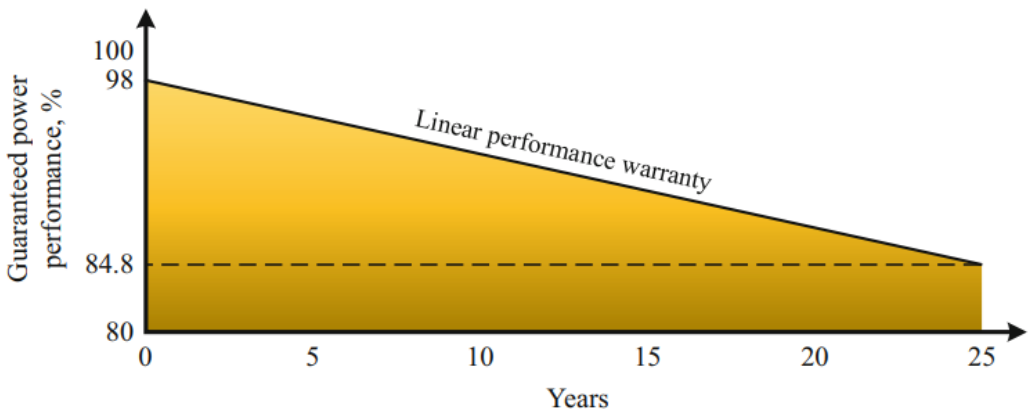
Figure I. 1: A average solar module's 25-year power production.[10]

Chapter I Solar Photovoltaic Power Generation Systems (Characteristics and integration impacts)

Module efficiency is guaranteed to be greater than the specified level for the duration of the warranty. The warranty is helpful since it suggests that performance decline would be minimal over time. Warranted power output is plotted against time in Figure I.1. The statistic indicates that after 25 years of operation, the module's working effectiveness will not fall below 84.8% of its initial efficiency. Due to manufacturing and crystal structure quality issues with the wafer, initial efficiency is less than 100%. The effectiveness of a module decreases by roughly 0.5% to 1.5% in the first few days after being exposed to sunlight, reliant on the type of module. This gradual loss of effectiveness is identified as light-induced degradation (LID)

6. No geographical necessities: PV modules can be deployed everywhere in the world, regardless of the weather, because they can still generate some electricity even in overcast conditions. However, PV systems function best when placed in a sunny location that is not shaded by any nearby trees or buildings.

7. Cheap: PV module prices have plummeted in the past two decades. Recent semiconductor advancements suggest additional price decrease.

8. Reprocessing of solar modules: Since solar modules are mostly made of glass, silicon, and some metal, they can all be recycled after they reach the end of their useful lives.

10. Less natural hazards: When compared to conventional power plants, PV systems are less likely to be destroyed by natural disasters.

I .3 Challenges es of Solar PV Systems

Certain difficulties with solar PV technology installations are also addressed here[10]

1. Exorbitantly priced to both start and recycle: PV applications are low-maintenance. For large-scale applications, the initial cost may be higher than conventional resources. It's possible that the price of recycling each module (by separating, melting, and breaking it) might exceed its retail value.

2. Irregular and inconsistent power supply: Solar module energy production is directly proportional to the fluctuating daily solar irradiation, which can be further affected by varying degrees of shade. Since solar energy production can be unpredictable, it is often viewed as a secondary source by electricity markets.

3. The necessity for energy storage: Energy storage technology offsets solar power's intermittency during shade times. Nevertheless, energy storage materials like batteries have a shorter lifespan than solar panels and must be replaced numerous times over the project. Hence, adding a new operational expense to the PV system raises its initial cost.

4. Occupied area: Since light-electricity conversion effectiveness is low, PV modules must cover a vast amount of ground to satisfy grid demand. Land cost and installation placement pose this problem.

I.4 Solar PV systems – Overview

In photovoltaic (PV) systems, the solar cell is the component that is responsible for transforming solar energy into direct current (DC) power. Figure I.2 illustrates an easy approach to converting sunlight into electrical energy. Silicon, which has a semi-conductive characteristic, is the material that is employed in the construction of this solar cell. Mono-crystalline, poly-crystalline, and amorphous silicon are the types of materials that are used nowadays for the manufacture of the bulk of solar cells [11].
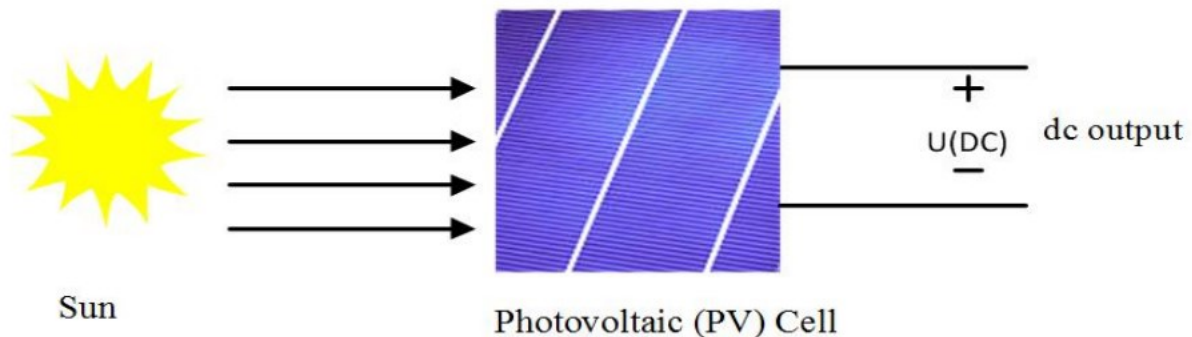
Figure I. 2: Photovoltaic (PV) Cell System [11]

Very little current and voltage can be produced by a single cell. Cells are linked in series to raise the output voltage, and cells are connected in parallel to raise the output current in order to increase voltage and current. The photovoltaic arrays that harness the sun's beams to generate power are built on solar cells as their primary building blocks .In order to generate a higher voltage across the terminal, a number of individual cells are connected in series, and these same cells are then linked in parallel with one another in order to produce a module. An array is formed by linking modules in series and parallel in order to achieve large-scale solar photovoltaic (PV) generation. Both the amount of solar irradiation and the temperature have an effect on the performance of a PV array [12].

I.4.1 Photovoltaic Cell and Theory

A p-n junction diode is a type of semiconductor that has properties that are comparable to those of PV solar cells made of silicon. There is evidence of both the p-region and the n-region. The n-region is the opposite of the p-region in that it contains a greater number of holes (+ positive particles) than electrons (- negative particles). Because of this, the material that makes up the p-n junction generates an electric field as a consequence of the mobility of electrons and

holes that is inherent to the material. When a photon from the sun's radiation strikes a p-n junction, it causes an electron to become dislodged across the n-side depletion zone. The electron is then accelerated by the field and pushed in that direction, while the matching hole is pushed in the opposite direction, toward the p-region. This causes the electron to be pushed in the direction of the depletion zone [13] [14]. Figure.I.3 demonstrates the arrangement of a p-n junction, a depletion layer, and the electric field that is generated.
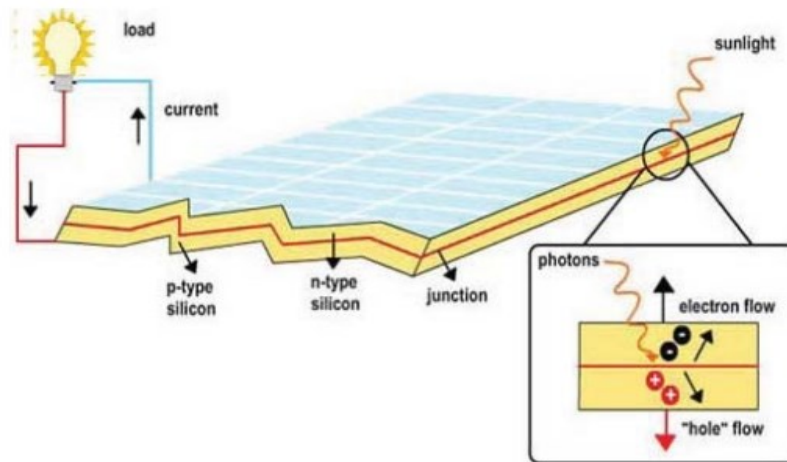
Figure I. 3: Photovoltaic effect principle and a p-n junction [15]

I.4.2 Modeling and Characteristics of Solar Photovoltaic Cell

Semiconductors, which can be created through a variety of techniques, are the primary element that go into the construction of solar cells. These semiconductors directly transform solar energy into electricity by utilizing a process known as the photovoltaic effect. The complete I-V curve of a cell, module, or array is defined as a continuous function for equivalent circuit models, regardless of the specific set of operating conditions that are being considered. A solar PV cell is depicted in Figure I.4. This cell is made up of a constant current source that is reliant on the amount of solar radiation, a diode that has a series resistance (RS), and a parallel resistance (Rsh) [16].
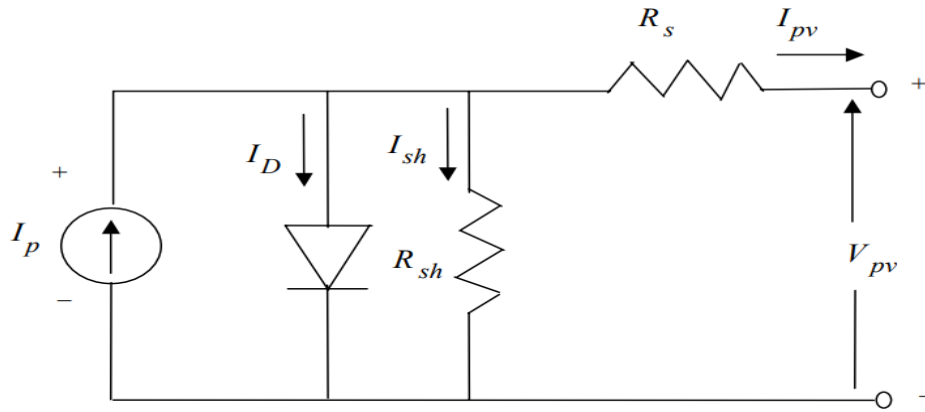
Figure I. 4: Solar cell equivalent model [16]

A dark current, also known as a backward current (Io), flows in a p-n junction when there is no solar radiation (G) from the sun. The cell produces the current I_p with a load connected when there is solar radiation. When there is no load connected, the voltage V_{pv} is the open circuit voltage that can be measured. The greatest current that a cell can produce at a specific level of solar radiation is known as the current I_p (G).

Following equation represents a PV cell:

$$\begin{aligned} I_{pv} &= I_p - I_D - I_{sh} \\ &= I_p - I_o \left[e^{\frac{q(V_{pv}+R_SI_{pv})}{NkT}} - 1 \right] - \frac{V_{pv}+R_SI_{pv}}{R_{sh}} \end{aligned} \tag{I.1}$$

Where

Ip = Photocurrent [A]

Vpv = Terminal voltage of the cell [V]

ID = Diode current [A]

Io = Saturation current [A]

Ish = Shunt current [A]

N = Ideality factor (a material constant)

q = Electron charge [C]

k = Boltzmann's constant (8.62 x 10-5 eV/K)

T = Junction temperature [K] (diode temperature)

Rs = Series resistance [Ω]

Rsh = Shunt resistance [Ω]

A current-voltage (I-V) representative and P-V curve of the solar module can are illustrated in Figure I.5 and figure I.6.
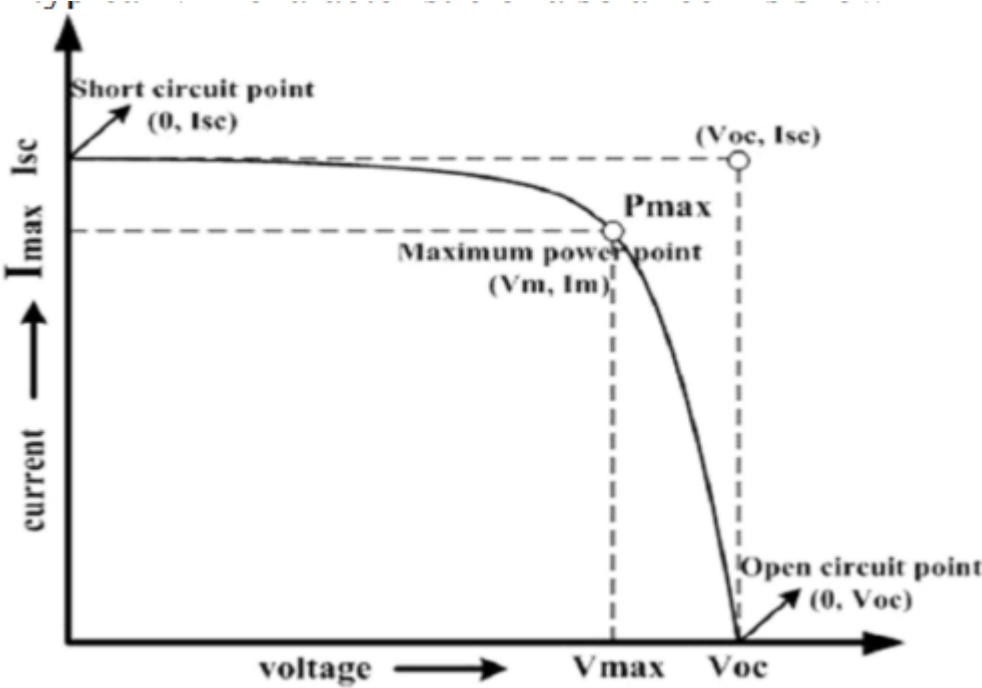
Figure I. 5: I-V curve of a solar module [17]
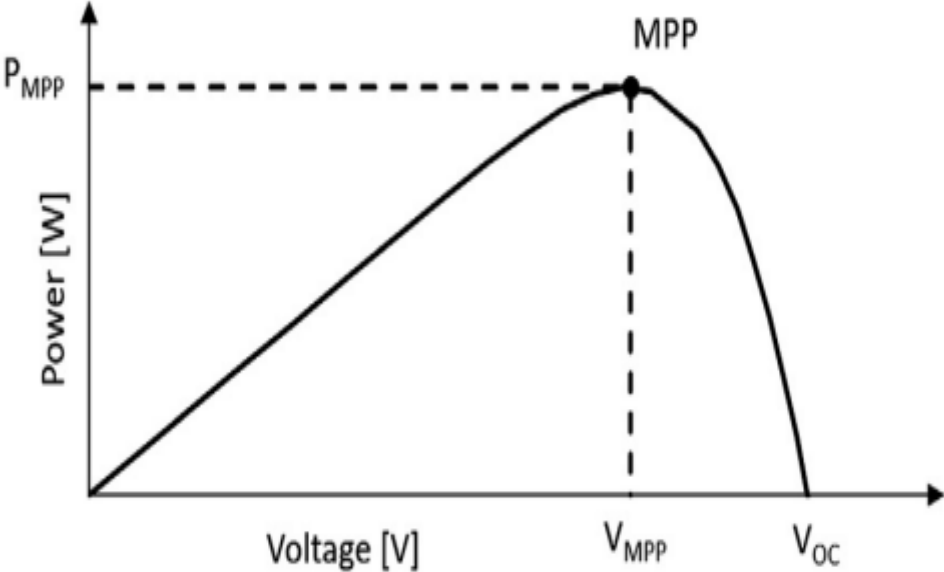
Figure I. 6: P-V curve of the solar module [18]

The highest current that it is capable of producing is referred to as the short-circuit current (Isc),), which is calculated by connecting the two ends with no load present and is depicted in Figure I.5. Each solar module's datasheet or the I-V curve can be used to calculate Isc; this value is found at the point where the y-axis and the curve meet. It is important to remember that the wires attached to the module terminals are built to withstand the high Isc. As a result, the short-circuit test can be performed by isolating the system from the solar modules and checking its

10

performance with a multimeter whose range is at least as great as the predicted value of the short-circuit current. In addition, the voltage between the terminals of the solar module is measured to be Voc If an infinitely-resistive load is applied. That's the maximum voltage this module can generate. With a digital multimeter linked in parallel to the terminals of solar module,the Voc can be read as a positive reading[10].

As can be seen in figure I.6, the power output of the solar cell is a function of both its voltage and its current. Power that can be given to an external circuit is what it is. The solar cell produces its greatest power at a specific voltage and current point. This point, which is referred to as the maximum power point, is the most optimal point of operation. The vast majority of commercially available solar cells have an efficiency of between 15 and 20 percent (%), which indicates that a considerable amount of surface area is necessary to generate greater amounts of power. It is absolutely necessary to ensure that the solar cell is consistently delivering the maximum quantity of power. It is the responsibility of the MPPT to ensure that the solar cell is always operating at its maximum possible power [10, 11].

The photovoltaic array, often known as the PV array, is a collection of individual PV cells that are connected together to form a single unit that has the desired power rating. It is feasible to compute the characteristic of a PV array by doubling the voltage of a single cell by the number of cells that are connected in series and the current by the number of cells that are linked in parallel [19].

I.4.3 Impact of irradiation and temperature on solar PV cell

The influence that irradiance has on the I-V characteristic curve is depicted in Figure I.7, and Figure I.8 depicts the effect that cell temperature has on that curve. Irradiation has an effect on the current that is produced by incident light, as shown in Figure I.7. The bigger the irradiation, the larger the current. Voltage, on the other hand, is practically stable and won't shift in any way. Irradiation has an obvious bearing on maximum power point; the more intense the irradiation, the higher the maximum power point will be.

As can be seen in figure I.8, the cell's voltage decreases as the temperature rises. Elevated temperatures cause a drop in voltage. As the temperature of a solar cell rises, the amount of power it can harvest from the sun drops dramatically. A solar photovoltaic (PV) cell's overall performance can be affected by a number offactors, including its efficiency, the amount of available light, and the temperature. These factors, which influence the power output of the cell in different ways, interact with the maximum power point [16].
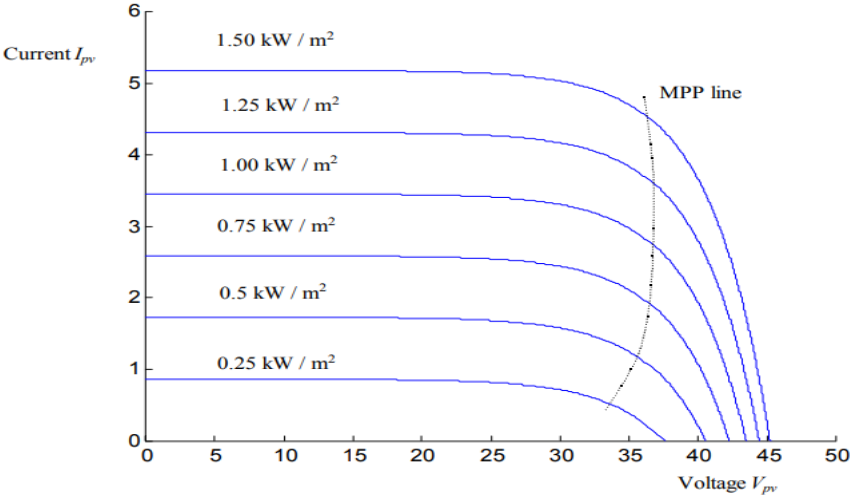
Figure I. 7: Effect of the irradiation on I-V curve [19]
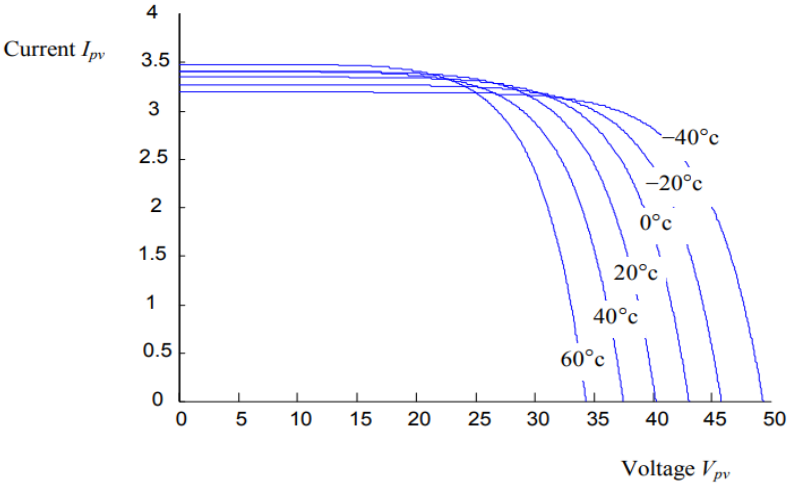
Figure I. 8: Effect of the temperature on I-V curve [19]

I.5 Main Components of Grid Integrated Solar PV System

The term "grid-connected energy system" or "grid-connected photovoltaic system" refers to a system that is linked to the grid. The system is able to collect solar energy, convert it into electrical power, and then send that electricity to residences, where it may be used to power a variety of electronic equipment. This is made possible by the grid-tied connection. As shown in figure I.10, the fundamental design of a PV system that is integrated to the grid contains of the below elements [20]:

(i)   PV Array: PV modules are vital components of any PV system because of the critical part they play in the generation of energy for the load. Every single photovoltaic (PV) module is made up of a fundamental component referred to as a solar cell. This solar cell is what performs the photovoltaic effect, which is the process of changing solar irradiance into direct current DC power. When a Silicon solar cell is exposed

to sunlight, an irradiance-proportional current flows between the cell's two poles, producing a voltage of 0.50 to 0.68 V. When the cell is called a "Silicon solar cell," this happens. In Figure I.9, we see an illustration of how a solar module is constructed by stringing together a number of solar cells in a serial arrangement. A string is created by connecting the modules together in a series order. After then, parallel connections are made between the strings to create an array. Important design factors include not just the orientation and tilt of these panels but also the shading that is provided by the surrounding impediments.
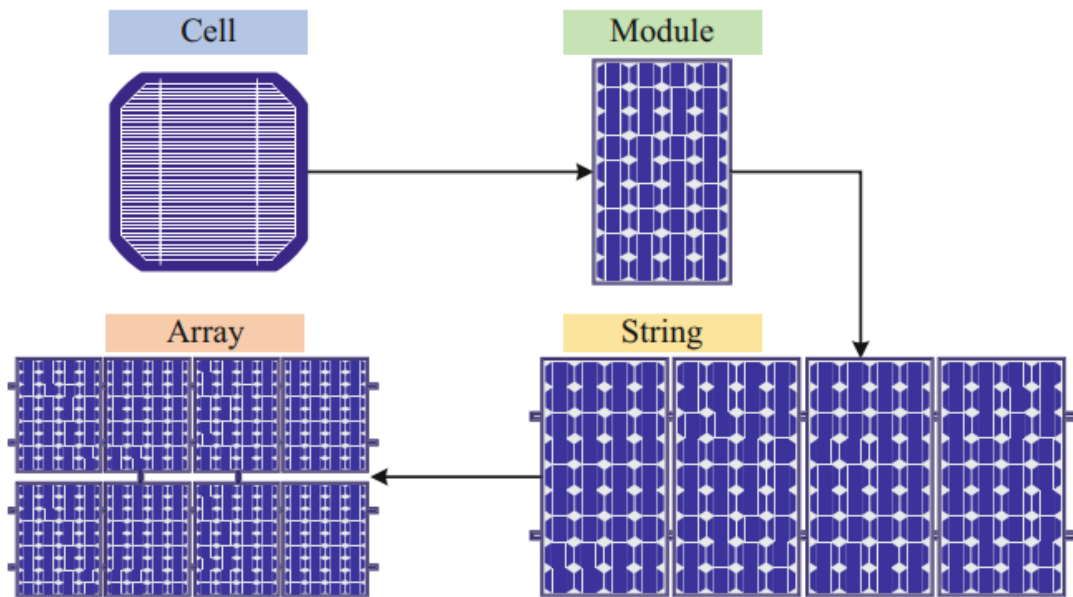
Figure I. 9: String, module, array, and cell diagrams[10]

(ii)　　PV array connection box (with protective devices)

(iii)　　DC current cable

(iv)　　Inverter: A power converter that "inverts" DC panel electricity into AC (AC). Output signals should match supply network voltage, frequency, and phase angle.

(v)　　AC cabling;

(vi)　　Transformer: A transformer can increase the AC output voltage of an inverter.

(vii)　　Meters: This shows energy flow between the PV and the grid or load.

(viii)　Protective Devices: Undervoltage relays, circuit breakers, etc. are also installed.

(ix)　　Additional devices, such as DC-DC converters and AC filters, can also be utilised to improve performance.
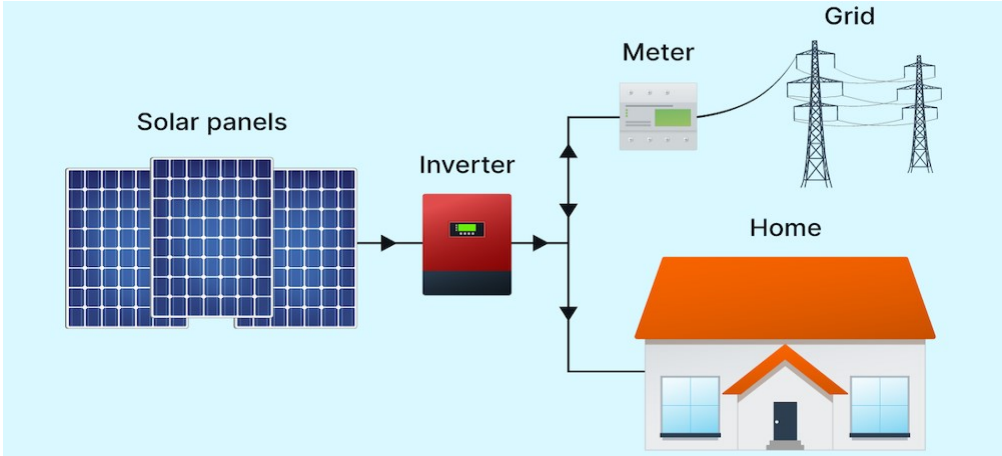
Figure I. 10: Chart of a PV system linked to the grid [21]

I.6 Solar Photovoltaic System Configuration for Grid Integration

In order to coordinate the PV power transfer to the grid, the state-of-the-art technologies generally fall into one of four configuration approaches, as shown in Figure I.11 Depending on the system's intended use, different setups may involve series and/or parallel connections of PV modules and various forms of converters (DC to AC inverters) [22].
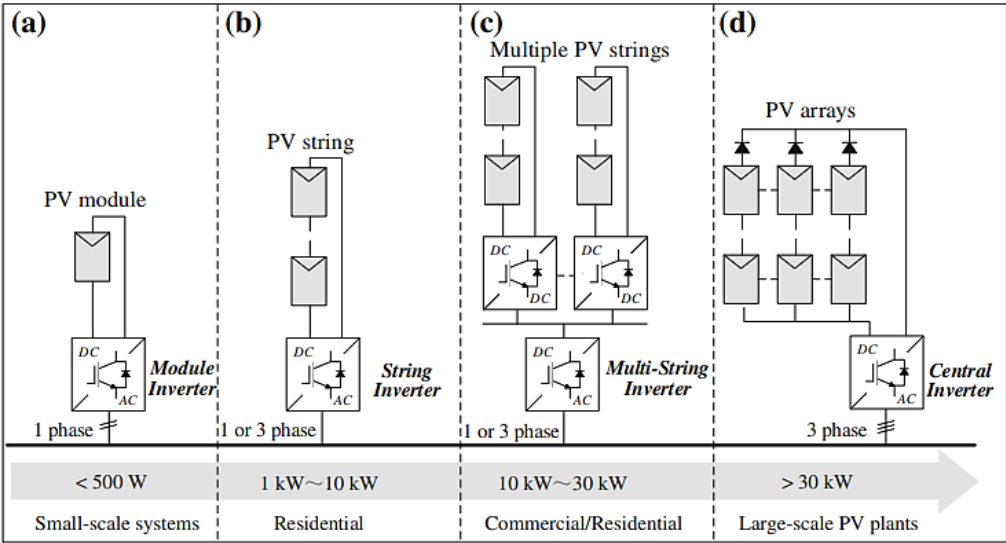
Figure I. 11: Configuration of solar PV systems connected to grid: (a) module inverter, (b) string inverter, (c) multi-string inverter, (d) central inverter [22]

I.6.1 Centralized configuration

This design is referred to as a central inverter. Figure I.11.d depicts what happens when many PV modules are linked to a single 3-phase inverter. In order to generate a suitably high voltage, the PV modules are linked together in series, which is sometimes referred to as strings. In order to obtain a high-power output, these PV strings are then linked in parallel, which is called an array. In order to prevent the flow of reverse current, a blocking diode is linked in series with

14

each PV string section. In large-scale photovoltaic plants, central inverters are typically installed. The usage of a central inverter for large-scale applications is made more economically viable as a result of its centralized configuration, This utilises a unified sensor suite, control hub, and monitoring device. Nevertheless, the straightforward setup has a large variance loss between PV modules as a result of the use of a single MPPT for the entire PV arrays. This is a drawback of the straightforward configuration. Inverter outages show power generation loss. Centralized power plant expansion is difficult [23] [24] [25].

I.6.2 Module configuration

A micro-inverter is another name for a module inverter. In contrast to a centralized setup, as shown in Figure I.11.a, each micro-inverter is connected to its own PV module. Mismatch loss between PV modules is totally eradicated according to the "one PV module one inverter approach," resulting in increased energy yields. Installation and growth are simplified through module setup. The use of a micro-inverter does, without a doubt, make it possible to achieve a very high degree of flexibility; nevertheless, this comes at the penalty of higher initial costs and increased maintenance requirements. Large-scale applications necessitate the utilization of a significant number of inverters. The micro-inverter typically incorporates a DC–DC converter as a means of boosting the PV module's low voltage to match to the specifications of the grid [23, 24] [25].

I.6.3 String configuration

When using a string arrangement, each inverter is only linked to a single PV string. This eliminates the need for the blocking diode that is depicted in Figure I.11. b. The benefits of a central inverter with a simple structure and the benefits of a micro-inverter with a high energy yield are combined in the string inverter. When compared to centralized design, MPPT that operates at the string level results in a higher energy yield. This is accomplished by lowering the amount of mismatch loss that occurs between the PV modules. Since there is only one PV string connected to each inverter in this setup, string inverters are typically developed for low power applications, such as those found on residential rooftops [23] [24] [25].

I.6.4 Multi-string configuration

Combining the center and string topologies into a single device result in the multi-string inverter, which may be shown in Figure2.11. c. A single inverter is connected to a number of PV strings, each of which has its own separate DC–DC converter (MPPT). That is the inverter that is most commonly used nowadays. Each PV string has its own MPPT, so the mismatch loss between modules is kept to a minimum while still benefiting from the centralized

configuration's ease of use and low cost. Despite the higher initial cost and greater number of inverters needed for a multi-string design, the industry is moving in support of multi-string inverters for large-scale PV facilities because of their simplicity in installation, commissioning, and maintenance [23] [24] [25].

I.7 Benefits of Grid-Integrated Solar PV Power Systems

Because of their durability and ease of use, solar PV system devices offer significant benefits while requiring just minimal upkeep. As independent units, they can generate power on a scale from microwatts to megawatts. Thus, the use of solar PV continues to gain popularity. Since solar energy can be generated in nearly any location, it eliminates the need to transport fuel from other parts of the country or the world, hence reducing the negative effects of transportation on the environment and the reliance of consumers and engineers on imported fuels. Solar PV are modular, easy to install, environmentally friendly, fuel-free, long-lasting, and low-maintenance. [26].

Unlike isolated photovoltaic systems, grid-connected solar PV systems operate parallel to the power grid and do not require storage devices to store electrical energy. By substituting local connected load and supplementing the electric utility grid, the solar PV system helps reduce greenhouse gas emissions. Grid-connected solar PV sent power back onto the grid when generated electricity exceeded local connected load. Hence, few conventional power plants are needed during peak solar hours [27]. Losses in transmission and distribution part are also minimized in grid-integrated solar PV systems. So, in modern power systems, solar PV or DG incorporated to the grid help satisfy consumer load needs and are more effective and reliable in sending more power to the grid with the appropriate quality and regularity. [26]. If the solar PV system is grid-connected, it can feed excess power either back into the regional power system or into a battery. Linking the solar PV system to the local electric utility grid reduces owner electricity bills, simplifies operation, and reduces operating and maintenance costs. Since the grid-connected solar PV system feeds back extra power, it minimizes conventional energy use to produce electricity [28].

I.8 Challenges of Grid-Integrated Solar PV Power Systems

Grid-integrated PV systems face obstacles when setting up and incorporating. PV systems connected into the utility grid cause power quality concerns, harmonic injection, voltage, frequency, and power variation, islanding, protective limits, and more. Since solar power is delivered directly to the grid, most on-grid solar PV systems don't need storage. If the grid fails due to power shortages or other issues, this dependence can be problematic [29].

Chapter I Solar Photovoltaic Power Generation Systems (Characteristics and integration impacts)

PV output power is very harmonic due to its dynamic nature. Harmonics disrupt the AC waveform in the grid and lower power quality when they are incorporated into the utility system. A dependable inverter that can consistently create an output with the required voltage and frequency should be used to prevent voltage and frequency changes in the grid power that may be caused by the fluctuating PV output [30].

In most cases, the daily solar power output takes the form of a roughly bell-shaped curve and reaches its highest point at noon. This pattern suggests a problem that is referred to as the duck curve for PV systems that are grid-connected. When the PV output reaches its peak, the demand for power from the grid drops, which forces the grid to ramp down. Similarly, as the PV output drops, the demand for power from the grid shoots up, which forces the grid to have to increase its capacity. In addition to the typical daily load curve that would be seen in the nonappearance of PV systems, the new load curve creates a picture of a duck. Figure I.12 illustrates this phenomenon, which is referred to as the duck curve. The actual load curve may be seen here as the orange curve, and it has a peak in the evening. Only during particular times of the day is the solar PV production available for use. The blue graph illustrates how, when solar PV output is available, there is a corresponding reduction in the amount of power used from the grid. The combination of the orange curve and the blue curve looks like a duck, which is where the name duck curve comes from. The phenomenon known as the duck curve is a challenge for electricity-generating systems since it demands them to rapidly ramp up their output in order to keep up with the unexpected increase in load demand. A solution to the problem of the duck curve can be found through the utilization of hybridization of energy sources, energy storage, microgrids, and demand-side management [10] [31].

Another issue that is inherent to grid-incorporated PV systems is the potential for overgeneration, which occurs when the output of the PV system is greater than what is necessary. An excessive amount of generation can result in the grid becoming overloaded and sustaining lasting damage, both of which are extremely expensive to fix. The conventional types of generators producing electricity have what's known as a spinning capacity reserve that can be used if necessary. It is possible for the generator's output to be increased when there is a greater demand from the load. This feature is not available in solar PV systems that are based on inverters since these systems lack inertia and do not have reserve capacity unless storage devices are utilized. Because of this, if photovoltaic (PV) solar energy is added to the grid, a storage system will be required in order to ensure the grid continues to function in a dependable manner [10].
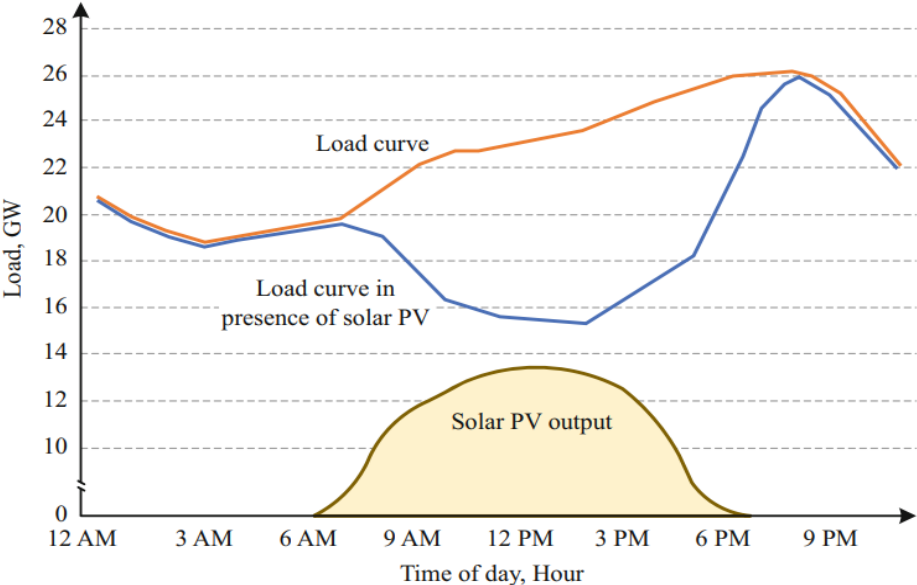
Figure I. 12 Diagram of the duck curve phenomenon—grid- PV challenge[10]

I.9 Impacts of Integration of Solar PV Power Systems

As the amount of energy produced by solar PVs continues to rise, it becomes more difficult for the companies in control of the transmission and distribution of electricity to incorporate this power into the grid. Consequently, it is crucial to comprehend the effects of adding a solar PV power plant to the current electricity system, both at the transmission and distribution levels [6]. In most cases, grid-connected photovoltaic systems are installed in order to improve the functionality of the electric network; solar photovoltaic systems deliver power to the load side of the distribution network, thereby lowering the amount of energy lost in the feeders and increasing the amount of active power loading, which ultimately results in an improvement in the voltage profile [32]. However, solar photovoltaic (PV) systems that are linked to the grid can also have a number of unfavorable impacts on power networks, particularly when the penetration level of these systems is high. The magnitude of these effects is largely determined by the geographic location and size of the PV system[32].

I.9.1 Impact of integration solar PV power systems on the voltage profile

One definition of voltage profile is the numerical depiction of the voltage level at a bus of a grid under various operational conditions. Conditions of no load, light load, full load, and overload, for instance, can all be accounted for by measuring the voltage level. The voltage level of the grid needs to stay within a certain range for the vast majority of power systems. This is because of the fact that there are loads whose operation is adversely affected by even small variations in the supply voltage. It is possible that voltage instability will occur if the voltage profile undergoes a significant change. Utility companies and transmission and

18

distribution grid operators all have a shared goal of preserving a healthy voltage profile, consistent grid characteristics, and reliable voltage. Grid characteristics have to be kept within stable operating conditions at all times, even during periods of system upgrades, incorporation of additional power units, and operations. Alterations in the operating conditions can also potentially have an effect on the loading and losses of the power system [11].

A two-port system with a short line, end voltage (V2), transmitting end voltage (V1), and load (P, Q) is used to demonstrate voltage profile. With the two-port system, we may derive the ideas of system behavior in terms of voltage level and stability. Figure I.13 is a depiction of a two-part system's representation.
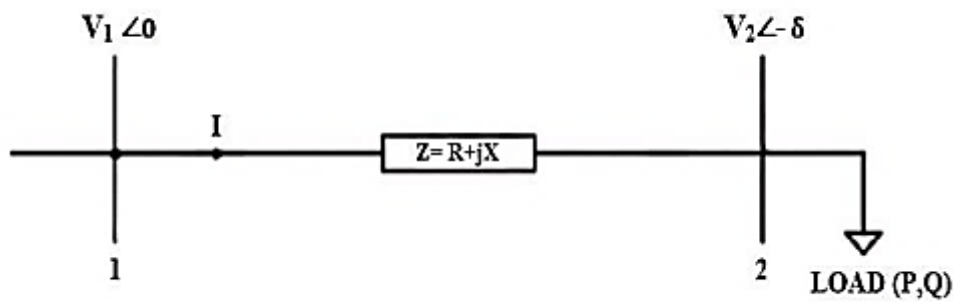
Figure I. 13: Two-bus power system [33]

In (I.2) is derived from analysis of Figure I.13 for the voltage relationship between bus 1 and bus 2;

$$V_1 = V_2 + IZ \tag{I.2}$$

Calculate the receiving bus voltage as;

$$|V_2| = |V_1| - (RP + XQ)/|V_1| \tag{I.3}$$

According to (I.2), under specific operating and loading conditions, bus 2's voltage magnitude and profile are expressed as |V2|. With the third term, we can calculate the voltage loss. Voltage drop is a result of the line parameters (R and X). Yet, at the bus 2 that's receiving the load, both active and reactive power are used. is written as, as illustrated in (I.4).

Voltage drop :

$$\Delta V = (RP + XQ)/|V_1| \tag{I.4}$$

The two-part system with a solar photovoltaic power is depicted in Figure I.14. A solar PV plant may be connected to a two-pole grid if active power with a power factor of 1 is added to bus 2.
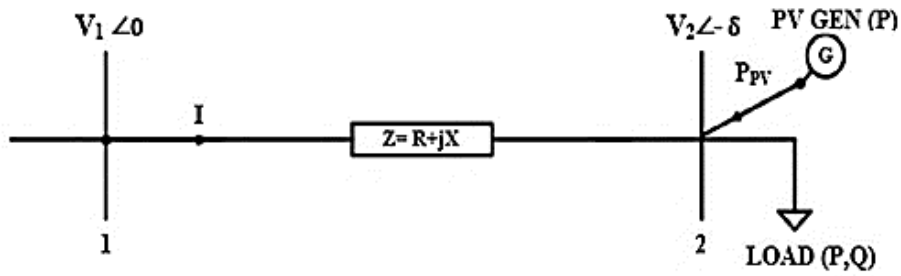
Figure I. 14: Two-node system with solar PV at load bus [33]

Figure I.14 illustrations the adjustment of two port equations for voltage level and drop for with solar PV power resulting in (I.5) and (I.6).

$$|V_2| = |V_1| - (R(P - P_{PV}) + XQ)/|V_1| \qquad (I.5)$$

$$\Delta V = (R(P - P_{PV}) + XQ/|V_1| \qquad (I.6)$$

Solar photovoltaic (PV) power implementation at bus 2 raises voltage at this bus and lowers voltage drop down the line.

I.9.2 Impact of integration solar PV power systems on power losses

As power is transported and distributed to the loads, as well as when major power plants are erected long distances from the supply and demand centres, there is often a significant amount of energy that is wasted in each of these processes. The conditions of each area have an effect on the proportionality and distance of power loss that occurs when it travels over transmission lines. PV systems provide power at the points of consumption, and the amount of power produced is dependent on the amount of solar radiation that is available. These systems offer minimal power loss. There is no requirement for land because photovoltaic panels can be integrated into or mounted on the structure that requires electricity. As a consequence of this, the value that the PV system contributes to the grid is increased. If power is generated at the point of consumption, transmission and distribution losses decrease[33].

In (I.7) and (I.8) demonstrate the active and reactive losses

$$P_{Loss} = |I|^2 R = ((P^2 + Q^2)/|V_2|^2)R \qquad (I.7)$$

$$Q_{Loss} = |I|^2 X = ((P^2 + Q^2)/|V_2|^2)X \qquad (I.8)$$

Figure I.14 depicts the change of two port equations for power losses consequential of the addition of solar PV power, as illustrated in (I.9) and (I.10).

$$P_{Loss} = |I|^2 R = (((P - P_{PV})^2 + Q^2)/|V_2|^2)R \qquad (I.9)$$

$$Q_{Loss} = |I|^2 X = (((P - P_{PV})^2 + Q^2)/|V_2|^2)X \qquad (I.10)$$

Chapter I Solar Photovoltaic Power Generation Systems (Characteristics and integration impacts)

A reduction in the flow of current via the lines is brought about by the installation of PV units in the distribution posts. The load correction that is carried out by the integrated PV system helps to cut down on the losses. owing to the fact that the power that is lost in the various components of an electrical network is proportional to the square of the current. This effect is more noticeable when the highest loads are being experienced. Because of the decrease in active power, there has been a discernible decrease in the active power losses as well as the active component of the line current. This is a direct result of the reduction in total losses [33].

The influences of solar PV addition on the voltage profile of the grid as well as power losses have been the subject of investigation in a number of studies. Authors in [11]. looked analyzed how adding solar power to the system might affect the distribution of electricity. Distribution grids were simulated in power modeling software with and without solar photovoltaics. The goal of the modeling was to look at the impact during steady state on the distribution networks. Based on the results, it was determined that the voltage level profile for distribution grids was greatly improved with the incorporation of solar PVP. As a result, the examined grids' state voltages became more stable, and voltage losses and drops were greatly reduced. According to [34] depending on the grid's design and distance from the main power supply, the addition of a PV system can result in a rise in both the level and profile of the voltage.. The study [35]found that when solar PV power is integrated into the grid, active and reactive power losses are reduced, and line load is lowered as a result. According to study by [36], integrating PV at different penetration rates effectively offsets active power use, reduces load and line losses, and improves voltage profile. The effects of interconnecting large-scale solar PV power facilities to Jordan's national grid were studied in [33] Incorporation of photovoltaic solar systems was shown to minimize power losses by a relatively small amount. The voltage profile on the grid is improved, especially when the solar system is linked to the grid in close proximity to the load centre.

I.9.3 Impact of solar PV power system integration on grid stability

The influence of this non-constant source of electricity on the grid is getting bigger as more photovoltaic are linked to the grid. Because of the properties of solar irradiation, a high penetration of PV systems can have a major effect on the stability of the power system [37]. The most significant factor that contributes to variations in the output power of PV systems is the variable amount of solar irradiation that occurs whenever clouds pass in front of a photovoltaic array. The degree to which oscillations in PV power on the electric network are severe is determined by a number of factors, including the following: [7]

Chapter I Solar Photovoltaic Power Generation Systems (Characteristics and integration impacts)

1. clouds type, 2. Penetration level, 3. Size of PV system, 4. PV system location, and 5. Topology of the electric network

The cloud- impacts on the Mölndal grid with various PV penetration rates on voltage stability were studied in [38]. In this particular investigation, the cloud transients were imitated by lowering the solar irradiation from 1000 W/m2 to 0 W/m2 over the course of a period of twenty seconds (from 10 to 30 seconds). The results indicated that the residential network that was located in the Molndal area (the real network) was able to keep its voltage stability without experiencing any problems even when cloud-induced power swings occurred in the grid at varying penetration levels.

When there is a substantial penetration of PV power systems into the power grid, there is a potential for considerable problems to be imposed on grid stability due to a lack of reactive power supply and system inertia [37]. It is commonly known that photovoltaic (PV) modules lack a spinning component; hence, no inertia response can be given during network interruptions. After PV power is included into the grid, the total system inertia will decrease. Reduced system inertia will result in increased system oscillations. Large angle discrepancies in the bus voltages caused by the injection of PV power also have an effect on the system's performance.[39] . The impact that huge PV systems have on the voltage levels and the stability of transmission systems after fault circumstances was investigated in [40]. The findings indicate that during normal operating conditions, there is an impact on the system's voltage levels caused by the replacement of conventional generating with large PV powers. As a result of the presence of photovoltaic (PV) units in the network, the rotors of some of the conventional generators that are part of the system may swing at greater magnitudes in the event of a fault. In addition to this, there is a possibility of voltage collapse occurring at very high penetration levels of PV systems.

Authors in [41] investigate the effects of increased penetration of PV systems on the static and transient stability of a big power system, with a focus on the transmission system. Both the negative and positive effects of higher PV penetration on performance of steady-state stability and transient stability are clearly identified by the simulation results. Furthermore, in [39] several effects on the stability of a power system are explored. These impacts include the integration of utility-scale PVs and rooftop PVs, as well as the replacement of the existing traditional generators. The findings showed that the benefits of PVs are significantly reliant on a variety of criteria like the criticality of nodes, the kind, position, and penetration of PVs, as well as the type of transients.

Chapter I Solar Photovoltaic Power Generation Systems (Characteristics and integration impacts)

The effects of incorporating photovoltaic (PV) plants with high penetration rates into Egypt's national grid are illustrated in [42]. Frequency stability findings indicated that the national grid would remain stable with PVP penetration of up to 3,000 MW. Furthermore, voltage stability analysis reveals that the voltage's dynamic behavior depends significantly on the grid's short circuit capacity at the time of integrating the PVPs.

The authors of [43] look into how large penetrations of solar-photovoltaic (PV) generation affect rotor angle stability (small-disturbance and transient). The research shows that small-signal stability has increased due to the integration of solar-PV production, with the exception of remote fault scenarios in which generators with PSS are replaced by solar-PV generation. The rising penetration of solar photovoltaics has degraded transient stability in the event of a fault at a node of vital importance. Nonetheless, fault closeness to solar PV generation is a significant predictor of transient stability, and this proximity is enhanced when faults occur at less important sites. Small-signal stability and transient studies of large multi-machine systems with PV connections are also conducted in [44]. The findings demonstrated that both small signal stability and transient stability of the system are enhanced when PV generation is increased without the replacement of traditional generators. While the addition of PV makes the system less stable in terms of tiny and big signal disturbance, conventional generators are still being phased out. Furthermore, the study found that parameters including PV penetration, fault clearance time, and fault location all have a role in determining the system's stability. Also, in [45], the effects of a large percentage of PV generation on the power system small signal stability were studied. Based on the position and penetration rate of solar PV power, the simulation findings demonstrate that the effect on small signal stability might be positive or negative.

In addition, a number of research have been carried out to explore the impacts of integrating solar PV on the static voltage stability of the power system. The effects of large-scale PVs on voltage stability in power transmission systems were investigated by the authors of [46]. The findings of the study indicate that static voltage stability is significantly affected by PV size, location, and operation mode. Modal analysis and CPF were studied in [47] to determine how distributed generation (PV and wind) installations in the distribution network could improve voltage stability. In addition, the effects of DG on the power distribution system, such as the enhancement of the voltage profile and the reduction of power losses, have been analyzed. When the load factor was 3.68, the system displayed signs of instability. The integration of DG at select key buses, however, has solved this problem. Authors in [48]]used CPF analysis o determine maximum loading limit, which is used as an indicator to measure the voltage stability

of the system. The incorporation of a solar PV generator at the system's weakest bus increases voltage stability, as shown by a simulation study. The findings indicate that voltage stability is significantly impacted by factors such as geographical position, physical dimensions, and the operational power factor. The inverter's reactive power rating must be taken into account. The critical loading limit of the system can be improved with the help of solar PV generators by providing both real and reactive power assistance for the local load requirement. Modal analysis and CPF were utilized in [46] to evaluate the stability of voltage in heavily stressed power system with large-scale PV addition. The assessment of STATCOM and SVC performance with large-scale PV is also studied. Based on the findings, the static voltage stability of a power system is significantly affected by the PV array's location, size, and incorporation strategy (whether concentrated or dispersed). Furthermore, STATCOM offers a preferable choice to improve the static voltage stability margin of the system when large-scale PVs are present. Authors in [49] used modal analysis and CPF to assess the influence of large-scale PV penetration on voltage stability of power system. Evidence from simulations suggests that the static voltage stability of the system is significantly influenced by the PV location, size, and integration strategy (whether concentrated or dispersed). The P.F of PV generators also affects how steady the voltage is.
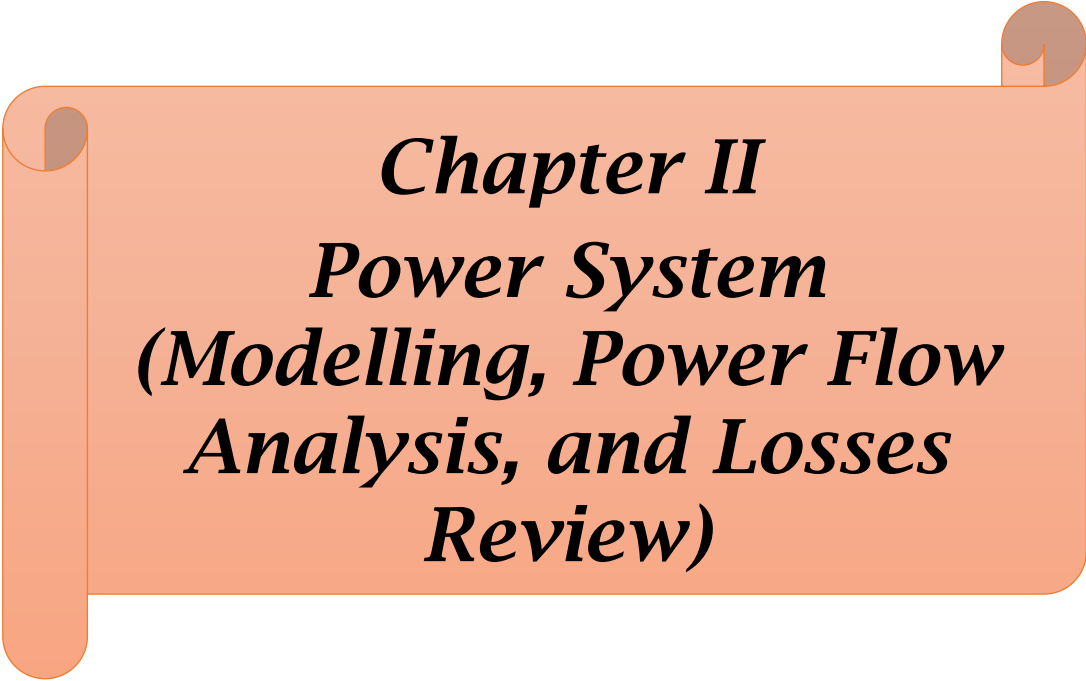
The primary contribution of this thesis is the presenting of several analyses for the power system stability of a grid-integrated solar PV power generation system. different scenarios are considered with various software. ETAP software is used to analyse transient stability of the power system. Real power grid is considered for analysis. Different cases are conducted. Moreover, NEPLAN software is used to analysis the static voltage stability of electrical grid connected to solar PV power system as well as steady state analysis. In order to enhance the effectiveness and accuracy of the analyses, provide a comprehensive understanding of the problem of voltage stability, and identify the root causes of instability, we employ a combination of four methodologies (modal analysis, sensitivity analysis, CPF, and Q-V curve). Furthermore, the impact of incorporation of solar PV generation system on small signal stability is analyzed used PSAT toolbox.

I-10 Conclusion

In this chapter, we covered the characteristics of solar PV as well as the influence that temperature and irradiance have on the I-V and P-V curves of the PV module. Both of these factors have the potential to have an impact on the overall performance of the module. This chapter also provides an overall picture of the major components that make up a PV system that

is linked to the grid. This chapter also talks about the benefits of a PV system that is linked to the grid and the problems that come with integrating it with the grid. Furthermore, the chapter looks at the influence that this has on the stability of the system. In addition to that, relevant findings from the earlier studies have been highlighted.

Chapter II
Power System (Modelling, Power Flow Analysis, and Losses Review)

Chapter II Power System (Modelling, Power Flow Analysis, and Losses Review)

II.1 Introduction

An electric power system is a grid of electrical components that generate (produce), transmit, and distribute electrical power. An electric grid is a power network that distributes power to households and businesses over a vast geographic area. Electric power system are three-layered complex interlinked networks made up of generation, transmission, and distribution elements. A power grid also contains control software and accompanying equipment for transmitting electricity from its source to residential, industrial, or commercial customers. This is achieved by transporting power from generation station to distribution substations via transmission lines. [50]. Power plants must be able to provide enough power to satisfy consumer needs. Transmission systems must carry large amounts of power over great distances without overheating or compromising the reliability of the system [51].

II.2 Power System Elements

The basic elements of a power system are illustrated in Figure.II.1

II-2-1 Generation station

The generation stations are responsible for generating electric power with a certain voltage level, which is raised to another level in proportion to the transmission lines using step-up transformers. The location of the generation stations depends on several factors, including proximity to the load centre and transportation facilities for the fuel sources used in the generation process. Also, the environmental factor is important for determining the location of the generation stations. Mostly, a generating station contains generating units complete with control elements and step-up transformers. The fuels used in the generating system are conventional fossil fuels (e.g., gas, oil, and coal), nuclear fuel, and water. Renewable energy sources such as wind, solar, etc. are also used for stand-alone systems.[52].

II.2.2 Transmission system

Power plants create electricity in large quantities, which is subsequently delivered across great distances to where it is needed (load or demand points). All the power plants and key load centers are linked together by the transmission network. As such, it is essential to the reliability of the electrical grid. As a result of the fact that power is constantly being lost during transmission line is proportional to the square of the line current, transmission lines often run at very high voltages (275 kV and higher). To guarantee that power can be transmitted from generators to load locations in a variety of ways, the transmission network is typically designed as a mesh. The system's dependability benefits from this enhancement [53].

Substations are the places where transmission lines of high voltage (HV) come to an end. There is the potential for very large industrial users to get power directly from these substations. These substations are responsible for reducing the voltage to a more manageable level before it is fed into the sub-transmission system. The step-down transformers are what connect the high voltage substation to the distribution substation, which is connected to this portion of the transmission system. In most cases, the voltage levels of the sub-transmission range from 66 kV to 132 kV. There is a possibility that the sub-transmission system will service some of the larger industrial consumers directly. A grid is formed as a result of the transmission lines connecting the electricity systems in the surrounding areas at the transmission level. The grid is a network that consists of various sources of generation and multiple layers of transmission networks [53].

II.2.3 Distribution system

The power is finally transferred to each individual consumer during the distribution step, which is the last stage in the process. In most cases, the connections between nodes in the distribution network take on a radial form. The voltage of the primary distribution system normally ranges from 11kV to 33kV. Primary feeders deliver power at this voltage level to customers who operate small industrial facilities. The residential and business areas are served by the secondary distribution feeders, which operate at 415/240 V. In most cases, smaller power facilities that are located close to load centers have direct connections to either the sub-transmission or distribution system [53].

II.2.4 Load

The population and average income in an area are two of the biggest factors in determining the overall loads there. Power systems have various types of loads, including the ones listed below [54]:

1. **Domestic Load:** The term "domestic load" is used to describe the aggregate total of the energy utilised by all of the electrical equipment in a home. Climate, living conditions, and the style of home all play a role. The majority of what makes up residential loads include things like lights, fans, refrigerators, air conditioners, mixers, grinders, heaters, ovens, tiny pumping, and motors, among other things. The home load accounts for a relatively small portion of total power consumption and is not affected by frequency. This load is mostly lighting, cooling, or heating.

2. **Commercial Load:** Commercial loads comprise fans, heating, air conditioning, and other electrical equipment in marketplaces, restaurants, and other businesses. The majority of

the lighting in stores, offices, advertisements, and other similar places is considered to be part of the commercial load.

3. **Industrial Loads:** Many types of manufacturing operations contribute to the overall industrial load, including those that are large, medium, small, heavy, and cottage. An important part of the total load is contributed by the induction motor. The composite load consists of the many industrial loads. The composite load represents a significant portion of the total system load, and it is a function of both frequency and voltage.

4. **Agriculture Load:** This kind of load consists primarily of motor pump sets that are used for agricultural irrigation.

So, the following fundamental conditions need to be satisfied by a power system in order for it to be correctly designed and operated: [55]

➢ The requirement for both active and reactive power must be met by the system, despite the fact that load conditions are constantly shifting.

➢ The system should provide energy at the lowest possible cost while also having the least possible impact on the environment.

➢ The reliability of the power supply must achieve at least the specified levels of excellence with respect to each of the following aspects:

(a) The bus voltages are well within the constraints that have been established.

(b) The frequency of the system is not outside of the adequate range.

(c) The system maintains a healthy equilibrium between its active and reactive power.
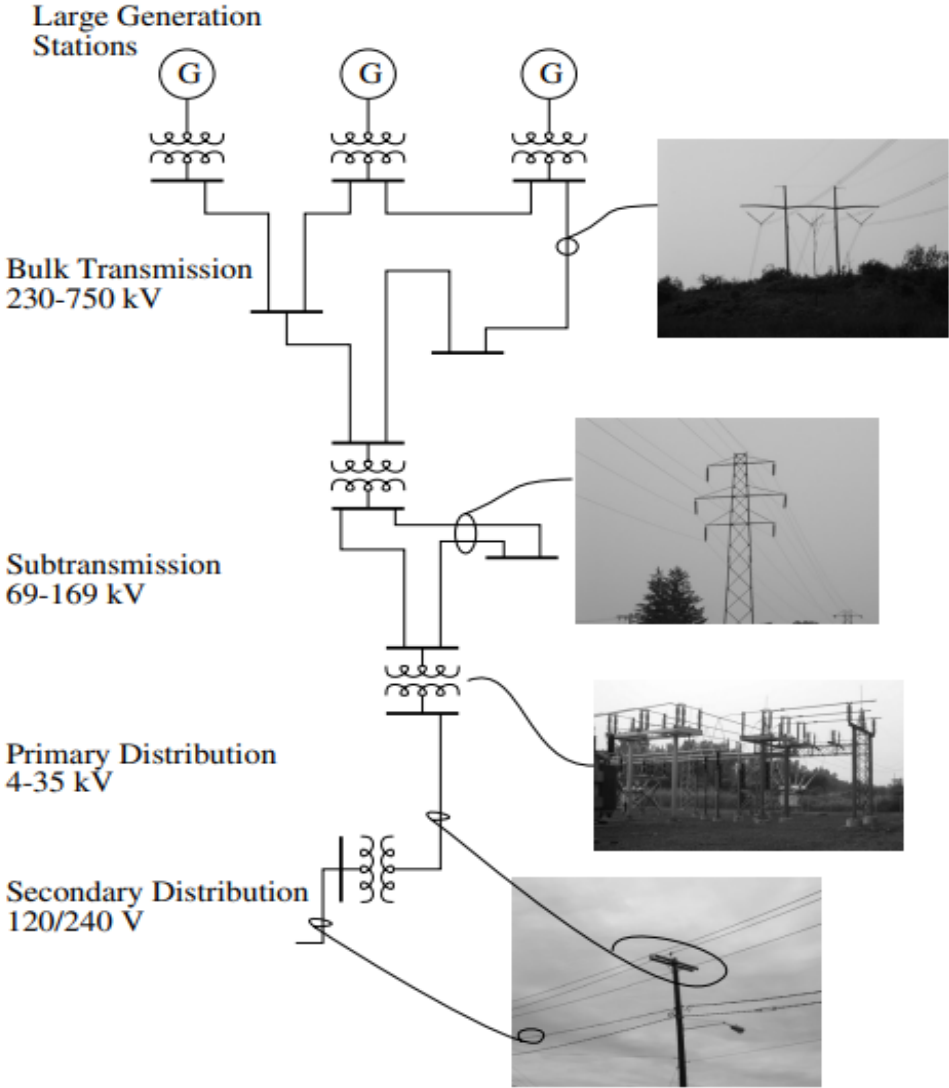
Figure II. 1: Basic elements of electric power system [56]

II.3 Modelling of Electrical Power System Components

II.3.1 Generator model

A simple per phase model for a cylindrical rotor generator is exposed in Figure (II-2)
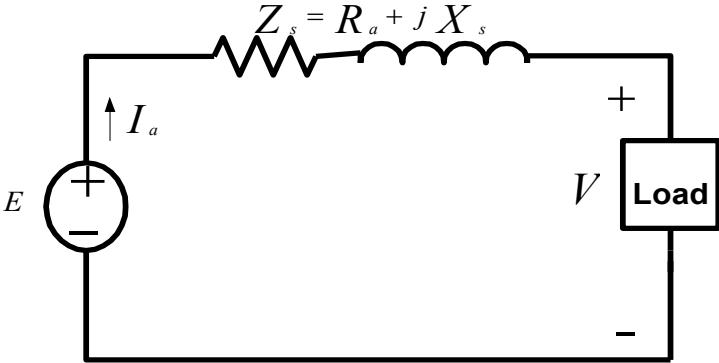
Figure II. 2: Equivalent circuit of synchronous machine [57]

Generated voltage is given by

$$E = V + I_a(R_a + jX_s) \tag{II.1}$$

Where

E= generated voltage

V= generator terminal voltage

X_S = synchronous reactance

R_a = armature resistance

As the armature resistance is typically a lot lower than the synchronous reactance and is frequently disregarded, the equation (II.1) can be reduced to its simplest form.

$$E = V + jX_s I_a \tag{II.2}$$

II.3.2 Modeling of transmission lines

The electrical qualities of resistance, inductance, capacitance, and conductance may be observed in every transmission line that makes up a power system. The model that is utilized to determine the voltages, currents, and flows of power along a line based on its length.

II.3.2.1 Short line model

When the line length is about 80km is called short line. The capacitance is ignored without match error. on a per-phase short line model basis is revealed in figure (II.3).
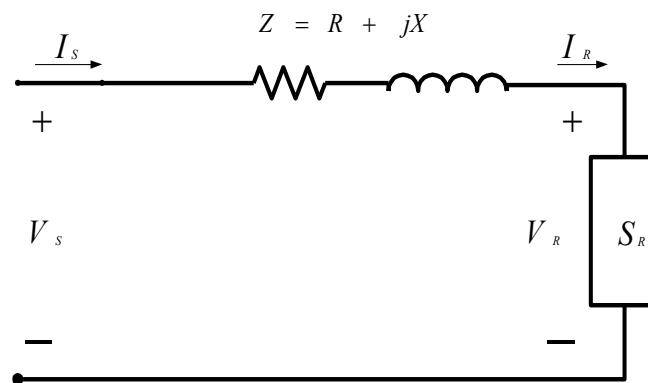
Figure II. 3: Short line model [58]

In order to calculate the short line model, simply multiply the series impedance per unit length by the line length, which can be found by using:

$$Z = (r + j\omega L)\ell$$

or

$$Z = R + jX \tag{II.3}$$

Where

X is reactance of the line.

r and L are the per-phase resistance and inductance.

V_S and I_S are current and voltage in the sending phase.

V_R and I_R where are the phase voltage and current at the other end of the line, respectively.

It is possible to write the aforementioned equations in terms of the generalised circuit constants, also known as the ABCD constants, and to depict the transmission line as a two-part network, as illustrated in Figure (II.4).
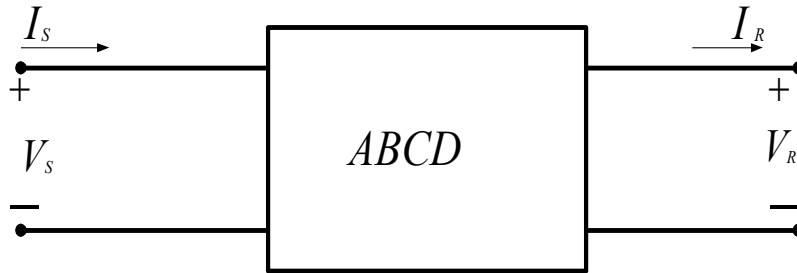
Figure II. 4: Two-part illustration of a transmission line [59]

When measured at the transmitting end of the line, the phase voltage and current are [60]

$$\left.\begin{array}{l} V_S = AV_R + BI_R \\ I_S = CV_R + DI_R \end{array}\right\} \tag{II.4}$$

II.3.2.2 Medium line model

In this context, "medium length lines" refer to those that are longer than 80 kilometres (50 miles) but shorter than 250 kilometres (150 miles). Half of the shunt capacitance can be assumed to be concentrated at each end of a medium-length line, as shown in figure (II.5), this is referred to nominal π model[60].
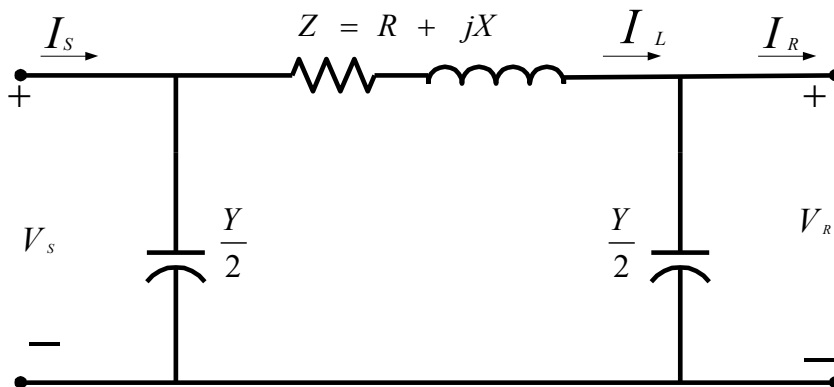
Figure II. 5: The standard mode for lines of medium length [60]

The total shunt admittance of the line is given by

$$Y = (g + j\omega C)\ell \tag{II.5}$$

Where

C is the line to neutral capacitance per km

ℓ is the line length

The ABCD constant for the nominal π model are given by

$$A = \left(1 + \frac{ZY}{2}\right) \quad , \quad B = Z$$

$$C = Y\left(1 + \frac{ZY}{4}\right) \quad , \quad D = \left(1 + \frac{ZY}{2}\right)$$

The sending voltage and current for the π model are calculated as

$$\left.\begin{array}{l} V_S = AV_R + BI_R \\ I_S = CV_R + DI_R \end{array}\right\} \tag{II.6}$$

II.3.2.3 Long line model

Assuming the line parameters to be lumped, relatively accurate models were constructed for the short and medium length lines. The precise effect of the scattered parameters must be thought about for lines 250 km (150 miles) or longer and for a more precise solution. One configuration of a distributed line L km in length is depicted in figure (II.6) [61].
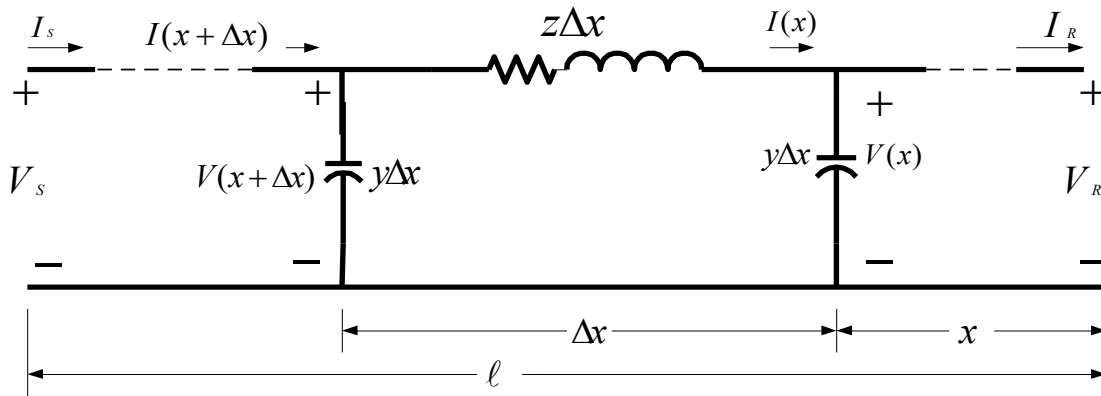
Figure II. 6: long line model [61]

Where

$$z = (r + j\omega L)$$
$$y = (g + j\omega C)$$

Where

z = length series impedance per unit

y = phase shunt admittance

The following formula can be used to model the long line.

$$V(x) = \cosh \gamma x V_R + Z_c \sinh \gamma x I_R \tag{II.7}$$

$$I(x) = \frac{1}{Z_c} \sinh \gamma x V_R + \cosh \gamma x I_R \tag{II.8}$$

Where

γ is propagation constant. Is given by

$\gamma = \sqrt{zy}$

Z_c is characteristic impedance. Is given by

$$Z_c = \sqrt{\frac{z}{y}}$$

There's a special connection between the two ends of the wire that we want to know more about. Setting x= ℓ, $V(\ell) = V_S$ and $I(\ell) = I_S$ .the result is

$$V_s = \cosh \gamma\ell V_R + Z_c\sinh \gamma\ell I_R \qquad\qquad\qquad (II.9)$$

$$I_s = \frac{1}{Z_c}\sinh \gamma\ell V_R + \cosh \gamma\ell I_R \qquad\qquad\qquad (II.10)$$

The ABC D constants are

$$A = \cosh \gamma\ell, \qquad B = Z_c\sinh \gamma\ell$$

$$C = \frac{1}{Z_c}\sinh \gamma\ell , \qquad D = \cosh \gamma\ell$$

II.3.3 Power transformer model

Electrical systems can't function properly without transformers. With their help, the comparatively modest voltages produced by generators can be amplified to very high levels, allowing for more efficient transmission of electrical power. In order to make the system usable, transformers are installed at the user end to decrease the voltage to safe levels[62].

Transformer equivalent circuit

Figure (II-7) provides a comparable circuit model of a single-phase transformer.
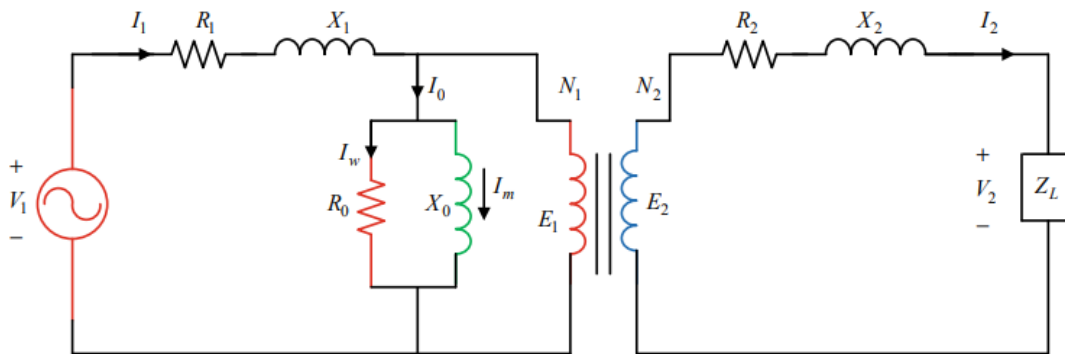
Figure II. 7: Equivalent circuit of a transformer [62]

An ideal transformer with the ratio N 1: N 2 is included in the equivalent circuit, along with components that stand in for the flaws that are present in the actual transformer.

Where

R_1 and X_1 represent the primary side's resistance and reactance.

R_2 and X_2 represent the secondary side's resistance and reactance.

V_1 and V_2 are the voltage at primary side and secondary side.

I_0 is no load current.

X_0 is magnetizing reactance.

Figure (II.7) can be redrawn as shown in figure (II.8)
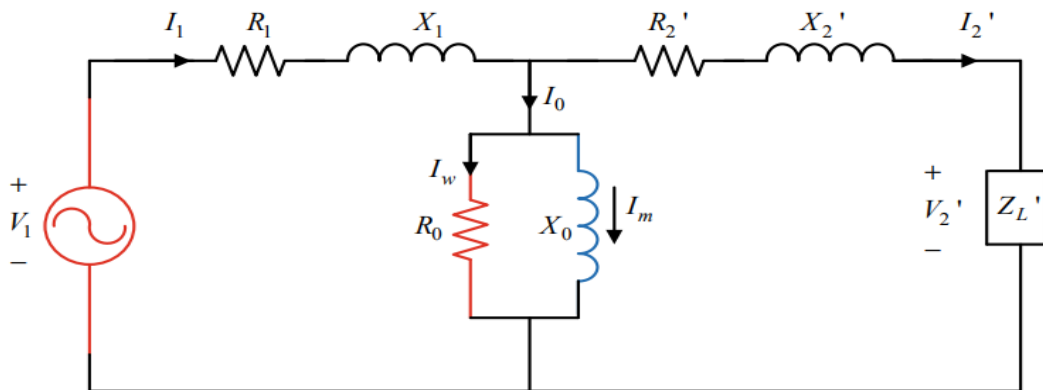
Figure II. 8: The identical equivalent circuit on the primary side [62]

Where

$$R'_2 = a^2 R_2 \;;\; X'_2 = a^2 X_2 \;;\; Z'_L = a^2 Z_L \;;\; V'_2 = a^2 V_2 \;;\; I'_2 = \frac{I_2}{a} \;; a = \frac{V_1}{V_2} = \frac{I_2}{I_1}$$

where a is the turns ratio of a transformer.

The core of power transformer is typically intended to have a very high permeability and, thus, a very low core loss; the shunt branch can be shifted across the supply voltage. So, approximate equivalent circuit can be drown as depicted in figures (II.9) and (II.10).
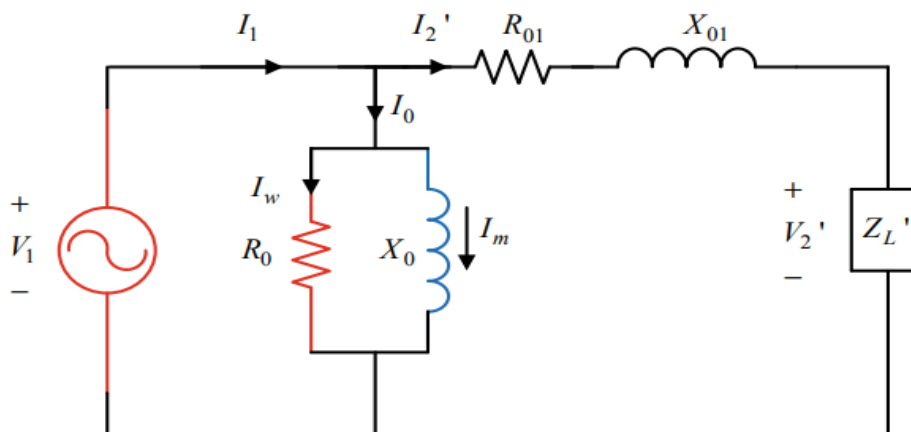
Figure II. 9: Approximate circuit referred to primary [62]

Where

$R_{01} = R_1 + R'_2 = R_1 + a^2 R_2$

$X_{01} = X_1 + X'_2 = X_1 + a^2 X_2$

$Z_{01} = R_{01} + jX_{01}$

The no-load circuit resistance and reactance are,

$$R_0 = \frac{V_1}{I_w} \quad ; \quad X_0 = \frac{V_1}{I_m}$$

The approximate equivalent circuit referred to secondary side is given in figure (II.10)
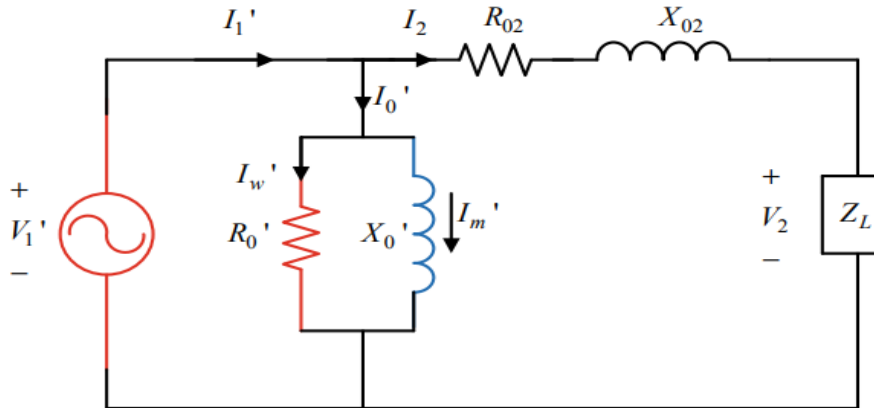
Figure II. 10: Approximate circuit referred to secondary [62]

Where

$$R_{02} = R_2 + R'_1 = R_2 + \frac{R_1}{a^2}$$
$$X_{02} = X_2 + X'_1 = X_2 + \frac{X_1}{a^2}$$
$$Z_{02} = R_{02} + jX_{02}$$

The no-load circuit resistance and reactance are,

$$R'_0 = \frac{V'_1}{I'_w} \quad ; \quad X'_0 = \frac{V'_1}{I'_m}$$

II.3.4 Model of load

Traditional classification of load models for boards divides them into static models and dynamic models.

1- Static load model:

The characteristic of the load at each instant in time can be expressed using a static load model as an algebraic function of the bus voltage magnitude and the frequency at that instant in time. These models can be written in two fundamental forms: the exponential form and the polynomial form [63].

Exponential models

It has been shown how the load's voltage dependence is expressed by:

$$P = P_0 \left[\frac{V}{V_0}\right]^a \tag{II.11}$$

$$Q = Q_0 \left[\frac{V}{V_0}\right]^a \tag{II.12}$$

Where

P and *Q* are active and reactive parts of the load when the bus load magnitude is V and base voltage is V_0 . The subscript 0 indentifies the value of particular variables at the initial conditions or base values.

a and *b* are exponents parameters of the model. *a* usually ranges between 0.5 and 1.8, and *b* ranges between 1.5 and 6.

Polynomial models

It has been shown how the load's voltage dependence is expressed by

$$P = P_0 \left[p_1 \left[\frac{V}{V_0}\right]^2 + p_2 \left[\frac{V}{V_0}\right] + p_3 \right] \tag{II.13}$$

$$Q = Q_0 \left[q_1 \left[\frac{V}{V_0}\right]^2 + q_2 \left[\frac{V}{V_0}\right] + q_3 \right] \tag{II.14}$$

Where

The coefficients p_1 to p_3 and q_1 to q_3 are the parameters of the model

Because to its characteristic constants of impedance (Z), current (I), and power (P), this model is known as the ZIP model (P).

In order to describe the frequency dependence of the load characteristic, the Exponential Model or Polynomial Model is typically multiplied by a factor as shown below:

$$P = P_0 \left[\frac{V}{V_0}\right]^a \left(1 + K_{pf}\Delta f\right) \tag{II.15}$$

$$Q = Q_0 \left[\frac{V}{V_0}\right]^a \left(1 + K_{qf}\Delta f\right) \tag{II.16}$$

Or

$$P = P_0 \left[p_1 \left[\frac{V}{V_0}\right]^2_1 + p_2 \left[\frac{V}{V_0}\right] + p_3 \right] \left(1 + K_{pf}\Delta f\right) \tag{II.17}$$

$$Q = Q_0 \left[q_1 \left[\frac{V}{V_0}\right]^2_1 + q_2 \left[\frac{V}{V_0}\right] + q_3 \right] \left(1 + K_{qf}\Delta f\right) \tag{II.18}$$

Where

Δf = the variation deviation $(f - f_0)$

K_{pf} = dampening coefficient for real power frequency

K_{qf} = damping coefficient for reactive power frequency

The following is a complete static load model that can accommodate several types of load expression.

$$P = P_0(P_{ZIP} + P_{EX1} + P_{EX2}) \tag{II.19}$$

Where

$$P_{ZIP} = p_1 \left[\frac{V}{V_0}\right]^2 + p_2 \left[\frac{V}{V_0}\right] + p_3$$

$$P_{EX1} = P_4 \left[\frac{V}{V_0}\right]^{a1} \left(1 + K_{pf1}\Delta f\right)$$

$$P_{EX2} = P_4 \left[\frac{V}{V_0}\right]^{a2} \left(1 + K_{pf2}\Delta f\right)$$

The expression of the reactive component of the load has a similar structure.

2 - Dynamic load models

Most composite loads have a rapid response to voltage and frequency changes, and their responses stabilise quickly. This holds true for voltage/frequency changes of even a relatively small amplitude. Nonetheless, there are numerous scenarios where considering the dynamic nature of the load component is essential. Investigations of inter-area oscillations, voltage stability, and long-term stability sometimes include modelling of load dynamics. For a comprehensive understanding of a system with many motors, it is necessary to model the load dynamics [55]

II.4 Power Flow Analysis (Load Flow Analysis)

The goal of power flow study is to offer a detailed overview of the operational status of a whole power system, which can range in scale from a single city to many states. This system involves of multiple power generations, transmission lines, and end-use consumers. Power flow analysis is a technique for determining unknown numbers from known ones, most commonly the amount of generated and consumed of power at various locations. The voltages at various points in the transmission system are the most crucial of these measurements; voltage for alternating current (a.c.) consists of two parts: the magnitude and the time element or phase angle. The currents in each transmission connection may be computed with ease once the voltages are known. Consequently, the term "power flow," often known as "load flow" in the industry, describes the process by which power is sent from its source to its final consumer. [64]. The issue, "What is the current operational condition of the system given certain known quantities?" is addressed through power flow analysis. For this purpose, it employs the iterative approximation algorithm, which performs calculations repeatedly until an acceptable result is found. Planning, economic programming, and management of an existing system, as well as its expansion, necessitate knowledge of the power flow[58].

The power flow problem is solved by assuming that the system is in a balanced state and use a single-phase model. Every bus can be mapped to one of four different metrics. These are the voltage's absolute value V, its phase angle, its real power P, and its reactive power Q. There are typically three distinct varieties of system buses:[65]

- Slack bus, also known as swing bus, It is utilized as a reference when the voltage's magnitude and phase angle are provided. This bus recompense for the discrepancy between planned loads and produced power caused by network losses.

- Load bus, The active and reactive powers are indicated at these bus. Unknown are the magnitude and phase angle of the bus voltages. These are known as P-Q buses.

- Regulated bus or generator buses or voltage-controlled buses. These buses specify real power and voltage. Calculate the phase angles of voltages and reactive power. Reactive power restrictions are gives. These are identified as P-V buses.

II.4.1 Power flow equations and solution methods

Figure (II.11) depicts a basic bus of an electrical system.
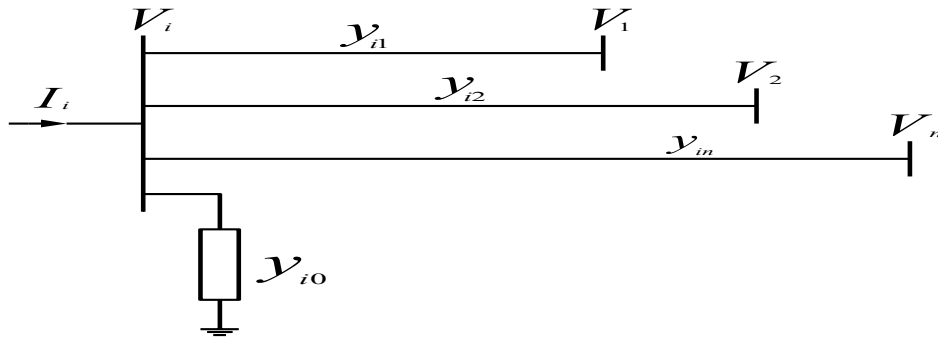
Figure II. 11: A representative the power system bus [66]

When applied to a common MVA base, impedance conversion to per-unit admittance yields the corresponding models for transmission lines. When KCL is applied to this bus, the result is

$$I_i = V_i \sum_{j=0}^{n} y_{ij} - \sum_{j=1}^{n} y_{ij} V_j \qquad\qquad j \neq i \qquad\qquad (II.20)$$

Where

V_i = bus i voltage

I_i = bus i current

V_j = bus j voltage.

y_{ij} = admissions per unit between buses I and j.

The active and reactive power at bus i is

$$P_i + jQ_i = V_i I_i^* \qquad\qquad\qquad (II.21)$$

$$I_i = \frac{P_i - jQ_i}{V_i^*} \qquad\qquad\qquad (II.22)$$

In the equation (II.22), the result of substituting Ii is

$$\frac{P_i - jQ_i}{V_i^*} = V_i \sum_{j=0}^{n} y_{ij} - \sum_{j=1}^{n} y_{ij} V_j \qquad j \neq i \qquad\qquad (II.23)$$

Iterative methods are required in order to solve the algebraic nonlinear equations that are produced as a result of the mathematical formulation of the power flow problem, which is determined by the relation described above [66].

II.4.1.1 Gauss-seidel solution method

In order to achieve a power analysis, you need to solve the set of nonlinear equations described by (II.23) for two unknown parameters at each node. Once that is done, the equation (II.23) can be solved for, and the iterative sequence may be written as [67]

$$V_i^{(k+1)} = \frac{\frac{P_i^{sch} - jQ_i^{sch}}{V_i^{(k)}} + \sum y_{ij} V_j^{(k)}}{\sum y_{ij}} \qquad j \neq i \tag{II.24}$$

Where

P_i^{sch} and Q_i^{sch} are the net real and reactive powers expressed in per unit

Y_{ij} is actual admittance in per unit

If (II.23) is solved for P_i and Q_i we have

$$P_i^{(k+1)} = R\left\{V_i^{*\ (k)}\left[V_i^{(k)} \sum_{j=0}^{n} y_{1j} - \sum_{j=1}^{n} y_{ij} V_j^{(k)}\right]\right\} \qquad j \neq i \tag{II.25}$$

$$Q_i^{(k+1)} = -\text{Im}\left\{V_i^{*(k)}\left\{V_i^{(k)} \sum_{j=0}^{n} y_{ij} - \sum_{j=1}^{n} y_{ij} V_j^{(k)}\right]\right\} \qquad j \neq i \tag{II.26}$$

The equation that describes the flow of power is typically written in terms of the components of the bus admittance matrix. As a result of the fact that the off-diagonal elements of the bus admission matrix Y bus are represented in capital letters, are $Y_{ij} = -y_{ij}$, and the diagonal elements are $Y_{ii} = \sum y_{ij}$, equation (II.24) become

$$V_i^{(k+1)} = \frac{\frac{P_i^{sch} - jQ_i^{xch}}{V_i^{(k)}} - \sum_{j \neq i} Y_{ij} V_j^{(k)}}{Y_i} \tag{II.27}$$

And

$$P_i^{(k+1)} = R\left\{V_i^{*(k)}\left[V_i^{(k)} Y_{ii} + \sum_{\substack{j=1 \\ j \neq i}}^{n} Y_{ij} V_j^{(k)}\right]\right\} \qquad j \neq i \tag{II.28}$$

And

$$Q_i^{(k+1)} = -\text{Im}\left\{V_i^{(k)}\left[V_i^{(k)} Y_{ii} + \sum_{\substack{j=1 \\ j \neq i}}^{n} Y_{ij} V_j^{(k)}\right]\right\} \qquad j \neq i \tag{II.29}$$

Y_{ii} contains the admittance to ground of line charging susceptance and any other fixed admittance to ground. for the Gauss-Seidel technique, an primary voltage estimation of 1.0 + j0.0 for unknown voltages is acceptable, and the converged solution correlates with the actual operating states.

For P-Q buses, the active and reactive powers P_i^{sch} and Q_i^{sch} are known. Beginning with an preliminary estimate, (II.24) is solved for the real and imaginary parts of voltage. For the voltage-controlled buses (P-V buses) where P_i^{sch} and $|V_i|$ are definite, first (II.26) is solved for $Q_i^{(k+1)}$, and then is used in (II-27) to solve for V_i^{k+1} . Nevertheless, since $|V_i|$ is explained, only the imaginary part of V_i^{k+1} is preserved, and the actual part of it that will be used is chosen so as to

$$\left(e_i^{k+1}\right)^2 = \sqrt{V_i^{\ 2} - f_i^{\ k+1^2}}$$

Where e_i^{k+1} and f_i^{k+1} are the voltage's real and imaginary componentsV_i^{k+1}

- **losses and flows in Line:**

After bus voltage iteration, flows in line and losses are calculated. The line between buses I and j in Figure (II.12) [68] [69].
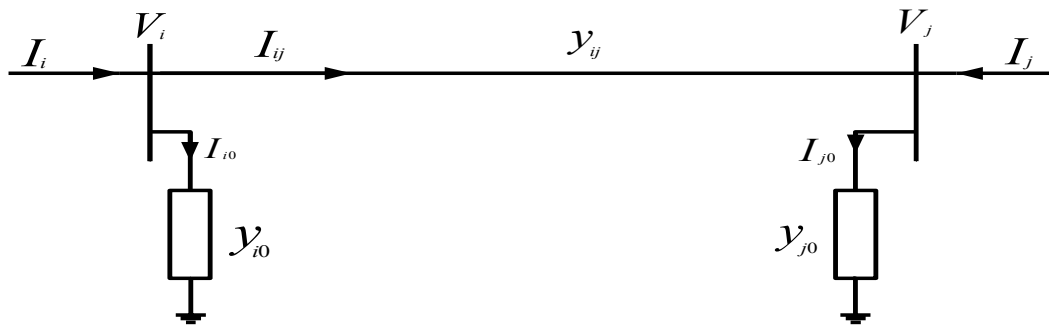
Figure II. 12: Model for determining line flows in transmission lines [68]

The current I_i measured at bus i is given by

$$I_i = I_{ij} + I_{i0} = y_{ij}(V_i - V_j) + y_{i0}V_i \tag{II.30}$$

Similarly, the current I_j measured at bus j is given by

$$I_j = -I_{ij} + I_{j0} = y_{ij}(V_j - V_i) + y_{j0}V_j \tag{II.31}$$

The complex powers S_{ij} from bus i to j and S_{ji} from bus j to i are:

$$S_{ij} = V_i I_{ij}^* \tag{II.32}$$

$$S_{ji} = V_j I_{ji}^* \tag{II.33}$$

The algebraic sum of (II.32) and (II.33) power flows is the power loss in line I ~ j.

$$S_{lij} = S_{ij} + S_{ji} \tag{II.34}$$

II.4.1.2 Newton-Raphson solution method

Newton's approach is more advanced mathematically than the Gauss-Seidel method, and it is less likely to diverge when used to ill-conditioned situations thanks to its quadratic convergence. For dealing with big power systems, the Newton-Raphson approach tends to be

more effective and convenient. Even if more functional evaluations are needed at each iteration, the total number of iterations needed to find a solution is unaffected by the complexity of the system. The power flow equation is written in polar form because in the power flow problem, the real power and voltage magnitude of the voltage-controlled buses are stated. For the bus in figure (II.11), the current entering bus i is given by (II-20). This equation can be rewritten in terms of the bus admittance matrix as [70].

$$I_i = \sum_{j=1}^{n} Y_{ij} V_j \tag{II.34}$$

This equation can be written in polar form as

$$I_i = \sum_{j=1}^{n} |Y_{ij}||V_j| < \theta_{ij} + \delta_j \tag{II.35}$$

The complex power at bus i is

$$P_i - jQ_i = V_i^* I_i \tag{II.36}$$

Substituting from (II.35) for I_i in (II.36),

$$P_i - jQ_i = |V_i| \angle - \delta_i \sum_{j=1}^{n} |Y_{ij}||V_j| \angle \theta_{ij} + \delta_j \tag{II.37}$$

Extrication the real and imaginary parts,

$$P_i = \sum_{j=1}^{n} |V_i||V_j||Y_{ij}| \cos(\theta_{ij} - \delta_i + \delta_j) \tag{II.38}$$

$$Q_i = -\sum_{j=1}^{n} |V_i||V_j||Y_{ij}| \sin(\theta_{ij} - \delta_i + \delta_j) \tag{II.39}$$

The variable, voltage magnitude in per unit and phase angle in radians, are nonlinear algebraic equations (II.38 and II.39). Each load bus has two equations, II.38 and II.39, and each voltage-controlled bus has one (II.39). Extending (II.38) and (II.39) in Taylor's series about the original estimate and ignoring higher order terms provides the following matrix-form linear equations.

$$
\begin{bmatrix} \Delta P_2^{(k)} \\ \vdots \\ \Delta P_n^{(k)} \\ \Delta Q_2^{(K)} \\ \vdots \\ \Delta Q_n^{(k)} \end{bmatrix}
=
\begin{bmatrix}
\frac{\partial P_2^{(k)}}{\partial \delta_2} & \cdots & \frac{\partial P_2^{(k)}}{\partial \delta_n} & \frac{\partial P_2^{(k)}}{\partial |V_2|} & \cdots & \frac{\partial P_2^{(k)}}{\partial |V_n|} \\
\vdots & \ddots & \vdots & \vdots & \ddots & \vdots \\
\frac{\partial P_n^{(k)}}{\partial \delta_2} & \cdots & \frac{\partial P_n^{(k)}}{\partial \delta_n} & \frac{\partial P_n^{(k)}}{\partial |V_2|} & \cdots & \frac{\partial P_n^{(k)}}{\partial |V_n|} \\
\frac{\partial Q_2^{(K)}}{\partial \delta_2} & \cdots & \frac{\partial Q_2^{(K)}}{\partial \delta_n} & \frac{\partial Q_2^{(K)}}{\partial |V_2|} & \cdots & \frac{\partial Q_2^{(K)}}{\partial |V_n|} \\
\vdots & \ddots & \vdots & \vdots & \ddots & \vdots \\
\frac{\partial Q_n^{(K)}}{\partial \delta_2} & \cdots & \frac{\partial Q_n^{(K)}}{\partial \delta_n} & \frac{\partial Q_n^{(K)}}{\partial |V_2|} & \cdots & \frac{\partial Q_n^{(K)}}{\partial |V_n|}
\end{bmatrix}
\begin{bmatrix} \Delta \delta_2^{(k)} \\ \vdots \\ \Delta \delta_n^{(k)} \\ \Delta V_2^{(K)} \\ \vdots \\ \Delta V_n^{(k)} \end{bmatrix}
\tag{II.40}
$$

Elements of the Jacobian matrix (linear equations in matrix form) are the partial derivatives of (II.38) and (II.39), evaluated at $\Delta \delta_i^k$ and ΔV_i^k. In short form, it can be written as

$$\begin{bmatrix} \Delta P \\ \Delta Q \end{bmatrix} = \begin{bmatrix} J_1 & J_2 \\ J_3 & J_4 \end{bmatrix} \begin{bmatrix} \Delta \delta \\ |V| \end{bmatrix} \tag{II.41}$$

The diagonal and the off-diagonal elements of J_1 are

$$\frac{\partial P_i}{\partial \delta_i} = \sum_{j \neq i} |V_i||V_j||Y_{ij}| \sin\left(\theta_{ij} - \delta_i + \delta_j\right) \tag{II.42}$$

$$\frac{\partial P_i}{\partial \delta_j} = -|V_i||V_j||Y_{ij}| \sin\left(\theta_{ij} - \delta_i + \delta_j\right) \qquad j \neq i \tag{II.43}$$

The diagonal and the off-diagonal elements of J_2 are

$$\frac{\partial P_i}{\partial |V_i|} = 2|V_i||Y_{ii}|\cos\theta_{ii} + \sum_{j \neq i} |V_j||Y_{ij}|\cos\left(\theta_{ij} - \delta_i + \delta_j\right) \tag{II.44}$$

$$\frac{\partial P_i}{\partial |V_j|} = |V_i \parallel Y_{ij}| \cos(\theta_{ij} - \delta_i + \delta_j) \qquad j \neq i \tag{II.45}$$

The diagonal and the off-diagonal dement of J_3 are

$$\frac{\partial Q_i}{\partial \delta_i} = \sum_{j \neq i} |V_i||V_j||Y_{ij}|\cos\left(\theta_{ij} - \delta_i + \delta_j\right) \tag{II.46}$$

$$\frac{\partial Q_i}{\partial \delta_j} = -|V_i||V_j||Y_{ij}|\cos\left(\theta_{ij} - \delta_i + \delta_j\right) \qquad j \neq i \tag{II.47}$$

The diagonal and the off-diagonal elements of J_4 are

$$\frac{\partial Q_i}{\partial |V_i|} = -2|V_i||Y_{ii}|\sin\theta_{ii} - \sum_{j \neq i} |V_j||Y_{ij}|\sin\left(\theta_{ij} - \delta_i + \delta_j\right) \tag{II.48}$$

$$\frac{\partial Q_i}{\partial |V_j|} = -|V_i||Y_{ij}|\sin\left(\theta_{ij} - \delta_i + \delta_j\right) \qquad j \neq i \tag{II.49}$$

The terms ΔP_i^k. And ΔQ_i^k is power residuals, defined as the discrepancy between planned and actual levels,

$$\Delta P_i^{(k)} = P_i^{sch} - P_i^{(k)} \tag{II.50}$$

$$\Delta Q_i^{(k)} = Q_i^{sch} - Q_i^{(k)} \tag{II.51}$$

The revised bus voltage estimations are

$$\delta_i^{(k+1)} = \delta_i^{(k)} + \Delta\delta_i^{(k)} \tag{II.52}$$

$$V_i^{(k+1)} = \left|V_i^{(k)}\right| + \Delta\left|V_i^{(k)}\right| \tag{II-53}$$

II.4.1.3 Fast decoupled solution method

Transmission lines in the power grid typically have a high X/R ratio. Changes in real power P are less sensitive to shifts in voltage magnitude and more responsive to shifts in phase angle for such a system. Similar to how reactive power is less affected by variations in angle and more dependent on changes in magnitude of voltage, a voltage's reactive power will increase or decrease accordingly. As a result, it makes sense to zero off the elements J_2, and J_3 of the Jacobin matrix, changing (II.41) to : [71]

$$\begin{bmatrix} \Delta P \\ \Delta Q \end{bmatrix} = \begin{bmatrix} J_1 & 0 \\ 0 & J_4 \end{bmatrix} \begin{bmatrix} \Delta \delta \\ |V| \end{bmatrix}$$ (II.54)

The diagonal elements of J_1 described by (II.42) may be written as

$$\frac{\partial P_i}{\partial \delta_i} = \sum_{j=1}^n |V_i||V_j||Y_{ij}|\sin\left(\theta_{ij} - \delta_i + \delta_j\right) - |V_i|^2 |Y_{ii}|\sin \theta_{ii}$$ (II.55)

Putting in (11.39) for Q_i in place of the first term in the previous equation yields

$$\frac{\partial P_i}{\partial \delta_i} = -Q_i - |V_i|^2 |Y_{ii}|\sin \theta_{ii}$$ (II.56)

$$\frac{\partial P_i}{\partial \delta_i} = -Q_i - |V_i|^2 B_{ii}$$ (II.57)

Where $B_{ii} = Y_{ii}\sin \theta_{ii}$ is the imaginary part of the diagonal elements of the bus admittance matrix. B_{ii} is the sum of susceptances of all the elements incident bus i. Simplification is obtained by assuming $|V_i|^2 \approx |V_i|$ and $B_{ii} \gg Q_i$ which yields

$$\frac{\partial P_i}{\partial \delta_i} = -|V_i|B_{ii}$$ (II.58)

In a typical working environment, $\delta_i - \delta_j$ is negligible. Then, the off-diagonal elements of J_1 in (11.43) under the assumption of $(\theta_{ij} - \delta_i + \delta_j \simeq \theta_{ii})$ becomes

$$\frac{\partial P_i}{\partial \delta_j} = -|V_i||V_j|B_{ij}$$ (II.59)

Further simplification is obtained by assuming $|V_j| \approx 1$

$$\frac{\partial P_i}{\partial \delta_j} = -|V_i|B_{ij}$$ (II.60)

Likewise, J_4's diagonal elements can be expressed as

$$\frac{\partial Q_i}{\partial |V_i|} = -|V_i||Y_{ii}|\sin \theta_{ii} - \sum_{j=1}^n |V_i||V_j||Y_{ij}|\sin\left(\theta_{ij} - \delta_i + \delta_j\right)$$ (II.61)

Putting the second term of the previous equation with $-Q$ i (11.39), yields

$$\frac{\partial Q_i}{\partial |V_i|} = -|V_i||Y_{ii}|\sin \theta_{ii} + Q_i$$

Again, since $B_{ii} = Y_{ii}\sin \theta_{ii} \gg Q_i, Q_i$ may be neglected

$$\frac{\partial Q_i}{\partial |V_i|} = -|V_i|B_{ii}$$ (II.62)

Similarly, in (II.49), supposing $\theta_{ij} - \delta_i + \delta_j \approx \theta_{ij}$ yields

$$\frac{\partial Q_i}{\partial |V_j|} = -|V_i|B_{ij}$$ (II.63)

From equation (II.53)

$$\Delta P = J_1 \Delta \delta = \left[\frac{\partial P}{\partial \delta}\right]\Delta \delta$$ (II.64)

$$\Delta Q = J_4 \Delta |V| = \left[\frac{\partial Q}{\partial |V|}\right]\Delta |V|$$ (II.65)

Equations (II.64) and (II.65) can take the following form

$$\frac{\Delta P}{|V_i|} = -B'\Delta\delta \tag{II.66}$$

$$\frac{\Delta Q}{|V_i|} = -B''\Delta|V| \tag{II.67}$$

Here, B' and B'' are the imaginary part of the bus admittance matrix Y_{bus}.

Now, the voltage magnitude and phase angle changes are

$$\Delta\delta = -\{B'\}^{-1}\frac{\Delta P}{|V|} \tag{II.68}$$

$$\Delta|V| = -[B'']^{-1}\frac{\Delta Q}{|V|} \tag{II.69}$$

It takes more iterations than the Newton-Raphson approach to find a solution for fast decoupled power flow. however, each iteration takes far less time than before. Thus, the answer to the flow problem is discovered quickly.

II.4.2 Importance of load flow analysis in power system

When looking at issues with the operation and planning of a power system, load flow analysis is the most crucial and vital method to use. The stable operation state, including node voltages and branch power flow, is solved using load flow analysis based on a defined generating state and arrangement of the transmission network. In the absence of considering the power system's transient processes, load flow analysis can result in a stable, steady operation situation [72].

A steady-state power flow analysis is the recommended technique for calculating bus voltages, phase angles, and active and reactive power flows along branches, generators, transformer, and loads. An electric circuit including generating, transmission, and distribution networks represents the power system. The non-linear power flow equations must be solved iteratively and quantitatively. Numerical approaches solve mathematical problems using arithmetic operations and provide an estimated answer. Manual computations can estimate operating parameters of small circuits, but load flows and short circuit evaluations require computer systems. Electrical power systems need load flow analysis for the following reasons: [73]

➢ We could measure bus voltages and angles in a steady condition. It's crucial because bus voltage magnitudes must be kept within a range. The load flow may estimate the active and reactive power flow over each line once the magnitudes and angles of the bus voltages are calculated.

➢ Line losses can be determined by measuring the power flowing from source to user.

➢ It is essential. to obtain a load flow of a power system in order to ascertain the most efficient mode of operation for the existing system and to plan for the extension of the present system in the future.

➢ It's useful for planning a new power grid.

➢ It contributes to the decrease of power losses and assists in the choosing transformer taps for efficient and economical operation.

➢ Researchers are able to detect both over and under load concerns based on the line flow data.

II.5 Power-Transfer Characteristic

On the basis of the two-machine system model presented in Figure II.4, an analysis of the transmission features of the transmission system is carried out. The fundamental Figure II.4 depicts a model for determining active and reactive power transmission. It is assumed that the voltages at both the transmitting and receiving ends are fixed. These values can be viewed as locations in big systems where voltages are stable or reliable. The equivalent reactance connects the transmitting and receiving ends of the circuit. Active and reactive power delivered by a transmission line is principally dependent on voltage amplitude and phase angle at both ends [74, 75].

(a)

(b)
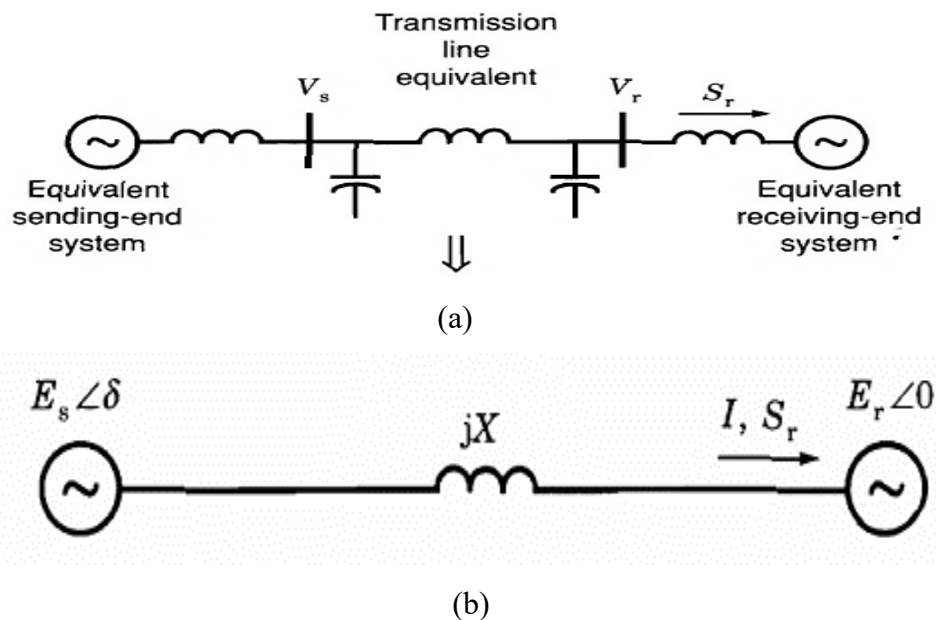
Figure II. 13: Elementary model for transmission of active and reactive power (a) one-line diagram (b) equivalent circuit [74]

The relations can be easily calculated:[74]

$$\bar{S}_r = P_r + jQ_r = \bar{E}_r I^*$$

$$= E_r \left[\frac{E_s \cos \delta + jE_s \sin \delta - E_r}{jX} \right]^*$$

$$= \frac{E_s E_r}{X} \sin \delta + j \left[\frac{E_s E_r \cos \delta - E_r^2}{X} \right]$$

$$P_r = \frac{E_s E_r}{X} \sin \delta = P_{max} \sin \delta \tag{II.70}$$

$$Q_r = \frac{E_s E_r \cos \delta - E_r^2}{X} \tag{II.71}$$

As for the sender's side:

$$P_s = \frac{E_s E_r}{X} \sin \delta = P_{max} \sin \delta \tag{II.72}$$

$$Q_s = \frac{E_s^2 - E_s E_r \cos \delta}{X} \tag{II.73}$$

Maximum power transfer occurs at a power or load angle of 90 degrees, therefore the standard formulae for P s and P r hold true. The power-angle curve, depicted in FigureII.14, is a plot of the two equations (II.70) and (II.72).
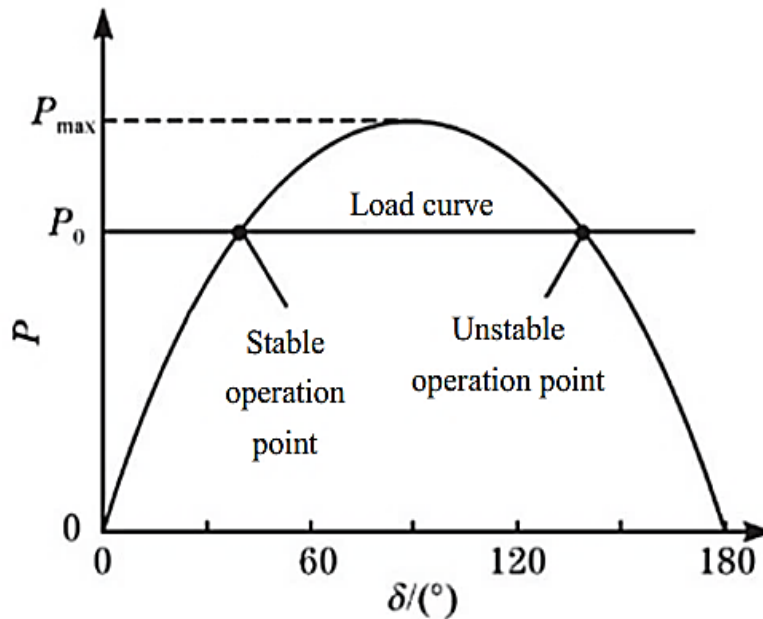
Figure II. 14: Power angle curve [74]

Figure II.14 shows two positions where the mechanical power curve and the electromagnetic power curve intersect: the stable operating point on the left and the unstable operating point on the right. A large receiving-end system, for instance, can be modelled as an infinite bus with a constant phase angle of voltage and speed. If the mechanical power at the transmitting end is increased, the generator's speed and rotor angle will increase. With respect to the right-hand

operating point in Fig. II.14, increasing the rotor angle decreases the electromagnetic power, which causes the generator speed to keep going up and the rotor angle to keep going up. At the left-hand operational position, the electromagnetic power will rise in step with the rotor angle, until the two are equal. Rotor angle has a crucial role in the transmission active power [74] [75].

The magnitudes of the voltages are usually what piques our interest. Our focus here is on the reactive power that can be conveyed through a transmission line or a transformer when the voltage at the load end drops suddenly or drastically due to an outage or collapse. Referring to the reactive power flow across the transmission line is now taken into account in Figure II.13, and Equations II.71 and II.73 are rewritten in terms of V s and V r. In addition, X now just stands for the transmission line reactance [75].

$$Q_r = \frac{V_s V_r \cos\theta - V_r^2}{X} \tag{II.74}$$

$$Q_s = \frac{V_s^2 - V_s V_r \cos\theta}{X} \tag{II.75}$$

When there is only a little phase angle variation between the beginning and finish of the line., $\cos\theta \equiv 1$: Hence, the following approximation is provided:

$$Q_r = \frac{V_r(V_s - V_r)}{X} \tag{II.76}$$

$$Q_s = \frac{V_s(V_s - V_r)}{X} \tag{II.77}$$

From Equations II.76 and II.77, We argue that the magnitude and direction of the flow of voltage from high to low are the most important factors in reactive power transfer. Moreover:

- P and δ are tied closely

- Q and V are tied closely

II.6 Power System Losses Review

While losses do occur at all stages (from generation to transmission to distribution to consumption to metering), they are typically more severe at the distribution stage. Electricity costs are rising because distribution losses raise utilities' operational expenses. Customer energy price increases are influenced by how regulators account for losses in the tariff [76]. The electric utility, its customers, and the country in which the company is operated all stand to benefit economically, financially, and socially from a reduction in losses. Losses can have negative and variable levels of financial repercussions on both the customers and the utility, and these effects can vary depending on the regulatory system [77].

There are two categories of electrical power losses that influence energy utilities: I- technical losses, and II- non-technical losses. Figure II.15 illustrates types of losses in electrical network. Total power losses are demarcated as the difference between the amount of electricity delivered and the amount of electricity sold to customers. By default, the amount of electrical energy created and consumed should be equal. In fact, however, the situation is different because losses are a natural consequence of energy transmission and distribution [78].

Considering the primary components of a typical power grid. Table II.1 displays the typical power losses at several levels during ordinary operating circumstances.

Table II. 1: Average percentage of power losses at various steps

component	average percentage
Step up transformer from generator to transmission line:	1-2 %
Transmission line	2-4 %
Step down transformer from transmission line to distribution network	1-2 %
Lines and transformers of distribution network	4-6 %

Total losses typically fall between 7% and 10% in wealthy countries, but hover between 30% and 50% in some African countries. The "optimal" range of system losses differs from system to system. Utilities with the lowest total system losses in the area typically fall below 20%. In poor countries, system losses continue to be a major problem, preventing most of the generated electricity from reaching its target places [76] [79] .
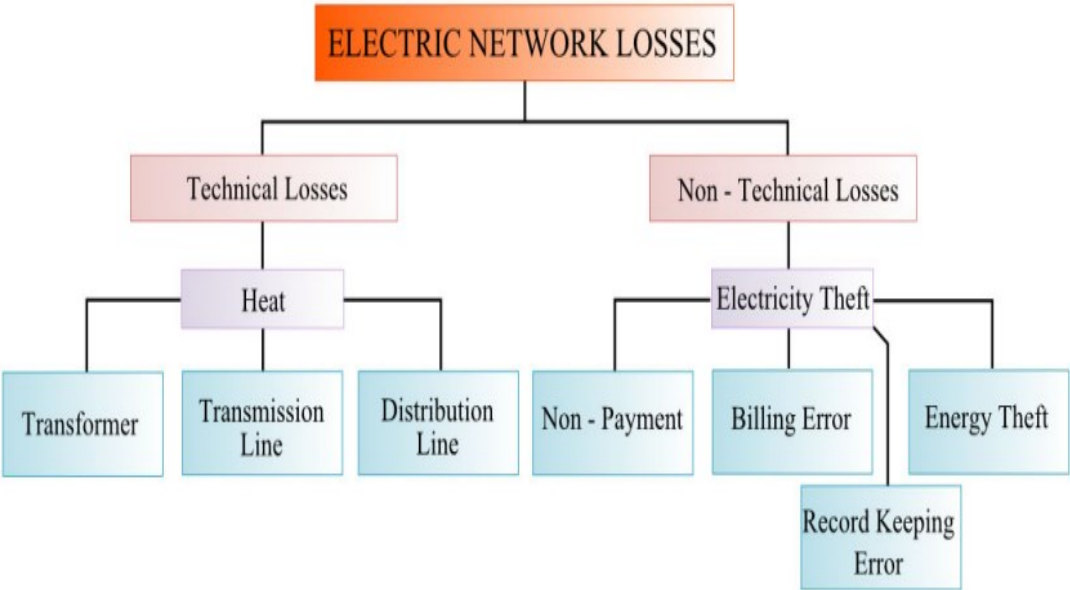
Figure II. 15: Types of electrical losses in power system [80]

II.6.1 Technical losses

Technical losses in power systems are losses that occur obviously because of actions inside the power system and are mostly generated as a result of power being lost in various components of an electrical system, such as transmission lines and power transformers, and monitoring devices. Technical losses might include substation, transformer, and line losses. Power squandered in lines and transformers owing to internal electrical resistance are two of the most prevalent instances of technical losses [81, 82].

The resistance, reactance, capacitance, voltage, and current of the power system are taken into account while calculating these losses. These are the natural features of the components that make up the power system. Loads are not counted as part of the technical losses because it is the objective of the system to supply them with the maximum amount of energy. Technical losses cover resistive primary losses, distribution transformer losses (winding and core losses), secondary networks, service drops, and metering. The load flow of a power system will determine technical losses [83].

The following are the most likely reasons for technical losses:

a- Unbalance load

b- Losses due to over loading and low voltage.

c- Losses incurred as a result of subpar equipment standards.

d- Lines that only use one phase that are several miles in length.

e- Improper earthing at consumer end.

f- Giving new connections without adequate reinforcement

II.6.2 Non-technical losses

In power systems, losses that are not due to technical issues are referred to as "non-technical losses" (NTLs). In addition to events outside of the power system, the loads and conditions that aren't accounted for in technical losses estimations also contribute to NTLs. NTLs can involve a variety of methods of purposeful interaction with customers and are thus related to customer management. NTLs can be thought of as undiscovered loads; customers' that the utilities are unaware of. Most NTLs are associated with power theft in one form or another[83].

Measuring NTLs is trickier since system operators generally don't account for them, hence there is little to no historical data available. Theft of electricity and malfunctioning components are two significant causes of NTLs. Seldom do equipment failures result in NTLs, but when they do, it could be due to anything from a lightning strike to simple carelessness or a lack of preventative maintenance. Failures caused by weather and natural events are taken into account during the selection of equipment and the planning of the distribution network[84].

Distribution firms must prioritise the reduction of NTLs because, despite their prevalence in the low voltage network, their sources are dispersed throughout the entire system and their impact is greatest at lower levels, where it is often used, such as in homes, businesses, and some light industries. Most, if not all, non-technical losses (NTLs) in power networks are thought to be the result of electricity theft and non-payment.

Expected losses in a power system can be calculated with load-flow analysis software given sufficient information about the system's power sources and loads. The actual losses equal the discrepancy between the amount of energy recorded as having left a certain source (say, a substation) and the amount of energy actually consumed by the customer (as indicated on the customer's bill). The level of non-technical losses in the system would be determined by the gap between forecasted and actual losses. In the first place, load flow studies have been used to determine the extent of technical losses [83].

The following are the non-technical losses that are most likely to have been caused by:**[85]**

(i)   Adjusting metres to lower usage.

(ii)   Mistakes in calculating technical losses.

(iii)   Connecting to low-voltage lines by tapping into them.

(iv)   Paying off metre readers to report inflated readings

(v)   Bypassing or illegally connecting to a metre is a kind of theft

(vi)   broken or unmetered electricity metres.

(vii)   Difficulty in obtaining accurate metre readings, which causes invoicing delays and mistakes

(viii) Customer's failure to make payment.

It's possible for utilities to make various kinds of calculations mistakes or have data loss that lead to NTLs, such as unexpected rises in power system losses due to equipment deterioration over time.

II.6.2.1 Electricity theft:

There are many ways in which electricity can be stolen, including metre manipulation, illegal connections, erroneous billing, and nonpayment. The theft rate is rising in most parts of the world, according to the data. Theft has monetary repercussions such as decreased profits from the selling of electricity and the have to increase prices for customers. Theft of electricity is associated with poor governance indices such as liability, government variability, and corruption. Reducing electricity theft requires a combination of technological solutions, such as tamper-proof metres, managerial measures, such as inspection and monitoring, and, in some

situations, a reorganisation of ownership and regulation of power systems. There is no way to completely protect an electrical grid from sabotage [86, 87].

- ➤ **Defining electricity theft**

Theft occurs in four common forms across all power grids. Several factors, including cultural norms and the administration of the power company, will determine the degree of the theft.

(i) Fraud:

When a customer intentionally tries to scam their utility company out of money, this is considered fraud. It is standard practise to tamper with the metre in order to reflect a lower reading of the amount of power being used than is actually being consumed. [86, 88].

(ii) Stealing electricity:

Theft of electricity can be accomplished by wiring a line from the power supply to the location where it is required to bypass the metre. The unlawful lines are generally above ground and very visible, making them simple to spot. Nonetheless, there are stories of personnel being beaten and requiring police protection to remove the lines. The organization's corrupt employees may accept bribes to allow the practise to continue. On a broader scale, firms may bribe power organisation employees to install direct electricity lines to their buildings or offices, bypassing the metre. The bribes can be significantly less than the price of power. Inspectors can also be paid to prevent them from discovering and/or reporting the crime [86] [87].

(iii) Billing irregularities:

Billing errors have several causes. Certain power companies may miscalculate the amount of electricity used. Unintentional abnormalities may even out over time. Certain methods make it simple to get significantly cheaper bills than for the power actually utilised. Workers can be persuaded to record a lesser metre reading. The consumer pays less and the meter-reader gets unofficial remuneration. Office employees can also change the decimal point to the left on a bill to charge $47.48 instead of $474.80. Customers may know that some power company workers are "on-the-take" for delivering these services. Workers can keep payment [86, 87].

(iv) Unpaid bills:

Some companies don't pay their electricity bills. Consumers may have moved or a business may have failed. Some networks have wealthy and politically influential chronic non-payers who know their electricity won't be cut. Government agencies are another chronic non-payer.

When electricity prices rise worldwide, some people struggle to pay their bills. This may promote metre manipulation to lower their expenses. Electricity theft may not include unpaid bills. The issue and its consequences are particularly serious in certain power systems [86] [87].

Electricity theft is estimated, not measured. Power theft is measured by losses in transmission and distribution. The method compares metered and sold electricity to generated electricity (excluding system use and free). The distribution network's non-technical line losses may be mostly theft if technical line losses are accurately calculated.

II.7 Decrease of Technical and Non-technical Losses

Technical losses in distribution system can be reduced by the following improvements: [89, 90]
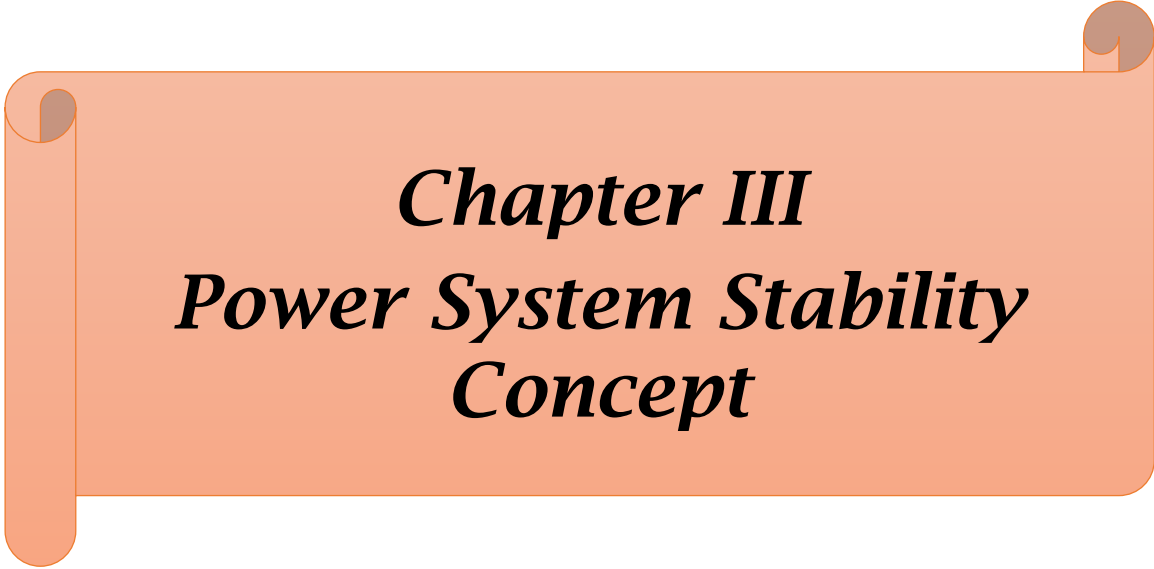
(i)   Conversion of L.T line into 11 kV line and providing additional transformers.

(ii)   Balancing of phase loads.

(iii)   Replace low efficiency transformers.

(iv)   Reduction of the cables, overhead lines and transformers loading.

(v)   Optimized cross section for overhead lines and cables.

(vi)   Adequate preventive maintenance.

(vii)   Use reactive compensation

Non-technical losses can be reduced by the various methods below:[91]

(i)   The following locations were the subject of investigations:

  ➢ the locations where there is no electricity use

  ➢ Completed accounts with unpaid sales taxes

  ➢ regions suspected of having unauthorized connections

(ii)   To ensure accuracy, bulk supply meters are tested as a whole

(iii)   Replacement of Meters (defective, tampered, old, etc).

(iv)   Implementation of seal management system

(v)   Energy consumption is being tracked statistically

(vi)   Electronic metres should be used for all types of consumers

(vii)   Auditing meter readings

II-8 Conclusion

The electrical power system and its fundamental components have both been elucidated in this chapter, as have the techniques that are applied to the problem of determining the flow of power. In addition to that, an explanation was provided for the many forms of power losses that might occur within the power system.

Chapter III
Power System Stability Concept

Chapter III Power System Stability Concept

III.1 Introduction

Because they are the most enormous and dynamic systems that have ever been developed by humans, power grids are considered to be one of the most significant technological achievements of all time. The stability factor is extremely important when taking into consideration the scale and complexity of the electrical system [92]. If no generators or loads trip, the power system can be considered intact. Only generators and loads that were purposefully tripped to maintain system integrity have been cut off. When two or more forces are evenly balanced against one another, the situation is said to be stable. A state of instability exists whenever there is a disruption that leads to an unbalanced relationship between the forces at play [93].

The loads, generator outputs, topology, and important variables of operation of the electric power grid are all in a constant state of change, making the grid a highly nonlinear system. The stability of the system is dependent not only on the initial operating condition, but also on the specifics of the disturbance being introduced. The disruption could be on a small or large scale. The system is subject to constant minor disturbances as a result of the load's fluctuation, yet it can adjust to its ever-changing environment. The viability of the system hinges on whether or not it can continue to operate normally and meet the load requirement in these circumstances. It needs to be able to handle big problems, like a short circuit on a power line or the loss of a main generator. In addition to this, it needs to be able to resist a significant number of disturbances of this kind [94]. If the power system is stable, it will quickly reach a new state of balance after a temporary disruption. Eventually, the system will return to its normal state due to the actions of automatic controllers and possibly human operators. In the event that the power system is not stable, it will never arrive at a condition of equilibrium. This can manifest itself in a number of ways, such as a progressive growth in the angular separation of the generator rotors or a progressive drop in the bus voltages. An unstable system state may result in a chain reaction of power outages and the suspension of operations for a significant component of the power system [93].

The definition of power system stability is the capacity of a power system to return to a state of operating balance following exposure to a physical disturbance with the majority of system variables restricted so that practically the entire system remains uninjured [95]. Depending on the nature and magnitude of disturbances the Power system stability problems studies can be classified in to the following types:

Chapter III Power System Stability Concept

III.1.1 Steady-state stability

The steady-state stability test examines how well a system performs under constant loads and generator outputs. In this case, the transmission line length plays a significant role in respect to the transmitted power [64]. The capability of the power system grid to maintain or remain in balance following a gradual system variation is referred to as steady state stability. Loads can be increased or decreased gradually, such as when additional megawatts (MW) are added at load terminals or when the primary mover's steam is switched out [96].The power system is able to withstand the after-disturbance changes and, as a result, remains in a stable state capable of preserving equilibrium. If a network is subjected to only mild disruptions, then its steady-state stability limit is the greatest amount of power that may be communicated between sources and loads[97].

Synchronous generators must rotate at the same speed and be in phase with one another so that their voltage output peaks at around the same time in order to provide a group of loads with a group of generator power contributions over a set of transmission lines. This is necessary so that all generators can feed power into the network at once; otherwise, they would have to alternate injecting and absorbing power during different parts of the cycle (In actuality, this would result in overloading of sections of the generator windings if somehow the circuit breakers were not initially opened) [97].

III.1.2 Transient stability

The capability of the power system to sustain synchronism in the face of a significant transient disruption, such as a breakdown on transmission lines, the loss of generation, or the loss of a major demand, is what is meant by the term "transient stability.". As a result of these disturbances, the system responds with significant swings in generator rotor angles, power flows, bus voltages, and other parameters [96].The power system's nonlinear properties have an effect on its stability. The machines in the system are considered to be in synchrony if and only if the resulting angular discrepancies between them stay within a narrow range. If synchronization is lost due to temporary instability, it will become noticeable within two to three seconds [97]. After an interruption in the power supply, many machines may be activated in order to restore service. As an example, if a critical element fails and is then isolated by protective relays, the resulting disturbance will cause changes in power flows, bus voltages, and speed rotor; the voltage differences will activate both generator and transmission system voltage controllers; the generator speed changes will activate prime mover governors; and the system loads will be affected by the voltage and frequency fluctuations to different degrees, depending on their specific features [64].

Protective devices usually avoid system instability. These devices safeguard power system components from fault currents, overvoltage, and overspeed. Monitoring system amounts and disconnecting generators, loads, and lines, protective devices identify abnormal system conditions. Protective devices need selectivity, quickness, and dependability to work well. A topology modification often restores power system stability by removing the failed component. Disturbances can change the stable operating point. If the disturbance or protection devices modify the power system's topology, this is the case. Load and generator trips are topological changes. Therefore, a fault that is removed without tripping any elements does not change the power system topology. After the event, the steady state is usually the same[19] . Hence, the primary stability condition in both regimes is that synchronous devices retain synchronism after minor and large perturbations.

III.2 A categorization of the Stability of Power System

The categorization of power system stability concerns based on [55] is the one that has been used most frequently in modern times. The following primary considerations are incorporated into this classification:[98] [95]

- The physical character of the ensuing mode of instability, as evidenced by the principal system variable exhibiting instability.

- The size of the perturbation examined determines the technique of stability computation and prediction.

- The equipment, procedures, and time span that must be considered in order to evaluate stability.

Figure III.1 gives an overview of the different kinds of power system stability by putting them into their own categories and subcategories.
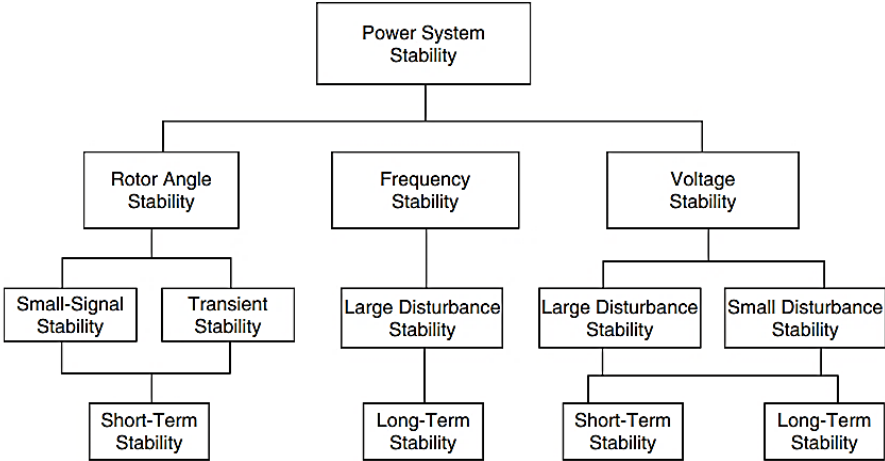
Figure III. 1: A categorization of power systems stability [99]

As a result of the widespread addition of variable forms of renewable energy like solar, system operators must work harder to maintain grid system stability to assure security and reliability and reduce the risk of blackouts. So, it is vital to analyze the grid system's operational reliability to help create methods to reduce the negative consequences of large-scale solar energy generation [92] .

A below is an explanation of each sort of stability phenomenon:

III.2.1 Voltage stability

voltage stability refers to the capacity of the power system to keep the voltage levels at all of its nodes at an appropriate level within ordinary operating circumstances and after it has been subjected to a perturbation. The potential instability that could result manifests itself as a gradual decrease or increase in the voltage across particular buses. Loss of load in the region where voltages achieve values that are inacceptable low or loss of integrity of the power system are both potential outcomes that can result from voltage that is unstable[100]. The next categories can be utilized to classify voltage stability: [74]

- large disturbance voltage stability refers to the condition in which the power system is required to maintain constant voltages after being expelled with a major perturbation such as the loss of a large generator. There are two possible time scales for the phenomenon of voltage stability: long term and short term. As a result, the time duration of this type of analysis might range anywhere from a few seconds to ten in order to accurately record the efficiency of the equipment used in the power system. Therefore, long term dynamic simulations are required for analysis [93]

- The capacity of a power system to maintain consistent voltages after being jolted by a relatively minor disruption, such as shifts in the system's load, is referred to as " Small disturbance voltage stability.". The nature of the fundamental mechanisms that contribute to minor perturbation voltage instability is primarily one that exists in a steady state. As a result, static analysis can be utilized efficiently to ascertain stability margins and recognize factors that influence stability. A requirement for small disturbance voltage stability is that, at a specified operating circumstance for every bus in the system, the bus voltage magnitude must raise in proportion to the increase in the amount of reactive power injection at the same bus. This is one of the conditions that must be met for the system to be considered stable [93].A system is considered to be voltage unstable if, for at least one of the buses in the system, the magnitude of the bus voltage drops when the amount of reactive power injection at the same bus is raised. To

put it another way, a system's voltage is said to be stable if the V-Q sensitivity of each bus in the system is positive, whereas the voltage of the system is said to be unstable if the V-Q sensitivity of at least one bus is negative.It is possible to analyze small perturbation voltage stability by linearizing the equations that describe the power system and taking into account the required calculation assumptions. Nevertheless, it is important to keep in mind that the linearized technique does not take into account non-linear factors such as time delays and tap changer controls [101]. This is something that should be kept in mind at all times. The amount of time needed to complete this investigation is comparable to the amount of time needed to ensure the stability of the voltage during large disturbances.

III.2.2 Frequency stability

The capability of the grid system to maintain frequency levels within permissible limits after being exposed to a perturbation that results in an imbalance between the generation and the load is what is meant by the term "frequency stability." [102]

The idea of frequency stability on the grid is depicted in Figure III.2. If the grid can't keep the balance between generation and load, or if it can't restore it, the result is unstable frequencies. The frequency of the grid is mostly dependent on the spinning speed of classic synchronous generators. These generators can either be sped up or slowed down depending on the load-power balance in order to raise or lower the frequency. As a result, this kinetic energy limits the initial degree to which the frequency drops when there is a power imbalance. This suggests that the conventional generators' inertial response is an essential component in the process of frequency regulation for the grid system [92].

Depending on the nature of the investigation, the time span could range from a few milliseconds to many minutes. Example responses for load voltage regulators take more time, while under frequency load shedding relays take less time [74].
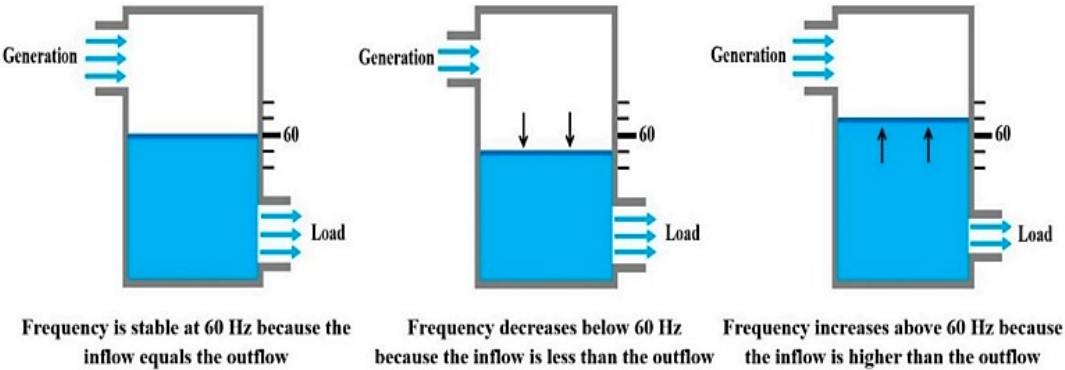
Figure III. 2: A theoretical framework for frequency stability in the grid [92]

III.2.3 Rotor Angle Stability

The ability of the grid's conventionally synchronized generators to keep synchronization in the face of a disturbance is called "rotor angle stability." [103]. In a normal state, all of the conventional generators that are interconnected to the grid are turning at the same speed range. This indicates that there is a equilibrium between the mechanical power input and the electromagnetic output of each conventional generator that is part of the grid. Nevertheless, if there were to be a perturbation, it would cause the classic generators to either speed up or slow down their rotational speed. This would change the angular location between the rotors, which would throw off the equilibrium between the mechanical input and the electromagnetic output [104]. The stability of the rotor angle can be maintained by the grid if the disparity in the angular positions of the rotors is decreased until the synchronized speed level is attained once more. In that case, the rotor angle stability will be lost, which will cause the generator to lose its synchronism with the remaining generators and cause in significant variations in the output of the generator in the form of power, voltage, and current. The phenomena known as rotor angle stability is considered to be of a short-term nature and can be broken down into the next categories[105].

- large disturbance rotor angle stability, is the capability of the power system to retain synchronism in the face of a significant transient disruption, such as a short circuit in a transmission line, is the focus of the concept that is more frequently referred to as transient stability. The basic normal operating condition of the system and the degree to which the disturbance was induced both have a role in determining the transient stability of the system. In studies of transient stability, the time range of interest is often limited to three to five seconds immediately following the disruption. In extremely large systems with strong inter-area swings, this time period could be extended to 10 seconds[105].

- small disturbance rotor angle stability, otherwise known as small signal stability or steady state stability, refers to the ability of a power system to preserve synchronism in the face of relatively minor disturbances such as shifts in the load being carried by the system. This ability is at the heart of the rotor angle stability concept. The power of the system, the initial operational condition of the system, and the sort of generator excitation controls that are employed are all factors that influence the small signal stability [106]

The categorization of stability has been based on a number of different criteria so as to make it suitable for the characterization of the reasons of instability, the application of appropriate

investigation tools, and the advancement of helpful measures that are suitable for a particular stability issue. Given that as systems fail, multiple types of instability may emerge, it is evident that There is some degree of intersection between the various kinds of unstable situations. The most important factor in classifying a system event is the primary initiating phenomena, which can be voltage, rotor angle, or frequency. Although while the categorization of power system stability is a useful and practical way to handle with the intricacies of the issue, it is essential to keep in mind that the whole stability of the system would always be a priority. The solutions to the stability issues faced by one category should not come at the expense of another category. It is imperative to examine not just all forms of the stability phenomenon, but also several perspectives on each individual feature [105].

III.3 Voltage Stability Analysis

Voltage stability difficulties are one of the most significant challenges in power system construction and operation. Voltage stability is defined as a system's ability to maintain adequate voltages at all system points under normal conditions and after a disruption. [55]. Voltage instability, on the other hand, is the inability of a system to maintain adequate voltages in all or some of its nodes when it is working normally and following disruptions such as increasing load rises or failures of crucial lines or producing units. It could also be the result of an imbalance between reactive power generation and demand, which occurs when a power system is unable to produce adequate reactive power [107]. If remedial efforts to prevent voltage instability are not made, a large fall in system voltage occurs due to substantial reactive power losses. Voltage collapse occurs as a result. Voltage collapse is the process by which a set of events caused by voltage instability result in an unacceptably low voltage scenario for a significant percentage of a power system network [107] [108]. In the last 20 years, voltage breakdown has become one of the biggest worries in the power industry, as it has been the main cause of many major blackouts around the world. As a consequence, for numerous systems, voltage stability assessment and prediction of voltage collapse or instability have become critical types of evaluation performed as part of system planning and operation. [109].

For analytical objectives, static or dynamic analysis could be utilized for the purpose of assessing voltage stability. The foundation of dynamic voltage stability is a set of differential equations that analyse the variation of bus voltages in response to changes in system operating parameters. Among the many methods that can be used to investigate dynamic voltage stability are bifurcation analysis, small signal stability analysis, time domain simulations, and the energy function method. Static voltage stability uses power flow equations to figure out why voltage

drops and how to stop them in many different situations. This method, needing less processing time, collects nearly all of the information needed to ensure the voltage stability of the system. [110].

Figure III.3 presents a straightforward example of a two-bus system, which can be used to illustrate the fundamental idea of voltage stability. The load is a type that uses a constant power. The real transfer of power from bus 1 to bus 2 is provided by

$$P = \frac{V_1 V_2}{X} sin \; \delta = P_{max} sin \; \delta \tag{III.1}$$

Transfer of reactive power from bus 1 to bus 2 is described by,

$$Q = -\frac{V_2^2}{X} + \frac{V_1 V_2}{X} cos \; \delta \tag{III.2}$$
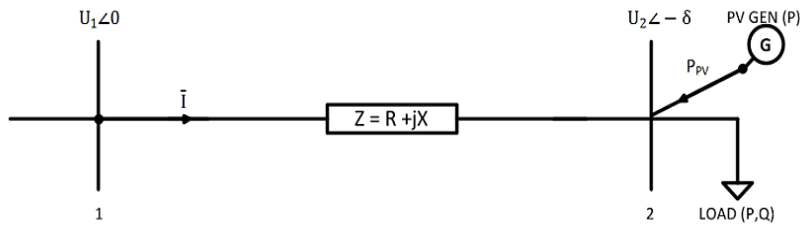
Figure III. 3: 2-bus test system [11]

According to equation (III.1) and (III.2), Both the active power and the reactive power are determined by the voltages at buses 1 and 2, the load angle (δ) and reactance (X).

From Equations III.1and III.2

$$sin \; \delta = \frac{PX}{V_1 V_2} \tag{III.3}$$

$$cos \; \delta = \frac{(QX + V_2^2)}{V_1 V_2} \tag{III.4}$$

We know: $sin^2 \; a + cos^2 \; b = 1$ $\tag{III.5}$

Use Eqs (III.5) to combine Eqs (III.3) and (III.4) into

$$\left(\frac{PX}{V_1 V_2}\right)^2 + \left(\frac{(QX + V_2^2)}{V_1 V_2}\right)^2 = 1 \tag{III.6}$$

The described in the previous expression is capable of being rewritten in the following:

$$\frac{V_2^4}{V_1^4} + \frac{V_2^2}{V_1^4}\left(2QX - V_1^2\right) + \frac{X^2}{V_1^4}\left(P^2 + Q^2\right) = 0 \tag{III.7}$$

It is possible to obtain the equations for the PV and QV curves for the two terminal grid using equation (III.7) as a starting point. When displayed, the equations that will be generated will explain how the voltage at bus 2 behaves in response to deviations in the load's active and reactive power. A formula for the voltage at bus 2 can be calculated by utilizing equation (III.7), and that expression is represented by equation (III.8). The equation illustrates how the voltage

at bus 2 is dependent on the voltage at the transmitting end of the line, the line reactance, as well as the active and reactive power of the load at bus 2 [11, 111].

$$V = \sqrt{\left(\frac{V_1^2}{2} - QX \pm \sqrt{\left(\frac{V_1^4}{4} - X^2 P^2 - X V_1^2 Q\right)}\right)} \qquad (III.8)$$

The PV curve for bus 2 can be determined by ensuring that the reactive power at the load remains unchanged despite shifts in the voltage and the active power. In a similar manner, a Q-U curve can be plotted by altering the reactive power and voltage while maintaining the load power at a constant level. The PV curve illustrates how much the voltage at bus 2 will vary depending on the magnitude of the power while assuming that Q will remain unchanged. The QV curve illustrates the amount of reactive power assistance that must be supplied in order to maintain a specific operating voltage while ensuring that the load is kept constant (P is constant). Both the PV curve and the QV curve for the two-port grid are depicted in Figure III.4 and Figure III.5, respectively, depending on the active power value[11, 112].
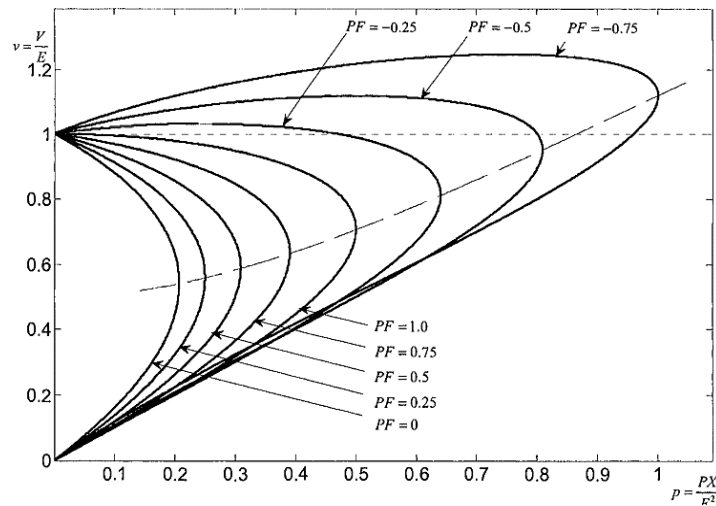
Figure III. 4: P-V Curves [111]

The behavior of the voltage in proportion to the active power that can be used at the bus by the load while maintaining a constant reactive power is illustrated by the P-U curves, which can be found above. There is a maximum power capacity and a voltage level that corresponds to it. These are the boundaries of the curve, and it is quite important to carry out operations at this point. The stable operating zone is located in the portion of the curve that is located above the critical voltage. The unstable operating region is located in the portion of the curve that is located under the critical voltage[113].

If solar photovoltaic power was integrated at bus 2, as seen in Figure III.3 and explained in equation III.9, the P-U curve will be moved outwards in the other direction. This would cause

a rise in the maximum amount of power that the load is capable of consuming. An examination of equation (III.9) reveals a rise in the voltage at the critical point. But nevertheless, this does not indicate that there has been an improvement in the grid's stability. This is due to the fact that, in practice, operating at the critical voltage and the maximum power is prevented at all costs. In addition, it is not recommended to operate the device at voltages lower than the critical voltage, even though doing so would be technically viable based on the formula (III.8). In accordance with equation (III.8), every power operation, P, possesses the potential to operate at two different voltage points. One of the voltages is higher than the critical voltage, while the other voltage is lower than the critical voltage [11].

$$V = \sqrt{\left(\frac{V_1{}^2}{2} - QX \pm \sqrt{\left(\frac{V_1{}^4}{4} - X^2(P - P_{PV})^2 - XV_1{}^2Q \right)} \right)} \tag{III.9}$$
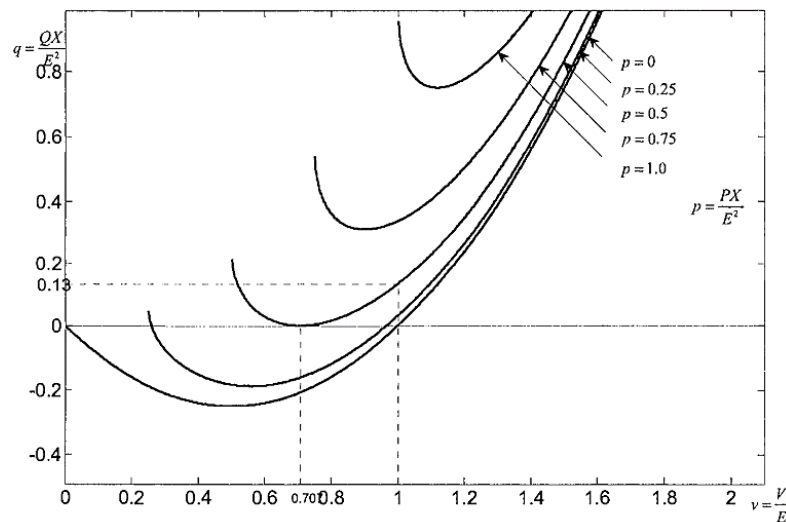
Figure III. 5: Q-U Curves [111]

Figure III.5 illustrates the connection between the voltage and reactive power support that is required at the bus 2 in order to maintain the same amount of active power (P). The curve has a point that is its lowest point. This point can be determined by separating the reactive power that acts reactively with regard to the voltage and bringing the result to an equal value of zero (dQ/dU=0). This is the upper limit of the system's voltage stability. The points on the curve that are located to the right of the lowest point represent the stable operating zone or a voltage stable zone, whereas the points that are located to the left of the lowest point represent an unstable operating zone or a voltage unstable zone. As indicated by equation (III.9), the integration of solar PV power causes a rise in voltage at the receiving bus, which in turn decreases the amount of reactive power that is required from the sending end. This leads to a rise in the reactive power

storage that is available in the grid, which could ultimately lead to an enhancement in the voltage stability of the grid [113].

III.3.1 Static voltage stability analysis techniques

Various works on static voltage stability analysis are conducted using various approaches, including QV curve, PV curve, sensitivity analysis, modal analysis, continuation power flow (CPF), and voltage stability indices[107]. In order to increase the effectiveness and accuracy of analyses, offer a thorough understanding of voltage stability, and pinpoint the sources of instability, this thesis analyses system network voltage stability utilising sensitivity analysis, modal analysis, P-V curve, and Q-V curve. Modal analysis is used to examine the system network's voltage stability state and identify the weakest bus and area. Sensitivity analysis is utilized to determine which buses in the system are the most sensitive by measuring their sensitivity. P-V curve is drawn. to calculate the maximum loading of power system as well as buses critical voltage. Q-V curve is also drowned to determine margin of reactive power of system buses.

III.3.1.1 Sensitivity Analysis

Voltage stability can be measured by plotting the magnitude of voltage fluctuations against the fluctuations in reactive power on a certain bus. If the V Q sensitivity for each bus is positive, then the system is stable in terms of voltage. However, it is prone to fluctuations. [114].

Reduced power system jacobian matrix is represented as follows:

$$\begin{bmatrix} \Delta P \\ \Delta Q \end{bmatrix} = \begin{bmatrix} J_{P\delta} & J_{PV} \\ J_{Q\delta} & J_{QV} \end{bmatrix} \begin{bmatrix} \Delta \delta \\ \Delta V \end{bmatrix} \tag{III.10}$$

$$\begin{bmatrix} \Delta P \\ \Delta Q \end{bmatrix} = [J] \begin{bmatrix} \Delta \delta \\ \Delta V \end{bmatrix} \tag{III.11}$$

Where

ΔP and ΔQ = gradual change in bus active and reactive power

$\Delta \delta$ and ΔV= gradual change in bus voltage angle and voltage magnitude

J= Jacobian elements of power flow

By taking into account the gradual change relationship between voltage and reactive power, voltage stability is evaluated. So, letting $\Delta P = 0$, equation (III.10) becomes

$$\Delta Q = \left[J_{QV} - J_{Q\delta} J_{P\delta}^{-1} J_{PV} \right] \Delta V \tag{III.12}$$

$$\Delta Q = J_R \Delta V \tag{III.13}$$

where,

$$J_R = \left[J_{QV} - J_{Q\delta}J_{P\delta}^{-1}J_{PV}\right]$$ is the system's reduced Jacobian matrix

equation (III.13) can be written as,

$$\Delta V = J_R^{-1}\Delta Q \qquad\qquad \text{(III.14)}$$

The Q-V curve's slope at a specific operating point is represented by the V-Q sensitivity at a bus. A positive V-Q sensitivity demonstrates stable behavior, and the lower the sensitivity, the more stable the system. A negative sensitivity represents an unstable operation. A particularly unsteady operation is represented by a small negative sensitivity [114].

III.3.1.2 Modal Analysis

The modal analysis method is one way to figure out when a power system's voltage will break down. It was proposed by Gao et al. [115]. This method essentially calculates the least Eigen value and related Eigen vectors of the power system's reduced Jacobian. The variations in voltage and reactive power are associated with the Eigen values. the system is deemed as stable voltage if all of the Eigen values are positive. On the other hand, if any of the Eigen values is negative, the system is deemed to be unstable voltage. A zero Eigen value means that the system is on the verge of instability of voltage [116].

The reduced Jacobian matrix's eigenvalues and eigenvectors, J_R, are calculated to figure out the voltage stability properties of a system. The J_R is written in the equation (III.15),

$$J_R = \xi\Lambda\eta \qquad\qquad \text{(III.15)}$$

where

ξ = J_R's right eigenvector matrix

η = J_R's left eigenvector matrix

Λ = J_R's diagonal eigenvalues matrix

equation (III.15) can be written as,

$$J_R^{-1} = \xi\eta\Lambda^{-1} \qquad\qquad \text{(III.16)}$$

replacing (III.16) in (III.4) gives

$$\Delta V = \xi\eta\Lambda^{-1}\Delta Q \qquad\qquad \text{(III.17)}$$

Or

$$\Delta V = \sum_i \frac{\xi_i\eta_i}{\lambda i}\Delta Q \qquad\qquad \text{(III.18)}$$

Where

$\lambda_i = i^{\text{th}}$ eigenvalue

$\xi_i = i^{\text{th}}$ column right eigenvector

$\eta_i = i^{\text{th}}$ row left eigenvector matrix of J_R

Considering that $\xi^{-1} = \eta$, equations (III.18) can be expressed as

$$\eta \Delta V = \eta \wedge^{-1} \Delta Q \tag{III.19}$$

or

$$v = \Lambda^{-1} q \tag{III.20}$$

Where

$v = \eta \Delta V$ = vector of modal voltage variation

$q = \eta \Delta Q$ = vector of modal reactive power variation

The equivalent i^{th} voltage variation modal is given by

$$v_i = \frac{1}{\lambda_i} q_i \tag{III.21}$$

The related modal voltage collapses if λ_i is equal to zero since any variation in reactive power reasons an endless fluctuation in the bus voltage. A system that has all positive eigenvalues for J_R is supposed to be stable, nevertheless if any of the eigenvalues is negative, the system is unstable [116].

Bus Participation Factors. The bus participation factor calculates the relative participation of bus k in mode I

$$P_{ki} = \xi_{ik} \eta_{ki} \tag{III.22}$$

Utilizing the bus participation factors of the small eigenvalues allows for the identification of weak buses as well as areas of the power system that are dangerously near voltage instability[110].

III.3.1.3 P-V Curve

Figure III.6 depicts the typical PV curve. It displays how the amount of total active power delivered to loads or sinking zones affects the voltage variation on a certain bus. It is clear that when there is an increase in load, the voltage rapidly decreases at the PV curve's knee. Beyond this point, load-flow solutions diverge, demonstrating that the system is becoming unstable. The critical point refers to this point. As a result, the collapse margin and critical operating voltage of the system may be calculated using the curve. Operating values that are above the vital point often denote a stable system, whereas operating values that are below the critical point typically denote an unstable system[117, 118].
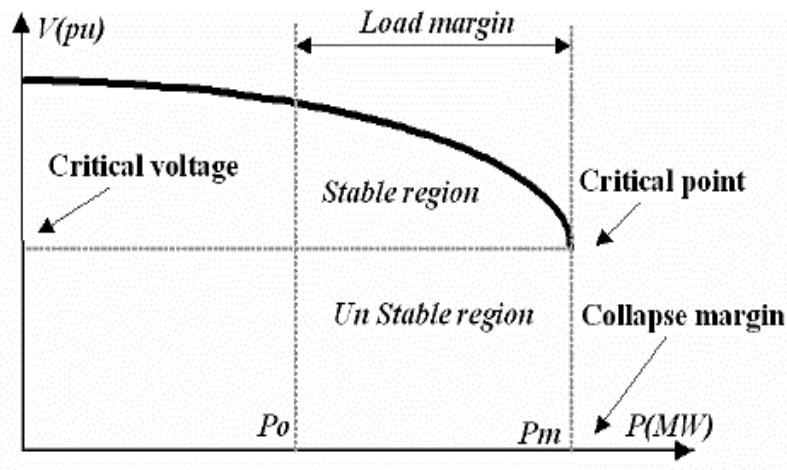
Figure III. 6: Standard PV curve [119]

III.3.1.4 Q-V Curve

A common QV curve is illustrated in Figure III.7, which is often produced by a number of load-flow solutions. Using this curve, one can determine the voltage safety margin or distance from collapse at a certain bus. The QV curve is a representation of the sensitivity and volatility of the bus voltage in response to reactive power injections or absorptions. [120]. The reactive power margin is determined by the Q-V curve's minimum MVAr point and the voltage axis. When the reactive supply is negative, the reactive load is increasing. The amount of load that may be applied to a bus before the voltage drops below its breakdown point is represented by its reactive power margin [121]. The bus with the largest reactive power margin is strong, while the bus with the shortest reactive power margin is the least strong.
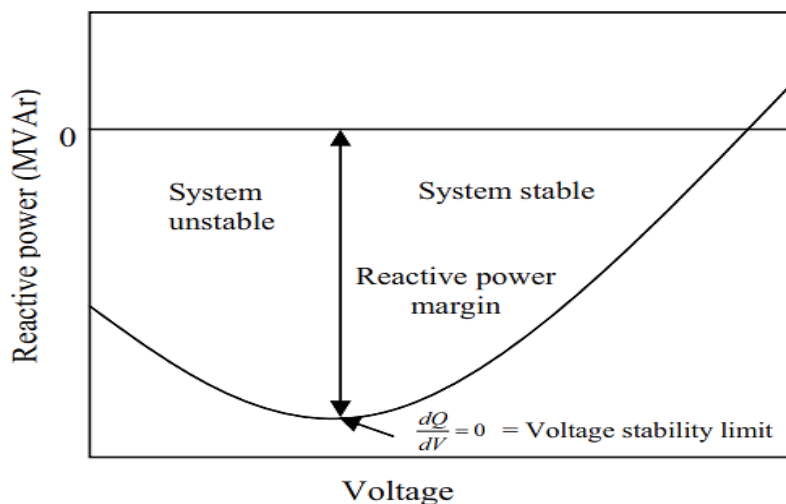
Figure III. 7: Common Q -V curve [121]

69

III.4 Steady-State Stability Analysis -Small Disturbances

- **Swing Equation**

Assume a synchronous generator operating at the synchronous speed ω_{sm} and producing an electromagnetic torque, Te. If T_m is the driving mechanical torque. Thus, if we assume a steady state operation and disregard losses, we have [122] [123]

$$T_{\mathrm{m}} = T_e \tag{III.23}$$

When a system is disrupted from its steady state, acceleration occurs.$(T_{\mathrm{m}}\rangle\ T_e\ )$ or decelerating $(T_m < T_e\ )$ torque T_a on the rotor.

$$T_a = T_{\mathrm{m}} - T_e \tag{III.24}$$

Ignoring the effects of frictional and damping torques, we can derive from the laws of rotation the following:

$$J\frac{d^2\theta_m}{dt^2} = T_a = T_m - T_e \tag{III.25}$$

where θ_m is the angular movement of the rotor regarding the stationary reference axis on the stator. The angular reference is selected with respect to a rotating reference frame that is moving at a constant angular velocity ω_{sm} in order to obtain the rotor speed in relation to the synchronous speed, that is

$$\theta_m = \omega_{sm}t + \delta_m \tag{III.26}$$

where δ_m is the location of the rotor prior to perturbation at time $t = 0$, as determined by the synchronously rotating reference point, The rotor angular velocity is given by the derivative of (III.26).

$$\omega_m = \frac{d\theta_m}{dt} = \omega_{ms} + \frac{d\delta_m}{dt} \tag{III.27}$$

and the rotor acceleration is

$$\frac{d^2\theta_m}{dt^2} = \frac{d^2\delta_m}{dt^2} \tag{III.28}$$

Substituting (III.28) into (III.25), we have

$$J\frac{d^2\delta_m}{dt^2} = T_m - T_e \tag{III.29}$$

Multiplying (III.29) by ω_m, results in

$$J\omega_m \frac{d^2\delta_m}{dt^2} = \omega_m T_{mn} - \omega_m T_c \tag{III.30}$$

Because angular velocity multiplied by torque equals power, we formulate the preceding equation in terms of power.

$$J\omega_m \frac{d^2\delta_m}{dt^2} = P_m - P_e \tag{III.31}$$

The quantity $J\omega_m$ is named the inertia constant and is meant by M. It is associated with the kinetic energy of rotating masses. W_k.

$$W_k = \frac{1}{2}J\omega_m^2 = \frac{1}{2}M\omega_m \qquad \text{(III.32)}$$

or

$$M = \frac{2W_k}{\omega_m} \qquad \text{(III.33)}$$

Although M is referred to as the inertia constant, it is not true when the rotor speed differs from the synchronous speed. Nevertheless, because ω_m does not vary much before stability is lost, M is assessed at the synchronous speed and is assumed to be constant.

$$M = \frac{2W_k}{\omega_{sm}} \qquad \text{(III.34)}$$

In perspective of inertia constant, the swing equation is

$$M\frac{d^2\delta_m}{dt^2} = P_m - P_e \qquad \text{(III.35)}$$

The swing equation is easier to write in terms of. If P is a synchronous generator's pole count, the electrical power angle is linked to the mechanical power angle by

$$\delta = \frac{P}{2}\delta_m \qquad \text{(III.36)}$$

also,

$$\omega = \frac{p}{2}\omega_m \qquad \text{(III.37)}$$

The electrical power angle swing equation is

$$\frac{2}{p}M\frac{d^2\delta}{dt^2} = P_m - P_e \qquad \text{(III.38)}$$

Because power system analysis is performed in per unit systems, the swing equation is typically given in per unit terms. Subtracting (III.38) from (III.34) and dividing by the base power S_B yields

$$\frac{2}{p}\frac{2W_K}{\omega_{sm}S_B}\frac{d^2\delta}{dt^2} = \frac{P_m}{S_B} - \frac{P_e}{S_B} \qquad \text{(III.39)}$$

The H constant, often known as the per unit inertia constant, is now defined.

$$H = \frac{\text{kinetic energy in MJ at rated speed}}{\text{machine rating in MVA}} = \frac{W_K}{S_B} \qquad \text{(III.40)}$$

The unit of H is seconds. The value of H varieties from 1 to 10 seconds, based on the machine's size and type. Replacing in (III-39), we get

$$\frac{2}{p}\frac{2H}{\omega_{sm}}\frac{d^2\delta}{dt^2} = P_{m(pu)} - P_{e(pu)} \qquad \text{(III.41)}$$

where $P_{m(pu)}$ and $P_{e(pt)}$ are the per unit mechanical power and electrical power, respectively. The relationship between the electrical angular velocity and the mechanical angular velocity is shown by $\omega_{sm} = (2/p)\omega_g$. (III.41) in terms of electrical angular velocity is

$$\frac{2H}{\omega_s}\frac{d^2\delta}{dt^2} = P_{m(pu)} - P_{e(pu)} \qquad\qquad (III.42)$$

The above equation is often written in terms of the frequency f_0. To make the notation easier to understand, the subscript pu is often left out, and it is assumed that the powers are in per unit.

$$\frac{H}{\pi f_0}\frac{d^2\delta}{dt^2} = P_m - P_e \qquad\qquad (III.43)$$

where δ is in electrical radian. If δ in electrical degrees, the equation for the swing is

$$\frac{H}{180 f_0}\frac{d^2\delta}{dt^2} = P_m - P_e \qquad\qquad (III.44)$$

Figure III.8 illustrates the steady-state stability problem by depicting the dynamic behavior of a single-machine system interconnected to an infinite bus [58].
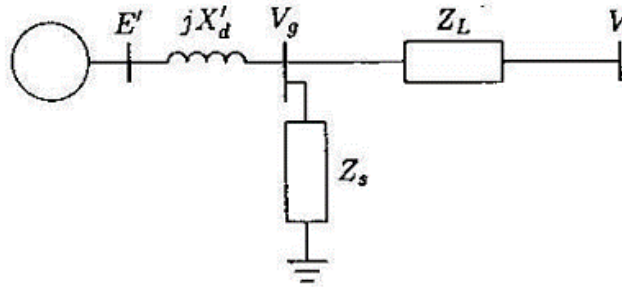
Figure III. 8: A single machine linked to an infinite bus [58]

The rotor dynamices for a synchrouns machine described by the swing equation given in equation (III.44). Substituting for the electrical power into the swing equation results in

$$\frac{H}{\pi f_0}\frac{d^2\delta}{dt^2} = P_m - P_{max}\sin \delta \qquad\qquad (III.45)$$

Power angle nonlinearly affects the swing equation. The swing equation can be linearized for small perturbations. Assume a modest power angle variation, i.e.,

$$\delta = \delta_0 + \Delta\delta \qquad\qquad (III.46)$$

Substituting in (III.45), we get

$$\frac{H}{\pi f_0}\frac{d^2(\delta_0+\Delta\delta)}{dt^2} = P_m - P_{max}\sin (\delta_0 + \Delta\delta) \qquad\qquad (III.47)$$

or

$$\frac{H}{\pi f_0}\frac{d^2\delta_0}{dt^2} + \frac{H}{\pi f_0}\frac{d^2\Delta\delta}{dt^2} = P_m - P_{max}(\sin \delta_0\cos \Delta\delta + \cos \delta_0\sin \Delta\delta) \qquad\qquad (III.48)$$

Since $\Delta\delta$ is small, $\cos \Delta\delta \cong 1$ and $\sin \Delta\delta \cong \Delta\delta$, and we have

$$\frac{H}{\pi f_0}\frac{d^2\delta_0}{dt^2} + \frac{H}{\pi f_0}\frac{d^2\Delta\delta}{dt^2} = P_m - P_{max}\sin\delta_0 - P_{max}\cos\delta_0\Delta\delta \qquad \text{(III.49)}$$

Since at the initial operating state

$$\frac{H}{\pi f_0}\frac{d^2\delta_0}{dt^2} = P_m - P_{max}\sin\delta_0 \qquad \text{(III.50)}$$

The linearized equation for incremental power angle adjustments is:

$$\frac{H}{\pi f_0}\frac{d^2\Delta\delta}{dt^2} + P_{max}\cos\delta_0\Delta\delta = 0 \qquad \text{(III.51)}$$

The quantity $P_{max}\cos\delta_0$ in (III.51) is the slope of the power-angle curve at δ_0. P s is the synchronization coefficient. System stability depends on this coefficient, which is given by

$$P_s = \frac{dP}{d\delta}\bigg|_{d_0} = P_{max}\cos\delta_0 \qquad \text{(III.52)}$$

Substituting in (III.51), we have

$$\frac{H}{\pi f_0}\frac{d^2\Delta\delta}{dt^2} + P_s\Delta\delta = 0 \qquad \text{(III.53)}$$

The roots of the characteristic equation provided by solve the above equation.

$$s^2 = -\frac{\pi f_0}{H}P_s \qquad \text{(III.54)}$$

One root in the right half of the s-plane, exponentially growing reaction, and loss of stability occur when P s is negative. At the positive P s limit, the motion is oscillatory and undamped, and there are two roots on the j - w axis. The system has a little margin of stability, and its natural frequency of oscillation is given by

$$\omega_n = \sqrt{\frac{\pi f_0}{H}P_s} \qquad \text{(III.55)}$$

If you look at the power-angle curve, you'll notice that the largest value of P s (the slope $dP/d\delta$) occurs at no-load $(\bar{\delta}_0 = 0)$, and that the range where P s is positive is between 0 and 90 degrees.

For as long as there is a discrepancy between the rotor's angular velocity and that of the resulting revolving air gap field, induction motor action will occur. , and a torque will be applied to the rotor in order to reduce the angular velocity differential. The damping torque measures how much an object can be moved without causing any noticeable movement. There is a roughly proportionate relationship between the speed difference and the damping force.

$$P_d = D\frac{d\delta}{dt} \qquad \text{(III.56)}$$

The damping coefficient D can be calculated from theoretical or experimental data. The prime mover's speed/torque feature and the load dynamic create additional damping torques, which are not considered here. The damping power of the synchronizing power coefficient Ps

dampens oscillations and restores equilibrium angle operation. Stability and synchronism are maintained.

The linearized swing equation becomes damping-corrected.

$$\frac{H}{\pi f_0}\frac{d^2\Delta\delta}{dt^2} + D\frac{d\Delta\delta}{dt} + P_s\Delta\delta = 0 \tag{III.57}$$

or

$$\frac{d^2\Delta\delta}{dt^2} + \frac{\pi f_0}{H}D\frac{d\Delta\delta}{dt} + \frac{\pi f_0}{H}P_s\Delta\delta = 0 \tag{III.58}$$

that is, in terms of the commonplace second-order differential equation, we have

$$\frac{d^2\Delta\delta}{dt^2} + 2\zeta\omega_n\frac{d\Delta\delta}{dt} + \omega_n^2\Delta\delta = 0 \tag{III.59}$$

where ω_n, the fundamental frequency of oscillation is determined by (III.55), and ζ ratio of damping, described in terms of a dimensionless quantity,

$$\zeta = \frac{D}{2}\sqrt{\frac{\pi f_0}{HP_s}} \tag{III.60}$$

The characteristic equation is

$$s^2 + 2\zeta\omega_n s + \omega_n^2 = 0 \tag{III.61}$$

Under typical operational circumstances, $\zeta = D/2\sqrt{\frac{\pi f_0}{HP_2}} < 1$, and the complex roots of the characteristic equation

$$\begin{aligned} s_1, s_2 &= -\zeta\omega_n \pm j\omega_n\sqrt{1-\zeta^2} \\ &= -\zeta\omega_n + j\omega_d \end{aligned} \tag{III.62}$$

where ω_d is the oscillation's damped frequency as determined by

$$\omega_d = \omega_n\sqrt{1-\zeta^2} \tag{III.63}$$

If the synchronization power coefficient P_S is positive, then it stands to reason that the roots of the characteristic equation will have a negative real portion for positive damping. The system is steady, and its response is constrained.

III.5 Model-Based Analysis for Small Signal Stability Analysis

When a power system is stable against small signals, it can withstand minor disruptions without losing synchronization. The resulting instability may take the shape of either (i) rotor oscillations with ever-increasing amplitude due to insufficient damping torque or (ii) a constant increase in generator rotor tilt due to insufficient synchronizing torque. Insufficient damping of system oscillations is typically the cause of the small-signal stability problem in real-world power systems today. Linear methods of small-signal analysis can reveal important facts about the power system's innate dynamic features and aid in its design [124].

Modal analysis is commonly employed in the analysis of nonlinear dynamic systems to investigate the stability of small signals in the system. Using modal analysis, nonlinear differential algebraic equations can be linearized at a specific operating point. The eigenvalues of the state matrix of the linearized model are then calculated to make an approximation of the oscillation mode and the form of the oscillation. System operators can evaluate the power system's dynamic properties at specific operating points using the model approach [125].

III.5.1 State-space representation

A power system is both dynamic and nonlinear. The system's state is the current information required for the system to accomplish the next task. It mixes the many information inputs of a system. The states change on a regular basis. It can be any of the physical variables. State-space is an approach to comprehending power system from n dimensions [126].

A set of n first order nonlinear ordinary differential equations of the following form can describe the behaviour of a dynamic system, such as a power system:

$$\dot{x}_i = f_i(x_1, x_2, \ldots, x_n; u_1, u_2, \ldots, u_r; t) \quad i = 1,2, \ldots, n \tag{III.64}$$

where n is the order of the system and r is the number of inputs. This can be written in the following form by using vector-matrix notation:

$$\dot{\mathbf{x}} = \mathbf{f}(\mathbf{x}, \mathbf{u}, t) \tag{III.65}$$

where

$$\mathbf{x} = \begin{bmatrix} x_1 \\ x_2 \\ \vdots \\ x_n \end{bmatrix} \quad \mathbf{u} = \begin{bmatrix} u_1 \\ u_2 \\ \vdots \\ u_r \end{bmatrix} \quad \mathbf{f} = \begin{bmatrix} f_1 \\ f_2 \\ \vdots \\ f_n \end{bmatrix}$$

The column vector x is known as the state vector, and its entries x_i are known as state variables. The vector of system inputs is represented by the colamn vector u. These are the outside signals that affect the system's efficiency. Time is represented by t, and the derivative of a state variable x with respect to time is represented by $\dot{x}$. If the derivatives of the state variables are not explicit functions of time, the system is said to be autonomous [55]. In this case, Equation III.65 simplifies to

$$\dot{x} = f(x, u) \tag{III.66}$$

We are frequently interested in the output variables that can be seen in the system. These can be represented in the form of state variables and input variables as follows:

$$y = g(x, u) \tag{III.67}$$

Where

$$\mathbf{y} = \begin{bmatrix} y_1 \\ y_2 \\ \vdots \\ y_m \end{bmatrix} \quad \mathbf{g} = \begin{bmatrix} g_1 \\ g_2 \\ \vdots \\ g_m \end{bmatrix}$$

III.5.2 Eigenvalue Analysis

The process of linearizing Equation is next on our agenda to discuss. (III.66) Let $\mathbf{x}_0$ represent the starting state vector, and let $\mathbf{u}_0$ stand for the input vector that corresponds to the equilibrium point that will be the focus of the investigation into the small-signal performance. Given that $\mathbf{x}_0$ and $\mathbf{u}_0$ are in agreement with Equation III.66, we have[55]

$$\dot{x}_0 = f(x_0, u_0) = 0 \tag{III.68}$$

Let us perturb the system from the above state, by letting

$$x = x_0 + \Delta x \qquad u = u_0 + \Delta u$$

where the prefix Δ means a small change.

Equation III.66 needs to be satisfied by the new state. Hence,

$$\begin{aligned} \dot{x} &= \dot{x}_0 + \Delta \dot{x} \\ &= f[(x_0 + \Delta x), (u_0 + \Delta u)] \end{aligned} \tag{III.69}$$

As the disturbances are considered to be small, the nonlinear functions $\mathbf{f(x, u)}$ can be explained in terms of Taylor's series expansion. With terms including second and higher order powers of Δx and Δu neglected, we may write

$$\begin{aligned} \dot{x}_i = \dot{x}_{i0} + \Delta \dot{x}_i &= f_i[(x_0 + \Delta x), (u_0 + \Delta u)] \\ &= f_i(x_0, u_0) + \frac{\partial f_i}{\partial x_1} \Delta x_1 + \cdots + \frac{\partial f_i}{\partial x_n} \Delta x_n \\ &+ \frac{\partial f_i}{\partial u_1} \Delta u_1 + \cdots + \frac{\partial f_i}{\partial u_r} \Delta u_r \end{aligned}$$

Since $\dot{x}_{i0} = f_i(\mathbf{x}_0, \mathbf{u}_0)$, we obtain

$$\Delta \dot{x}_i = \frac{\partial f_i}{\partial x_1} \Delta x_1 + \cdots + \frac{\partial f_i}{\partial x_n} \Delta x_n + \frac{\partial f_i}{\partial u_1} \Delta u_1 + \cdots + \frac{\partial f_i}{\partial u_r} \Delta u_r$$

with $i = 1,2, \ldots, n$. In a like manner, from Equation III.67, we have

$$\Delta y_j = \frac{\partial g_j}{\partial x_1} \Delta x_1 + \cdots + \frac{\partial g_j}{\partial x_n} \Delta x_n + \frac{\partial g_j}{\partial u_1} \Delta u_1 + \cdots + \frac{\partial g_j}{\partial u_r} \Delta u_r$$

with $j = 1,2, \ldots, m$. Therefore, the linearized forms of Equations III.66 and III.67 are

$$\Delta \dot{x} = A\Delta x + B\Delta u \tag{III.70}$$

$$\Delta y = C\Delta x + D\Delta u \tag{III.71}$$

Where

$$A = \begin{bmatrix} \dfrac{\partial f_1}{\partial x_1} & \cdots & \dfrac{\partial f_1}{\partial x_n} \\ \cdots & & \\ \dfrac{\partial f_n}{\partial x_1} & \cdots & \dfrac{\partial f_n}{\partial n_n} \end{bmatrix}, \quad B = \begin{bmatrix} \dfrac{\partial f_1}{\partial u_1} & \cdots & \dfrac{\partial f_1}{\partial u_r} \\ \cdots & & \\ \dfrac{\partial f_n}{\partial u_1} & \cdots & \dfrac{\partial f_n}{\partial u_r} \end{bmatrix}, \quad C = \begin{bmatrix} \dfrac{\partial g_1}{\partial x_1} & \cdots & \dfrac{\partial g_1}{\partial x_n} \\ \cdots & & \\ \dfrac{\partial g_m}{\partial x_1} & \cdots & \dfrac{\partial g_m}{\partial x_r} \end{bmatrix}$$

$$D = \begin{bmatrix} \dfrac{\partial g_1}{\partial u_1} & - & \dfrac{\partial g_1}{\partial u_r} \\ \cdots & & \\ \dfrac{\partial g_m}{\partial u_1} & - & \dfrac{\partial g_m}{\partial u_r} \end{bmatrix}$$

In order to get eigenvalues, the process of lineaization is necessary. The characteristic equation can be obtained from Equation (III.70)

$$\det(A - \lambda I) = 0 \tag{III.72}$$

Where λ is the eigenvalues of matrix A. The value of λ usually represents the stability of a system.

III.5.2.1 Eigenvalues and Stability

The roots of the characteristic equation of the system of first approximations, or the eigenvalues of A, convey information about the small stability of a nonlinear system. [55]. If all of the eigenvalues lie to the left of the imaginary axis in the complex plane, the power system is stable; otherwise, it is unstable. The system is unstable and its corresponding modes are considered to be unstable if any of the eigenvalues crosses over to the right side of the imaginary axis. When the real components of the eigenvalues are zero, no generalizations can be made using the first estimation. [127].

A non-oscillatory mode has an eigenvalue in the real number range. A declining mode is indicated by a negative real eigenvalue. The larger the original value was, the quicker it decayed. With a real eigenvalue greater than zero, aperiodic instability is present. Each conjugate pair of complex eigenvalues represents a different mode of oscillation. The frequency of an oscillation may be calculated from the imaginary portion of an eigenvalue, whereas the damping can be calculated from the real part. So, for a complex eigenvalue pair: [127].

$$\lambda = \sigma + j\omega \tag{III.73}$$

The formula for the oscillation frequency in hertz is [128]

$$f = \frac{\omega}{2\pi} \tag{III.74}$$

The damping ratio expressed as
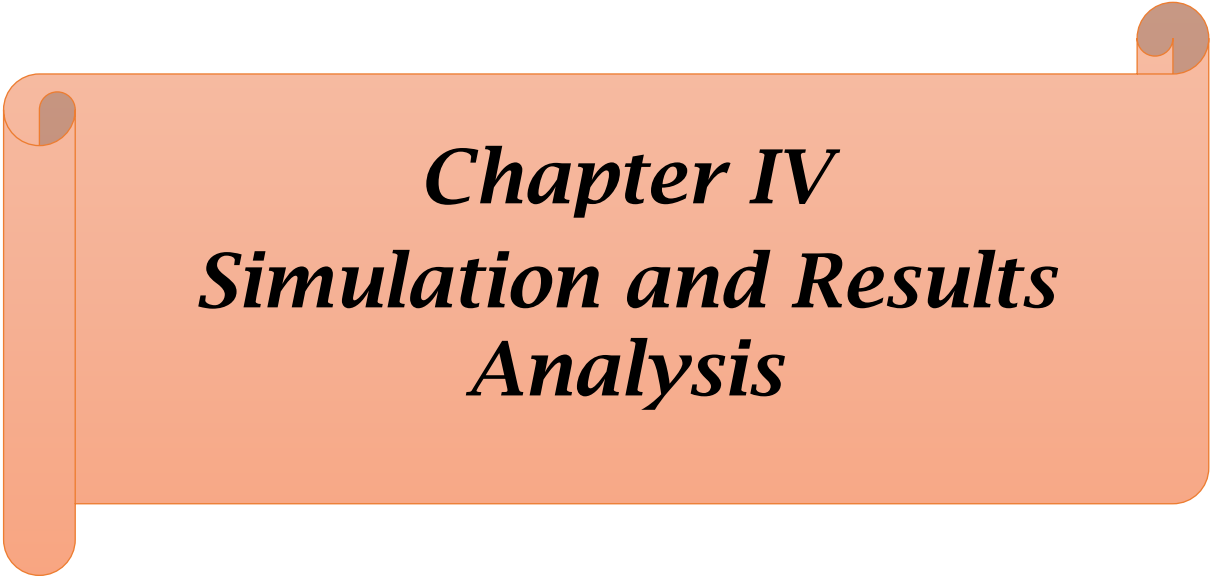
$$\zeta = \frac{-\sigma}{\sqrt{\sigma^2 + \omega^2}} \qquad\qquad\qquad\qquad\qquad\qquad\qquad\qquad\text{(III.75)}$$

Dominant modes are eigenvalues that are associated with an oscillatory mode that is either unstable or inadequately damped. This is due to the fact that their contribution dominates the time response of the system.

III.6 Conclusion

This chapter provides a summary of the concept of the power system stability, as well as the several forms and classifications of power system stability that were investigated throughout of this thesis. The analysis of the voltage stability also includes an explanation of the various methods utilized in the analysis. Moreover, the modal analysis method for small stability of the power system has been clarified.

Chapter IV
Simulation and Results Analysis

Chapter IV Simulation and Results Analysis

IV.1 Introduction

This chapter includes the discussions of the findings of a simulation performed on a solar photovoltaic power generation system that is connected to the electrical power grid. The results were acquired by employing three different kinds of software: the PSAT toolbox, the NEPLAN program, and the ETAP software for the various scenarios. The findings obtained reflect both the typical scenario, sometimes known as the base case, and those obtained with the addition of a solar photovoltaic power generation system. The findings are explored through the perspective of comparisons with the solar photovoltaic power system and the basic cases. The NEPALN program is used to discuss the influence of the integration of a solar PV system on the steady state stability in terms of how it affects the voltage level, system losses, and static voltage stability. In addition to this, a transient stability analysis of a real network is carried out. Using ETAP software, three different transient situations are simulated in order to investigate the effect that a solar photovoltaic power plant has on the overall performance of the network. With the use of the PSAT toolbox, an analysis of the effect that the integration of PV generation power has on the small signal stability of the power system was carried out, and its findings were addressed.

IV.2 Steady State Stability Analysis (Static analysis)

The method is based on a comparison of two situations; the first one reflects the regular case in which a solar PV power system is not integrated with the grid. The second scenario represents the case in which a solar PV power system is integrated with the grid. In the second possible scenario, the solar PV power system is connected into the grid so that the impacts of the system's integration can be studied. There are a different penetration levels that are considered. Figure IV.1 illustrates the methodology used for the analysis. In this study, IEEE 14- bus system is considered. It is made up of a main generator with a capacity of 615 MVA that is linked to bus 1, a generator with a capacity of 40 MW that is linked to bus 2, three compensators that are linked to buses 3, 6, and 8, 20 transmission lines, and 11 load buses. All of the loads equal 259 MW and 81.3 MVAr in total. [129]. Figure IV.2 illustrates the IEEE-14 bus system.
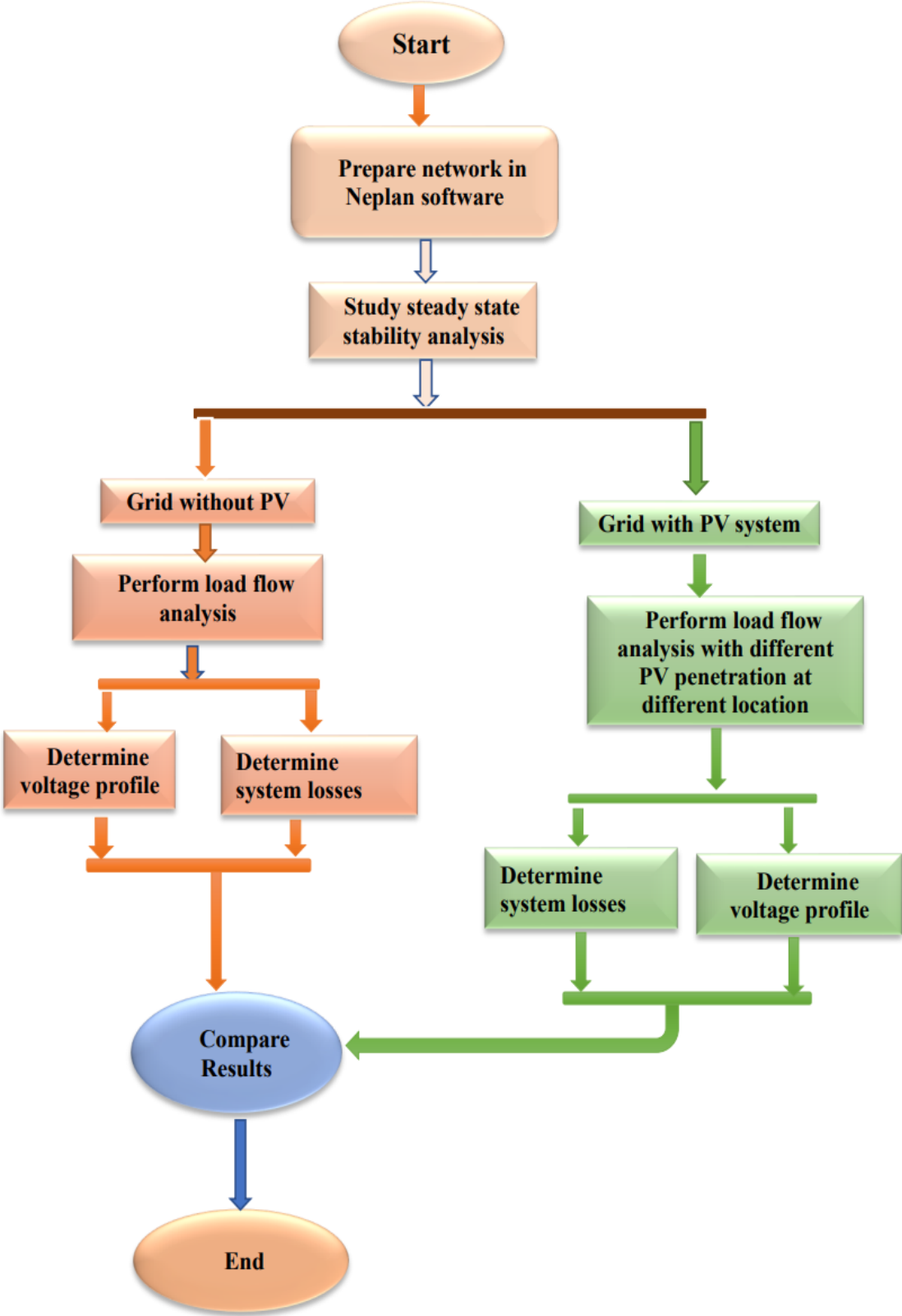
Figure IV. 1: Static analysis methodology flow chart
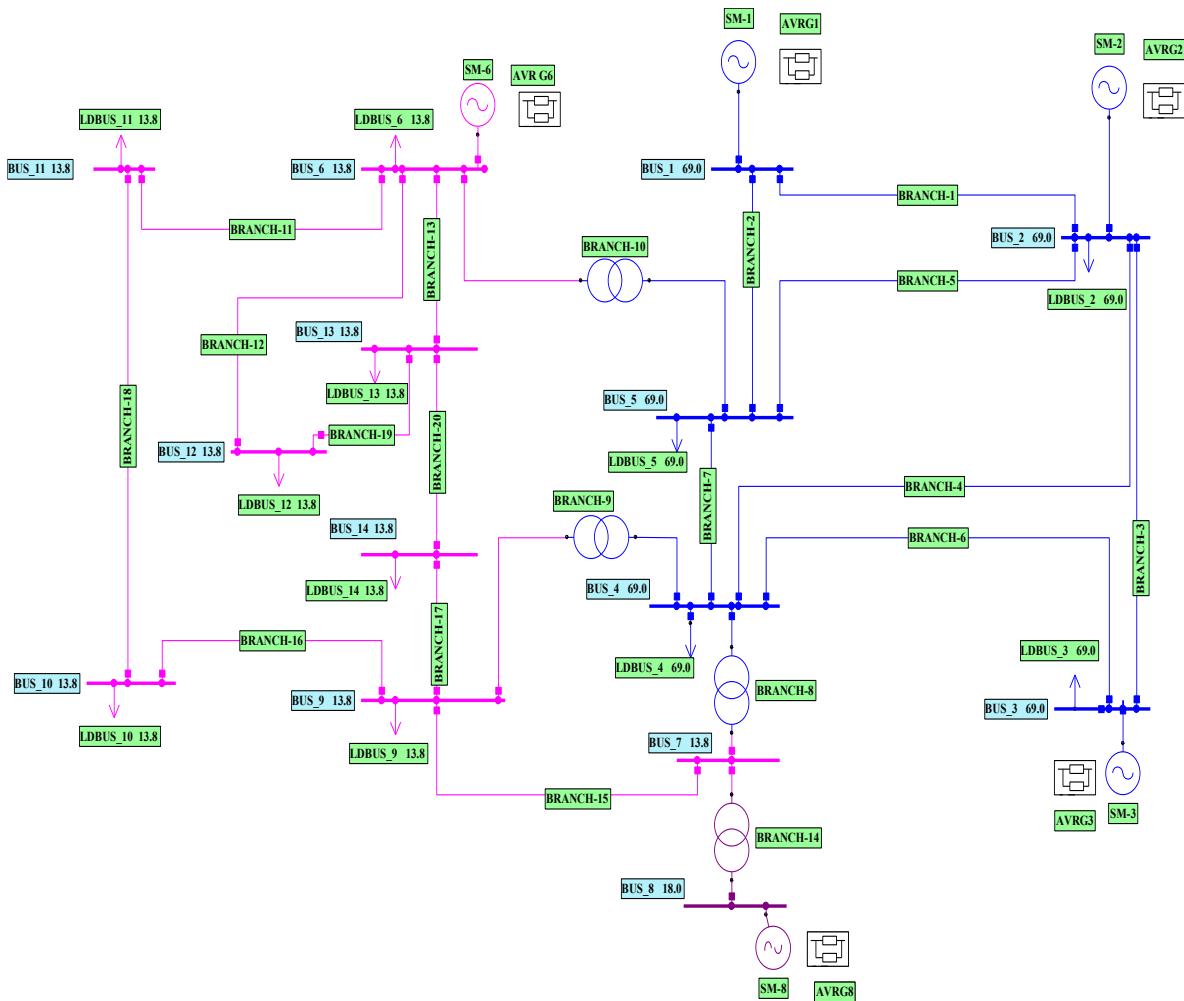
Figure IV. 2: Layout of IEEE14-bus system network in Neplan

IV.2.1 Normal case (Grid without solar PV power system)

The NEPLAN software performs simulations of the normal situation of the grids. Using the Newton–Raphson method, load flow is carried out in order to demonstrate the working conditions of the test grid. These conditions include the magnitudes of voltage on all system buses, which must be within the acceptable range in order for the test to be successful. It is clear from looking at figure 5.3 that the voltage across all of the buses falls totally within the acceptable range of (+/-) 5%. Bus 3 has the lowest voltage of all the buses, as compared to the other buses. Based on the results of the load flow study, it was determined that the total active power losses across the grid were 13.596 MW, and the total reactive power losses were 27.431 Mvar. The swing generator is the source of the absorbed reactive power that is represented by the reactive power, or Q_L, in bus 1.
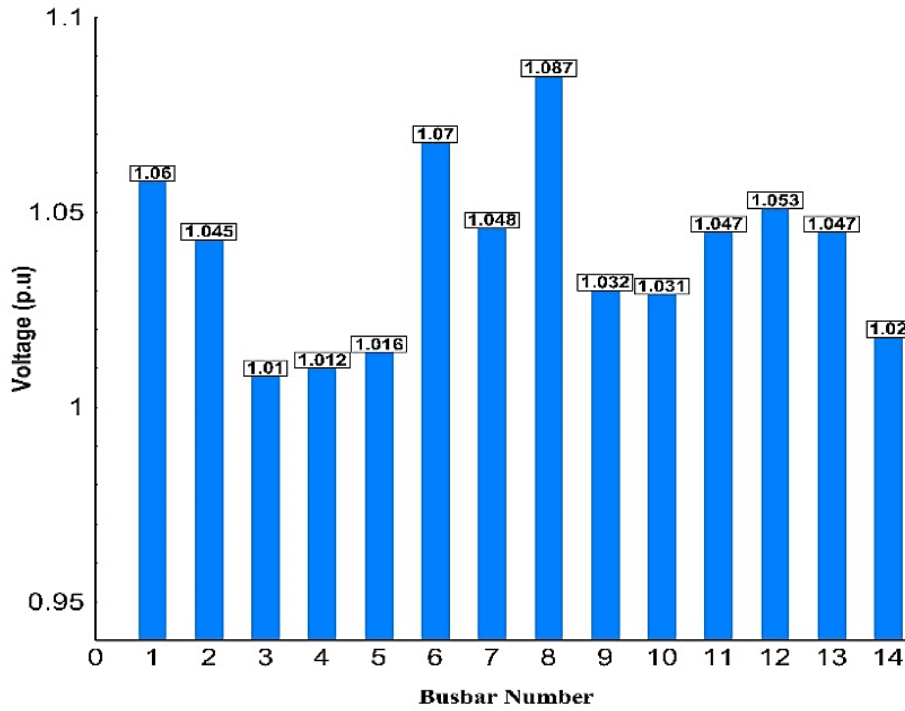
Figure IV. 3: Grid voltage magnitude of the normal case

IV.2.1.1 Power flow results for normal case (without PV system unit)

The power flow results of normal case and line flow results are shown in table IV.1 and IV.2

Table IV. 1: Power flow results without PV system unit

bus	V [p.u]	V ang	P gen	Q gen	P load	Q load
Bus 01	1.06	0	232.596	0	0	14.892
Bus 02	1.045	-5	40	49.114	21.7	12.7
Bus 03	1.01	-12.8	0	27.552	94.2	19
Bus 04	1.012	-10.2	0	0	47.8	3.9
Bus 05	1.016	-8.7	0	0	7.6	1.6
Bus 06	1.07	-14.4	0	22.957	11.2	7.5
Bus 07	1.048	-13.2	0	0	0	0
Bus 08	1.087	-13.2	0	24	0	0
Bus 09	1.032	-14.8	0	0	29.5	16.6
Bus 10	1.031	-15	0	0	9	5.8
Bus 11	1.047	-14.8	0	0	3.5	1.8
Bus 12	1.053	-15.28	0	0	6.1	1.6
Bus 13	1.047	-15.31	0	0	13.5	5.8
Bus 14	1.02	-16.1	0	0	14.9	5

Chapter IV Simulation and Results Analysis

IV.2.1.2 Line power flow results (grid without PV system unit)

Table IV. 2: Results of power flow in the grid branches

Element Name	Type	From Bus	To Bus	P flow	Q flow	P losses	Q losses
Branch-1	Line	Bus 01	Bus 02	157.138	-20.464	4.3118	7.3152
Branch-2	Line	Bus 01	Bus 05	75.458	5.572	2.7714	6.1381
Branch-3	Line	Bus 02	Bus 03	73.474	3.537	2.3381	5.2249
Branch-4	Line	Bus 02	Bus 04	55.931	1.769	1.6724	1.1185
Branch-5	Line	Bus 02	Bus 05	41.72	3.329	0.9217	-0.7964
Branch-6	Line	Bus 03	Bus 04	-23.064	6.864	0.3983	-2.5188
Branch-7	Line	Bus 04	Bus 05	-59.642	9.119	0.4764	0.1874
Braach-8	Trans	Bus 04	Bus 07	27.153	-5.917	0	1.5093
Branch-9	Trans	Bus 04	Bus 09	15.486	2.931	0	1.2675
Branch-10	Trans	Bus 05	Bus 06	45.767	10.89	0	4.6952
Branch-11	Line	Bus 06	Bus 11	8.22	8.653	0.1182	0.2475
Branch-12	Line	Bus 06	Bus 12	8.048	3.146	0.0802	0.1668
Branch-13	Line	Bus 06	Bus 13	18.298	9.854	0.2495	0.4914
Branch-14	Trans	Bus 0	Bus 08	0	-23.141	0	0.8591
Branch-15	Line	Bus 07	Bus 09	27.153	15.715	0	0.9862
Branch-16	Line	Bus 09	Bus 10	4.452	-0.675	0.0061	0.0161
Branch-17	Line	Bus 09	Bus 14	8.687	0.468	0.0904	0.1922
Branch-18	Line	Bus 10	Bus 11	-4.554	-6.492	0.0485	0.1136
Branch-19	Line	Bus 12	Bus 13	1.868	1.379	0.0107	0.0097
Branch-20	Line	Bus 13	Bus 14	6.406	4.932	0.1019	0.2076
Total losses						**13.596**	**27.431**

IV.2.2 Electrical test grid with solar PV power system (case two)

The optimal penetration of solar photovoltaic (PV) power that can be incorporated into the system is determined by calculating the minimum loses of active power that can occur in the power of the system when solar PV is integrated into the different buses. In order to calculate the penetration, the amount of power that is injected into the designated bus by the solar photovoltaic power system is increased from 0% to 100% of the entire load in 5% increments. In order to determine the amount of loss that occurs at each stage, a load flow is carried out using the Newton–Raphson method. The photovoltaic (PV) generation system has been represented as a three-phase distributed generation system that operates with a power factor of one. Because the PV generation system has an inverter, it is able to provide both active and reactive electricity to the grid. This ability is made possible by the fact that the system is

equipped with one. However, at the domestic level, reactive power assistance from the PV inverter is typically not paid for by the utility companies; as a result, the PV generation system is typically run at a power factor of unity. In addition, the potential reactive power assistance provided by the inverter places an increased amount of stress on the switches of the inverter, which may have an effect on the inverter's life cycle operation. As a consequence of this, during the course of the simulation, each of the solar PV generation units contributes only active power to the grid.

IV.2.2.1 Impact on grid losses

The effect that the penetration of solar PV power systems has on both active and reactive power losses is illustrated in figure 5.4. This demonstrates that solar photovoltaic power has a positive impact on the power grid at low levels of solar PV power injection, because it reduces the overall amount of power that is lost by the network. But nonetheless, as the penetration increased, both the active and reactive power losses started to grow. This continued until the penetration reached its maximum. This suggests that as the penetration of solar photovoltaic (PV) power increases, the active and reactive power losses will also increase. Also, the figure illustrates the presence of a penetration level at which the losses of both active and reactive power are kept to a minimum. The difference, however, shifts from one bus to the next The appropriate penetration levels for each type of bus are outlined in Tables 5.3 and 5.4, along with the accompanying loss rates expressed as a percentage decrease rate. It is clear from the two tables that the incorporation of a solar PV power system into the power system has obviously contributed to the reduction of the percent of grid losses. This means that the amount of power generated at the generation stations as well as the amount of power lost in the transmission and distribution lines and transformers has decreased, which has resulted in an improvement in the performance and efficiency of the power system. For economic reasons, it is important to keep active power losses to a minimum, and keeping reactive power losses to a minimum helps keep investment in reactive power devices to a minimum as well.

(a)   (b)
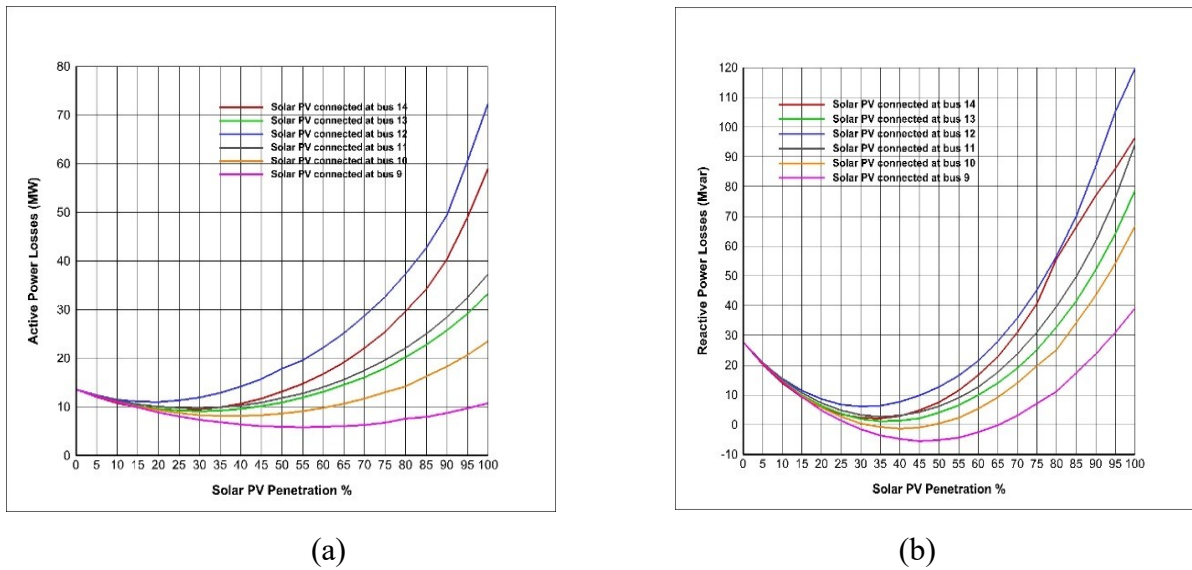
Figure IV. 4: Grid power losses(a) Active power losses (b) reactive power losses

Table IV. 3: Penetration level for minimum active power losses

Bus No	Optimal penetration (%)	Total active Power Losses	Reduction rate (%)
14	25-30	9.28	31.73
13	30-35	9.11	33.03
12	20-25	11.01	19.03
11	30-35	9.70	28.64
10	40-45	8.09	40.49
9	55-60	5.80	57.34

Table IV. 4: Penetration level for minimum reactive power losses

Bus No	Optimal penetration (%)	Total reactive Power Losses	Reduction rate (%)
14	35-40	2.045	92.54
13	35-40	1.136	95.86
12	30-35	6.064	77.89
11	35-40	2.687	90.20
10	40-45	-1.316	104.80
9	45-50	-5.489	120.01

IV.2.2.2 Impact on voltage level

The effect that adding solar photovoltaic (PV) power to the grid has on the voltage level is being studied. The findings that were achieved after integrating solar photovoltaic electricity at

various locations with the suitable level of penetration are presented in Table IV.5. It is clear from looking at the chart that the addition of solar photovoltaic panels results in an increase in the bus system's overall voltage. Figure IV.5 illustrates the voltage profile for the network. In this case, the optimal penetration is taken into consideration, and it is based on the electrical network having the least amount of active power loss, which is then studied in terms of how it affects the voltage level in the buses. The table reveals that there has been a discernible rise in the voltage level, which can be observed to be an improvement. It is also important to notice that the voltage level on some buses has increased to a point where it is above the maximum allowable voltage level. Because of this, when integrating solar PV power systems, their impact on the level of voltage must be taken into consideration, and an evaluation of the appropriate penetration must be carried out to ensure that the level of voltage does not exceed the permissible limits. Consequently, it is essential that this be done. As a result, photovoltaic (PV) solar power systems are always connected to the power network's bus that has the lowest voltage in order to circumvent the issue of the voltage increasing above the acceptable range. It is important to note that the loads are connected to buses 3 and 6, which include synchronous compensators. These compensators offer the reactive power that is required for the loads. Moreover, the generator on Bus 2 supplies the bus with reactive power. As a consequence of this, bus 14 is an acceptable option for connecting a photovoltaic (PV) system.

Table IV. 5: Voltage level of grid buses with solar PV power system penetration

Bus No	Bas case	25% PV at bus 14	30% PV at bus13	20% PV at bus 12	30% PV at bus 11	40% PV at bus 10	55% PV at bus 9
1	1.06	1.06	1.06	1.06	1.06	1.06	1.06
2	1.045	1.045	1.045	1.045	1.045	1.045	1.045
3	1.01	1.01	1.01	1.01	1.01	1.01	1.01
4	1.012	1.0218	1.0208	1.0175	1.0209	1.0274	1.0331
5	1.016	1.0255	1.0267	1.0232	1.0254	1.0299	1.0338
6	1.07	1.07	1.07	1.07	1.07	1.07	1.07
7	1.048	1.055	1.0502	1.0482	1.0533	1.0594	1.0649
8	1.087	1.09	1.0891	1.0871	1.09	1.09	1.09
9	1.032	1.0387	1.0295	1.0284	1.0354	1.0452	1.0557
10	1.031	1.0368	1.0283	1.0276	1.0415	1.067	1.051
11	1.047	1.0498	1.0445	1.0443	1.0773	1.0652	1.0571
12	1.053	1.057	1.0636	1.095	1.0537	1.0538	1.0536
13	1.047	1.0594	1.0793	1.0519	1.0472	1.0492	1.0507
14	1.02	1.0718	1.0315	1.0198	1.0223	1.0287	1.0345
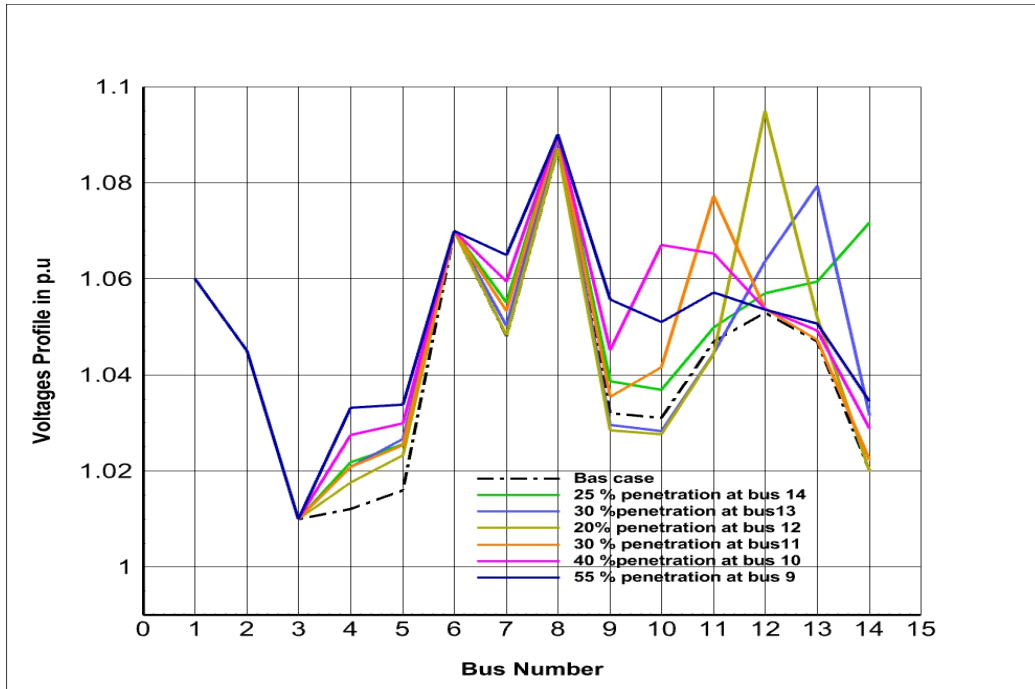
Figure IV. 5: Voltage profile of the test power system

IV.2.2.3 Power flow results of integration Solar PV system (case two)

Power flow in the power system grid lines is due to the integrated 25% solar PV system through bus 14, and power flow results are shown in tables IV.6 and IV.7.

Table IV. 6: Results of power flow of the grid with solar PV system

bus	V [p.u]	V ang	P gen	Q gen	P load	Q load
Bus 01	1.06	0	163.532	0	0	5.646
Bus 02	1.045	-3.503	40	29.603	21.7	12.7
Bus 03	1.01	-10.272	0	22.109	94.2	19
Bus 04	1.0218	-7.034	0	0	47.8	3.9
Bus 05	1.0255	-5.827	0	0	7.6	1.6
Bus 06	1.07	-7.982	0	17.04	11.2	7.5
Bus 07	1.055	-7.536	0	0	0	0
Bus 08	1.09	-7.536	0	21.632	0	0
Bus 09	1.0387	-7.801	0	0	29.5	16.6
Bus 10	1.0368	-8.116	0	0	9	5.8
Bus 11	1.0498	-8.167	0	0	3.5	1.8
Bus 12	1.057	-8.105	0	0	6.1	1.6
Bus 13	1.0594	-7.504	0	0	13.5	5.8
Bus 14	1.0718	-3.605	**64.75**	0	14.9	5

Chapter IV Simulation and Results Analysis

Table IV. 7: Results of power flow in the power grid branches with solar PV system (case two)

Element Name	Type	From Bus	To Bus	P flow	Q flow	P losses	Q losses
Branch-1	Line	Bus 01	Bus 02	112.464	-9.42	2.1888	0.8333
Branch-2	Line	Bus 01	Bus 05	51.068	3.775	1.2746	-0.0893
Branch-3	Line	Bus 02	Bus 03	64.424	4.502	1.8064	2.9848
Branch-4	Line	Bus 02	Bus 04	38.02	0.345	0.7722	-1.6512
Branch-5	Line	Bus 02	Bus 05	26.131	1.802	0.3631	-2.5357
Branch-6	Line	Bus 03	Bus 04	-31.582	4.626	0.682	-1.8301
Branch-7	Line	Bus 04	Bus 05	-50.07	6.663	0.3274	-0.3084
Braach-8	Trans	Bus 04	Bus 07	4.616	-5.123	0	0.0911
Branch-9	Trans	Bus 04	Bus 09	2.637	3.012	0	0.0802
Branch-10	Trans	Bus 05	Bus 06	17.565	13.574	0	1.0257
Branch-11	Line	Bus 06	Bus 11	5.72	8.157	0.0823	0.1724
Branch-12	Line	Bus 06	Bus 12	2.884	4.036	0.0264	0.055
Branch-13	Line	Bus 06	Bus 13	-2.239	9.895	0.0595	0.1171
Branch-14	Trans	Bus 07	Bus 08	0	-20.938	0	0.6938
Branch-15	Line	Bus 07	Bus 09	4.616	15.725	0	0.2654
Branch-16	Line	Bus 09	Bus 10	6.908	-0.273	0.0141	0.0374
Branch-17	Line	Bus 09	Bus 14	-29.155	2.064	1.0065	2.141
Branch-18	Line	Bus 10	Bus 11	-2.106	-6.11	0.0319	0.0746
Branch-19	Line	Bus 12	Bus 13	-3.243	2.381	0.032	0.0289
Branch-20	Line	Bus 13	Bus 14	-19.073	6.33	0.6151	1.2524
Total losses						**9.2823**	**3.4384**

In the load flow study, the power grid network variables are represented by tables IV.1 and IV.6 respectively. It can be seen from two tables that the incorporation of solar photovoltaic power into the power system resulted in the following outcomes:

1/ The quantity of active power produced by the main generator, also known as the swing generator, declined from 232.596 MW to 163.532 MW, while the amount of reactive power absorbed by it decreased from 14.962 Mvar to 5.646 Mvar. In addition, there is no question that this offers financial advantages for the power system.

2/ The reactive power generated by of generator 2 decreased from 49.114 Mvar to 29.603 Mvar

3/ For compensator generator 3, it decreased from 27.552 Mvar to 22.109 Mvar, for generator 6, it decreased from 22.957 Mvar to 17.04 Mvar, and for generator 8, it decreased from 24 Mvar to 21632 Mvar.

Chapter IV Simulation and Results Analysis

4/ It can also be noted that there is a clear improvement in the voltage and its angle, which is reflected in the direction of flow of both active and reactive power in the network branches.

The flow of active power and reactive power across the various branches of the test power system is depicted in Tables IV.2 and IV.7 respectively. It can be observed that the flow of the active power always depends on the angle that exists between the voltages at the two points, and that it flows from the voltage that exists at the angle with the greatest magnitude to the voltage that exists at the voltage with the smallest magnitude. Also, we take note of the fact that the transmission of the reactive power is dependent on the amplitude of the voltage, and that it travels from the voltage with the greater amplitude to the voltage with the lower amplitude. In every instance, however, it is essential to have knowledge about the placement of the busbar as well as the distance between it and the generator. When you see the indication (-), it means that the flow will go in the opposite direction to the one that was given.

It is clear from looking at Table IV.7 that the incorporation of the solar power system into the existing power system has the potential to change the direction of flow of both the active power and the reactive power. Thus, this modification needs to be taken into consideration, particularly when alterations are being made to protection systems such as directional protection.

IV.3 Steady State (Static) Voltage Stability Analysis

In order to enhance the effectiveness and precision of analyses, provide an extensive and in-depth grasp of the problem of voltage stability, and determine the causes of instability, the stability of voltage of the system network incorporated with distributed solar PV power system is looked at employing made up of four approaches: sensitivity analysis, modal analysis, P-V curve using CPF, and Q-V curve. These four techniques are used with the aim to enhance the analyses' effectiveness and precision. Modal analysis is used to evaluate the state of voltage stability in the system network as well as to identify the bus and area with the lowest strength. Sensitivity analysis is utilized to assess the sensitivity of the system's buses and identify the most sensitive of them. P-V curve is plotted to determine the maximum load percentage of power system as well as buses critical voltage. Q-V curve is also drowned to determine margin of reactive power of system buses. To make an analytical comparison, two most appropriate places to integrate solar PV generation is chosen. The impact of combining 70MW of distributed solar PV power unit operating at unity P.F into the grid is considered. IEEE 14-bus system described in figure 5.2 is considered for study. All analysis results are achieved using the NEPLAN software package. Figure IV.6 illustrates the methodology used for the analysis.
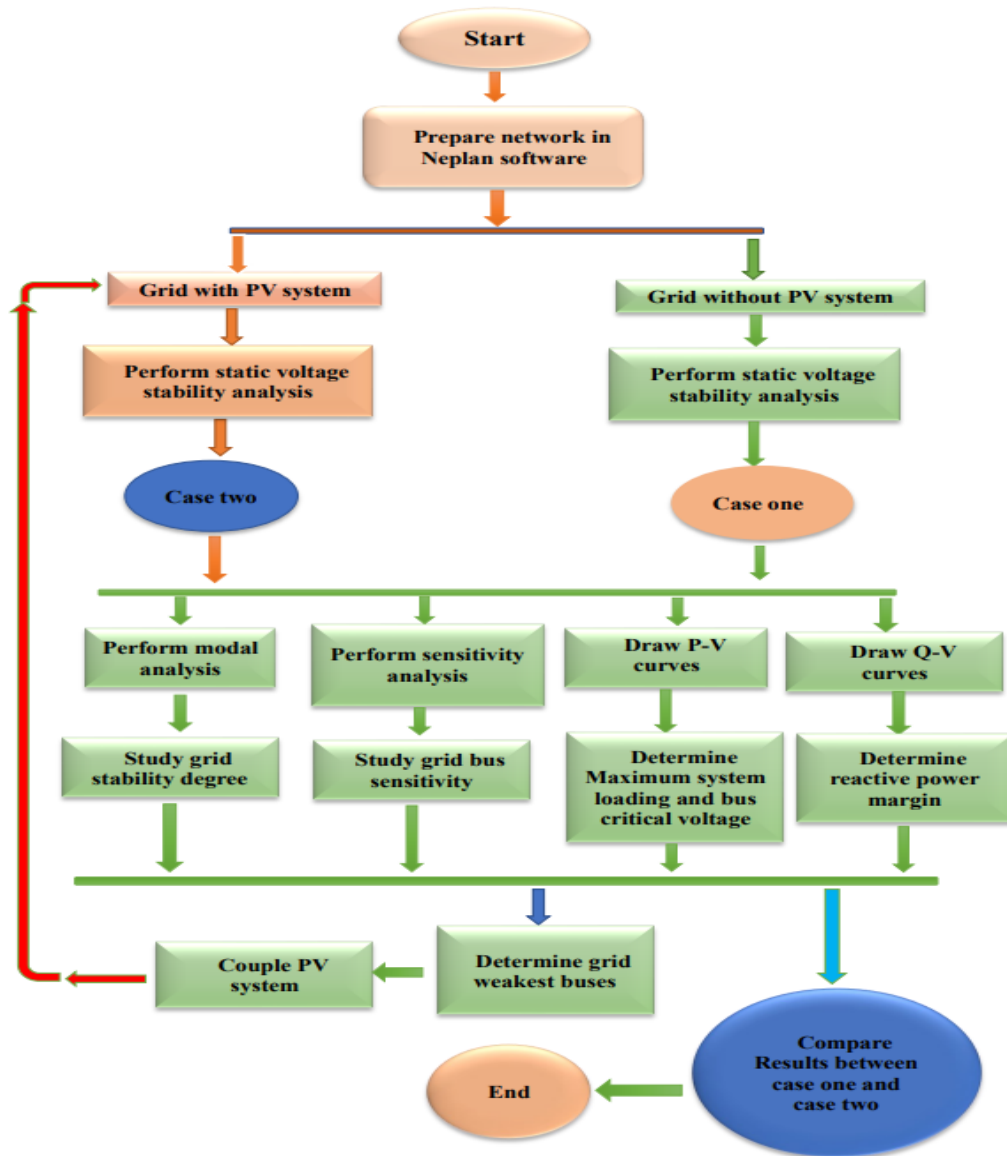
Figure IV. 6: Static voltage stability analysis methodology flow chart

IV.3.1 Determining the IEEE 14 system's weakest bus

A model analysis technique is utilized in order to examine the system's voltage stability. This allows for the measurement of the system's stability as well as the identification of the busses and weakest areas that could serve as suitable locations for the incorporation of distributed solar PV power. If there are any eigenvalues in the system that are negative, then we refer to the system as having unstable voltage. An eigenvalue of zero is a warning sign that voltage instability is about to occur. shows that a relatively minor adjustment to the amount of reactive power injection can result in a significant shift in the amplitude of the voltage. In addition to this, the small eigenvalues shed light on the degree to which the system voltage is unstable.

Table IV. 8: Eigenvalues of 14-bus system network

No	1	2	3	4
Eigenvalue	**2.0792**	5.3877	7.5987	9.4942
No	5	6	7	8
Eigenvalue	16.0985	18.8474	19.3553	38.8332
No	9			
Eigenvalue	64.9284			

As can be seen in Table IV.8, the test system has a total of nine different eigenvalues. This is because there are a total of 14 buses in the system, with one serving as a representation of the swing bus and four serving as representations of the PV bus. Table IV.8 shows that all of the eigenvalues are positive, which demonstrates that the testing system is stable. The smallest eigenvalue is = 2.0792, which denotes the critical mode and offers an indicator of how near the system is to being unstable. The bus participation factors may be seen in Figure IV.7, and they are determined by the eigenvalue that is the lowest. Figure IV.7 reveals that load buses 14,10,9, and 11 are the ones that are the closest to the point where the voltage will collapse. Furthermore, bus 14 has the highest bus participation factor of 0.2374, which indicates that it is the load bus that represents the weakest link in the test system. This is followed by buses 10,9, and 11, respectively. It is an ideal place for integrating the PV system unit into the system.
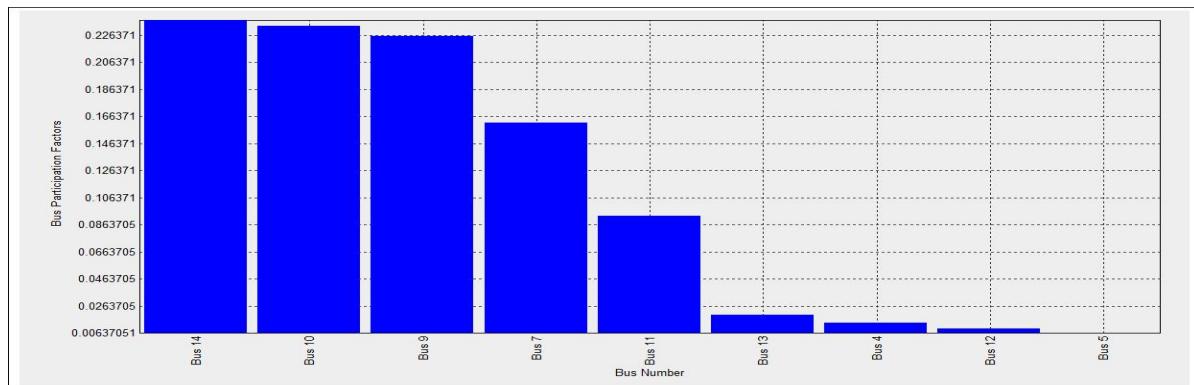
Figure IV. 7: Bus participation factors of IEEE 14- bus system

In other words, a test system's zone encompassing buses 14, 10, 9, and 11 signifies a weak stability region. Contrarily, the strongest nodes in the test system are bus 4 and bus 5, which have the lowest bus participation factors of 0.0139 and 0.0064, respectively. Additionally, it should be noted that only PQ load buses have a participation factor since buses 2, 3, 6, and 8 are PV buses, where the voltage is constant, whereas bus number 1 is a swing bus. Besides, the

model analysis considers how variations in reactive power and voltage in the particular bus relate to each other.

IV.3.2 Effect of incorporation of a dispersed solar PV power system

IV.3.2.1 Impact on the state of voltage stability

Table IV.9 illustrates how the integration of 70 megawatts power of distributed photovoltaic solar power generation that is running at unity power factor into the network of the testing system via buses 14 and 10 affects the stability of the voltage. In this case, an adequate evaluation of the system's stability is obtained by taking into account the four eigenvalues with the least absolute values. It can be noticed from the table that the stability of the test system voltage improved after the incorporation of distributed solar PV power. Specifically, it can be seen that the amplitude of the smaller eigenvalue increased from 2.0792 to 2.7389 in the case of adding distributed solar PV power generation to bus 14 and from 2.0792 to 2.7283 in the case of adding distributed solar PV power generation to bus 10.

Table IV. 9: Four smallest eigenvalues of the test system with solar PV power

Base case Eigenvalues [Mvar / %]	PV power at bus 14 Eigenvalues [Mvar / %]	PV power at bus 10 Eigenvalues [Mvar / %]
2.0792	2.7389	2.7283
5.3877	5.6029	5.5631
7.5987	7.7551	7.6399
9.4942	11.3257	11.3604

IV.3.2.2 Influence on the sensitivity degree of system buses

The sensitivity analysis method is applied to the process of analysing the IEEE 14-bus system network. It establishes the link between the change in voltage and the change in reactive power. It has been discovered that bus 14, which has a sensitivity amplitude value equal to 0.2233, is the bus that is the most sensitive. This is followed by buses 10, 9, 12, and 11. The bus 5 sensor had the lowest sensitivity value of any one that was measured, which was 0.0427, as can be shown in figure IV.8. The higher the level of the system's stability, the smaller the sensitivity amplitudes should be. Therefore, bus 5 is considered to be a powerful bus among all of the system's PQ load buses, with bus 4 coming in second. This indicates that these two buses have less fluctuation in their voltage and are therefore less likely to cause voltage instability. As the system's stability decreases, the amplitude of sensitivity will continue to increase. On the other hand, an unstable operation is indicated by a sensitivity rating in the negative range. A relatively low negative sensitivity indicates a process that is particularly prone to instability.

Chapter IV Simulation and Results Analysis

According to the data presented in Figure IV.8, the sensitivity amplitudes of voltage-controlled buses are equal to zero.
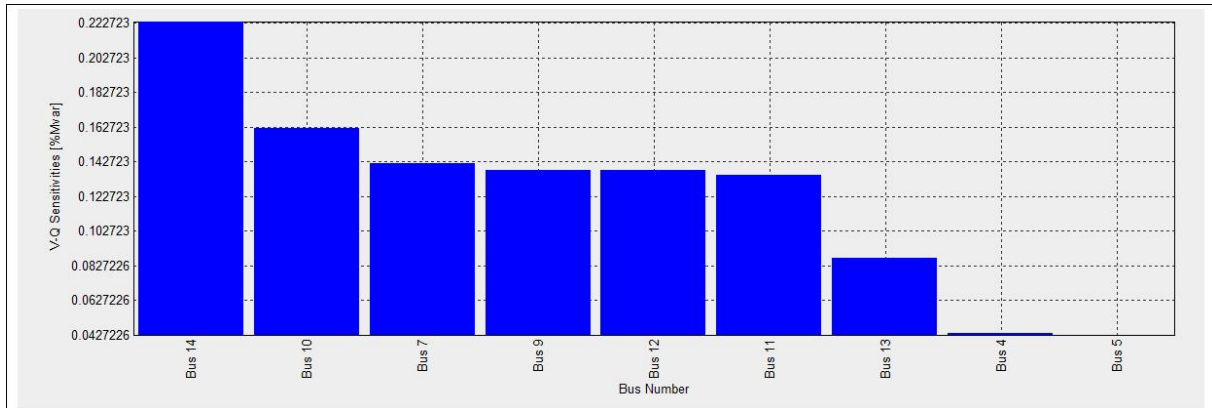
Figure IV. 8: V-Q Sensitivity [%/Mvar] of IEEE 14- bus system

The test system is subjected to a sensitivity analysis with the inclusion of distributed PV power, and the findings of the analysis may be found in table IV.10 below. The fact that the test system is now more stable can be inferred from the fact that the sensitivity of the buses has decreased, as shown in Table IV.10, which shows that the system has improved overall. The system's stability improves in direct proportion to the sensitivity amplitude's decrease. As can be seen, the sensitivity of buses 14 and 10 fell by 9.54% and 13.20%, respectively, when distributed solar PV power was incorporated at bus 14, and decreased by 6.18% and 14.74%, respectively, when distributed solar PV power was incorporated at bus 10.

Table IV. 10: Bus sensitivity of IEEE -14 bus system with and without solar PV power

Bus no	V-Q Sensitivities [%/Mvar] Base case	Solar PV power at bus14 [%/Mvar]	Solar PV power at bus10 [%/Mvar]
14	0.2233	0.2020	0.2095
10	0.1621	0.1407	0.1382
12	0.1377	0.1370	0.1374
11	0.1353	0.1295	0.1284
9	0.1377	0.1069	0.1064
13	0.0872	0.0857	0.0864
7	0.1417	0.0775	0.0773
5	0.0427	0.0407	0.0407
4	0.0440	0.0401	0.040

IV.3.2.3 Influence on the margin of the reactive power

As can be seen in Figures IV.9 and IV.10, the QV curve is sketched in order to determine the reactive power margin of the load buses used in the testing system. It is clear from reviewing the two statistics that bus number 14 has the least amount of reactive power of all the buses. This is followed by bus numbers 12, 13, 11, and 10. This indicates that there is a limited possibility of raising the reactive power load on these buses before exceeding the loading limit and prior to the occurrence of voltage collapse. On the other hand, it is observable that buses 5 and 4 have a high reactive power margin, which implies that they are very stable buses. This can be deduced from the fact that they are buses 5 and 4. It should be noted that the synchronous compensators in the buses 3 and 6 to which the loads are connected supply the reactive power needed for these loads. Bus 2's generator also provides reactive power to the bus. Therefore, these buses are classified as high-stability nodes.
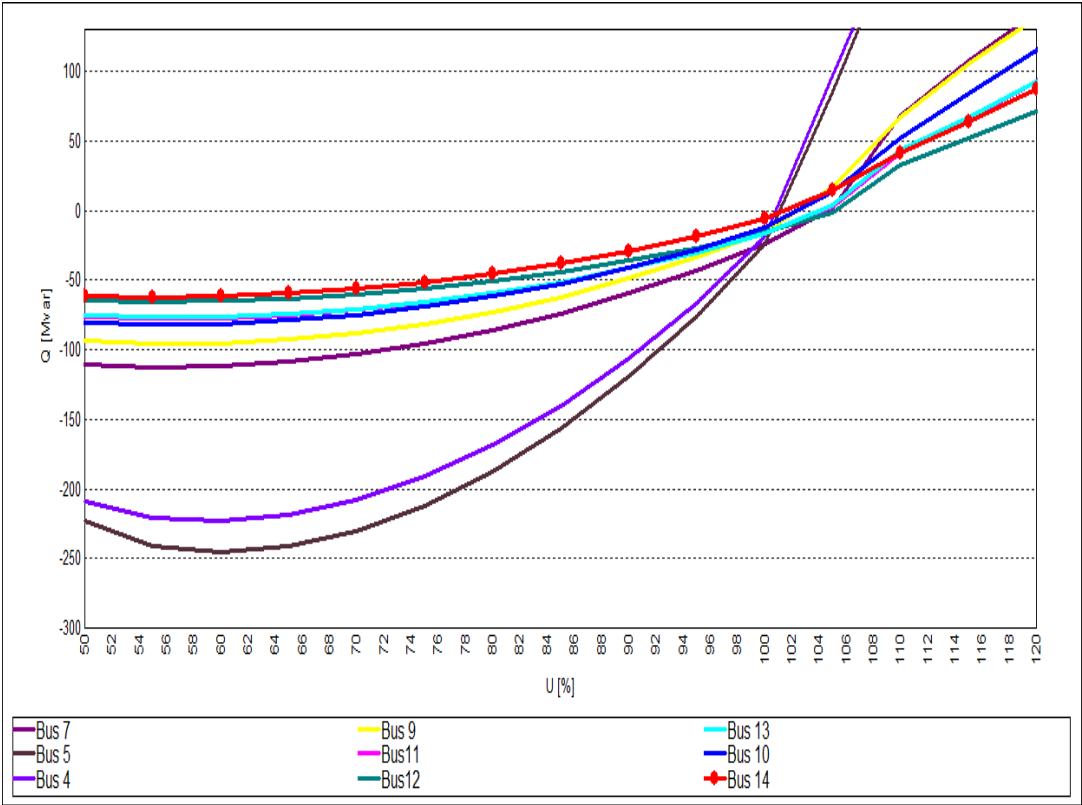
Figure IV. 9: QV curves of 14-node system grid for the baseline case
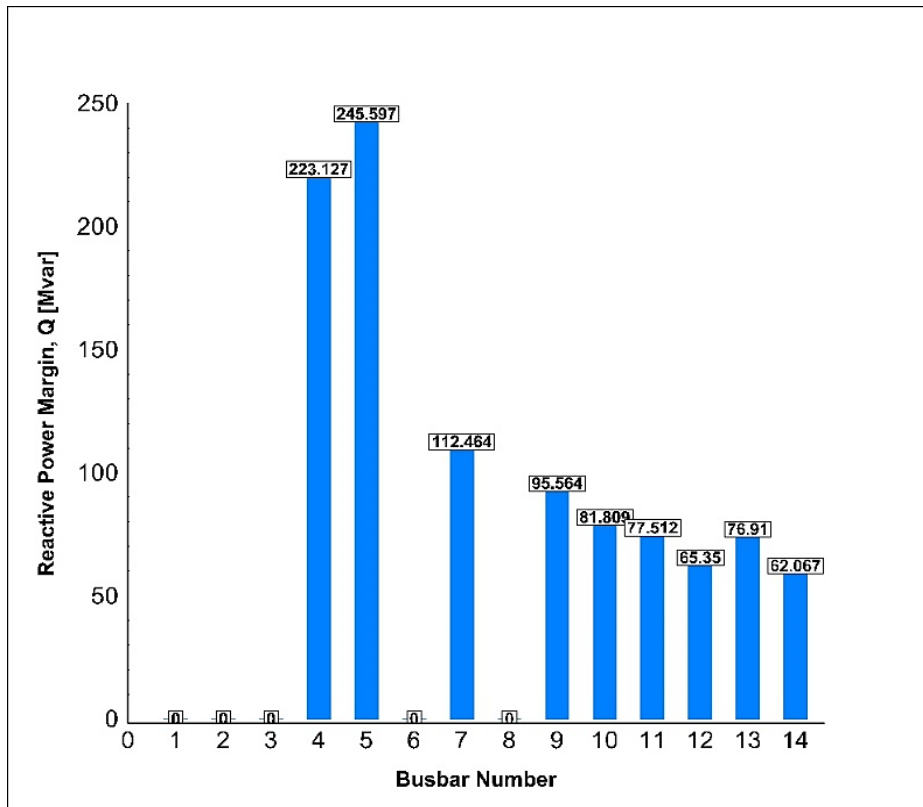
Figure IV. 10: Reactive power margin of 14-node network

It is common knowledge that the degree to which a system's reactive power margin is high determines the extent to which it can prevent the collapse of its voltage. However, the margin is smaller the closer the system runs to the critical point, and the more probable a voltage collapse is, therefore the margin gets smaller as well. As a result of incorporating distributed solar PV power generation into a test system through bus 14, the reactive power margin for the system buses has clearly improved, and the rate at which this improvement has occurred has increased, as shown in Table IV.11. This has led to an increase in the degree to which the system is protected against collapse. It is important to point out that the margins of reactive power for buses 14, 10, and 9 all increased by a value of 12.03%, 8.99%, and 8.58%, respectively. These buses, as was previously mentioned, are the source of the greatest contribution to the voltage decrease. The Q-V curve for the weakest buses is depicted in Figure IV.11, both before and after the integration of PV power at bus 14.

Chapter IV Simulation and Results Analysis

Table IV. 11: Reactive power margin enhancement as a result of adding solar PV power

Bus no	Reactive power margin [Mvar] Base case	Reactive power margin [Mvar] with PV power at bus14	Improvment rate [%]
Bus14	-62.083	-69.552	12.03
Bus13	-76.865	-84.440	9.85
Bus12	-65.334	-71.184	8.95
Bus11	-77.503	-84.463	8.98
Bus10	-81.820	-89.177	8.99
Bus9	-95.374	-103.553	8.58
Bus5	-245.682	-281.445	14.56
Bus4	-223.156	-254.299	13.96
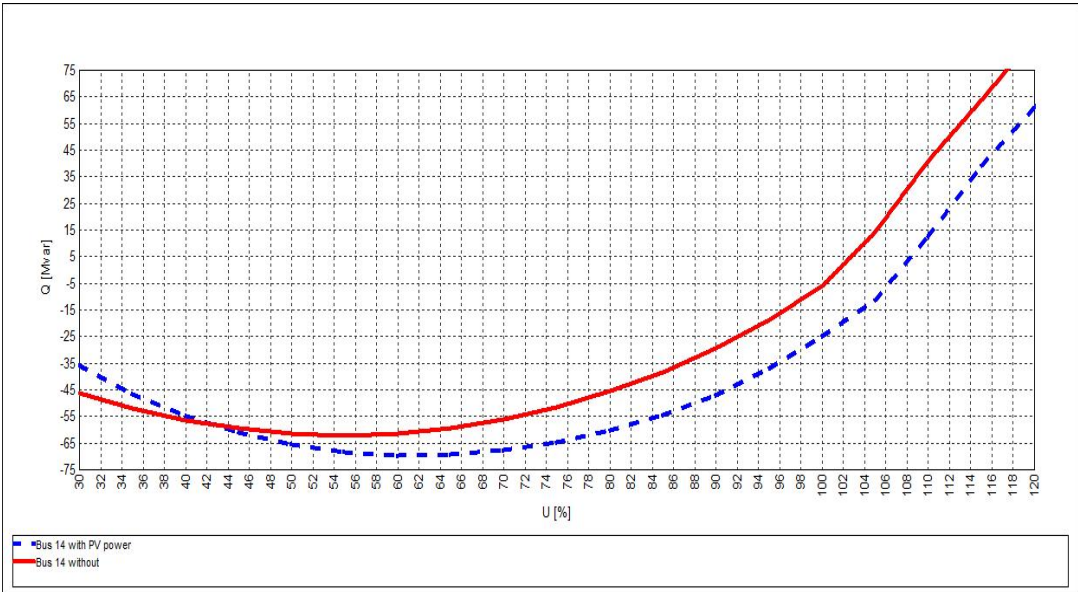
(a)
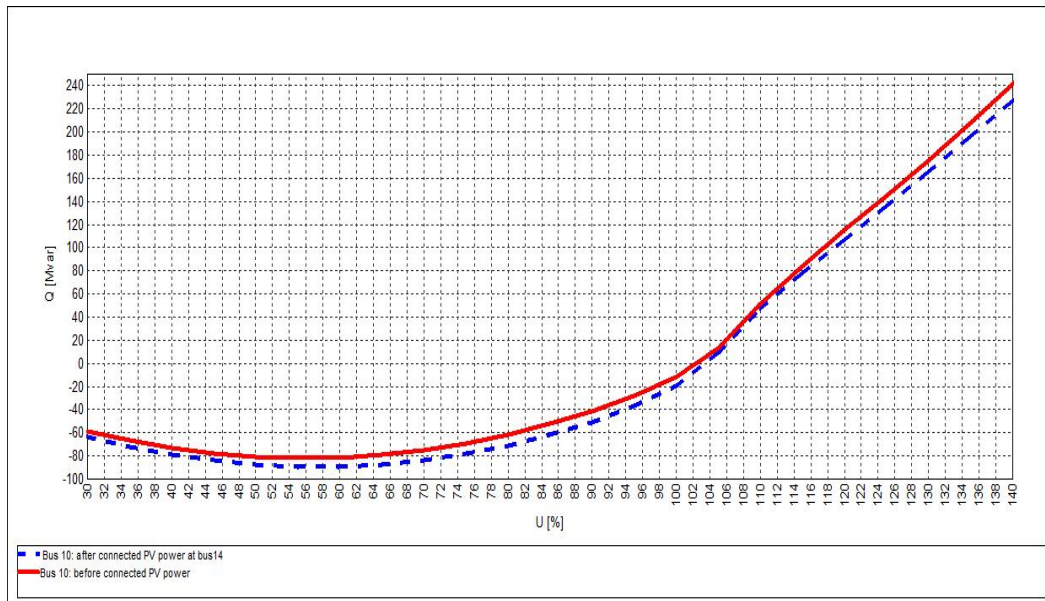
(b)
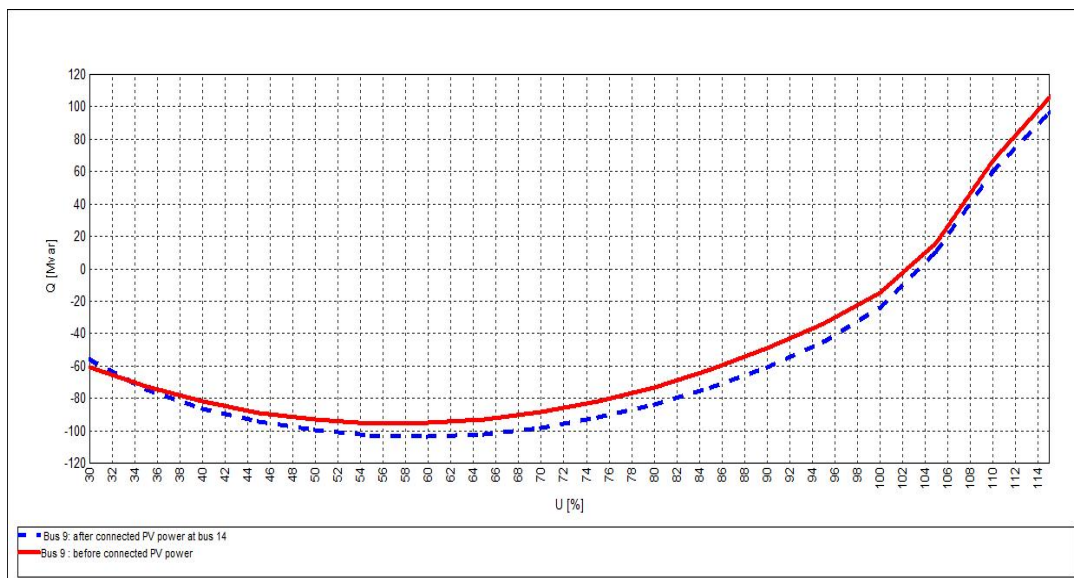
(c)

Figure IV. 11: Q-V curves prior to and after PV power inclusion at the weakest buses. (a) Bus 14. (b) bus 10. (c) bus9

IV.3.2.4 Influence on the percentage of maximum loading limit and the critical voltage

Plotting the PV curve allows one to determine both the maximum load percentage of the testing system and the bus's critical voltage, which is the point at which the voltage begins to collapse. The P-V curve of the system bus is depicted in Figure 5.12. It is possible to deduce from the figure that the voltage on bus 14 has the lowest voltage of all of the system buses, followed by bus 10 with the next lowest voltage. These buses are also regarded as being among the least reliable. Table IV.12 demonstrates how the critical voltage of the buses was affected as a result of the integration of distributed solar PV power into the testing power system through

98

buses 14. The favorable response of voltage at system buses and their tendency to enhance as a consequence of incorporating distributed solar PV power generation into the test system is observable as a result of looking at Table IV.12, which shows these characteristics. PV curves for the least powerful buses in the test system are depicted in Figure IV.13, both with and without a PV power unit.
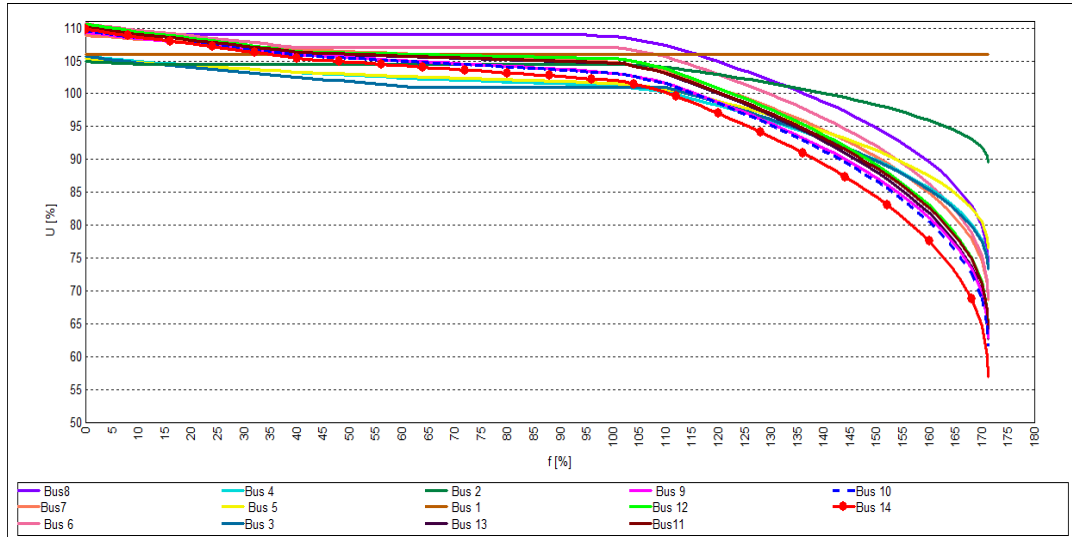
Figure IV. 12: P-V curves of IEEE14 -node network

Table IV. 12: Critical voltage of 14- bus system with and without solar PV power

Bus no	Bas Case V critial [%]	With PV power at bus 14 V critial [%]
Bus 1	106.00	106
Bus 2	90.49	90.49
Bus 3	74.99	74.99
Bus 4	75.19	75.82
Bus 5	78.07	79.03
Bus 6	71.54	72.79
Bus 7	71.04	72.35
Bus 8	76.56	77.78
Bus 9	65.66	66.68
Bus 10	64.64	65.42
Bus 11	67.09	68.00
Bus 12	67.19	68.58
Bus 13	65.63	68.33
Bus 14	60.18	68.75
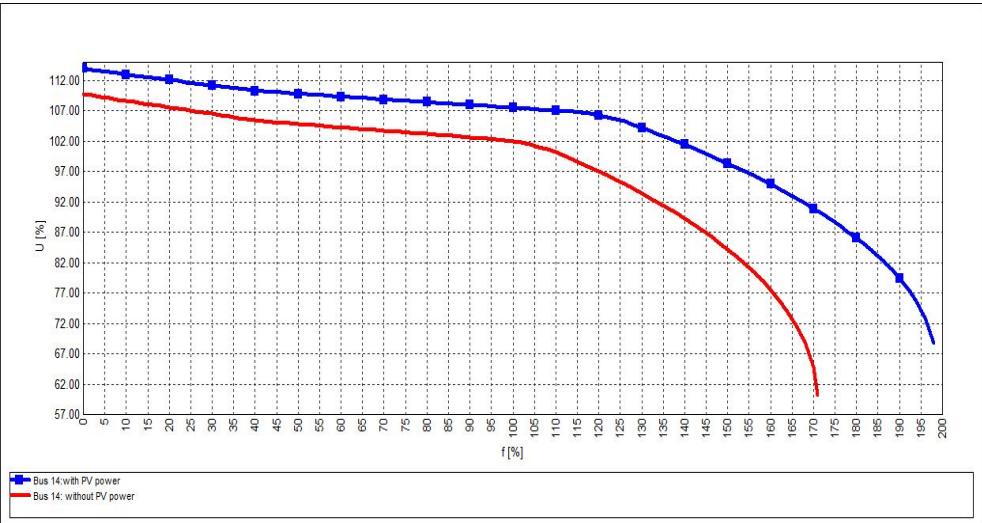
(a)
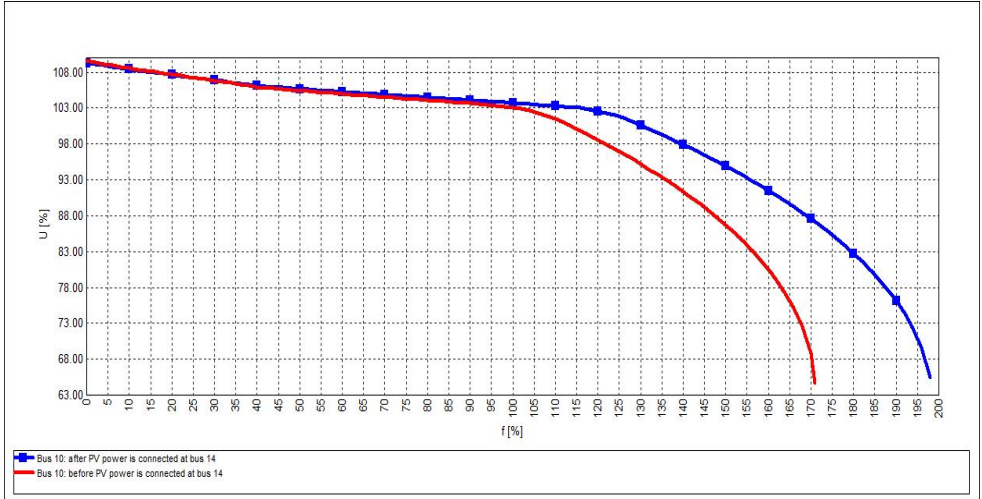
(b)
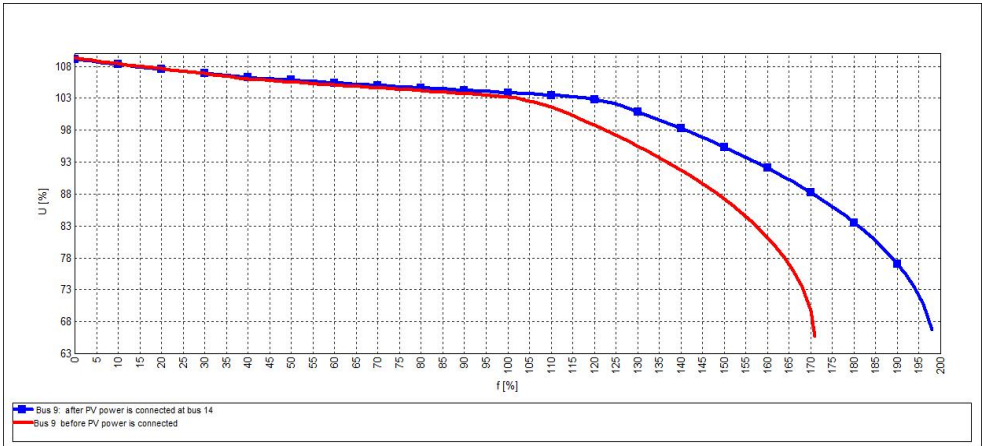
(c)

Figure IV. 13: curves prior to and after PV power inclusion at the weakest buses.

(a) bus 14, (b) bus 10, (c) bus 9.

Chapter IV Simulation and Results Analysis

The effect of adding distributed solar PV power on a test system loading is shown in table IV.13. In this analysis, different locations are considered to connect distributed solar PV power generation, and the resulting effect on test system MW loading is studied. It can be seen from Table IV.13 that the loading percentage increased and improved significantly when solar PV power was integrated into the testing system. Furthermore, it can be seen that the improvement rate of maximum loading reached 15.705% of the basic load in the case where bus 14 was chosen as the location for the integration. The above data is presented as a result of bus 14 being selected as the location for the incorporation. In other words, the system becomes less prone to collapse with the presence of solar PV power. It can also be observed that the addition of distributed solar PV power in weak buses gave a significant improvement in the system loading compared to strong buses. Because the inclusion of distributed solar PV power generation into a test system expanded system loading, new loads can be added without the requirement to replace the equipment of the power system with capacities corresponding with the added loads. This is because the system loading increased when distributed solar PV power generation was included. Therefore, this is a significant economic benefit for the people in charge of planning and operations. The amount of active and reactive power that can be added to each load bus due to integrated solar PV system in the grid through bus14 is shown in the table.IV.14 and table.IV.15 respectively. Which are illustrated in figure IV.14 and IV.15 respectively.

Table IV. 13: Maximum loading level of 14-bus system network with solar PV power

Grid status	Maximum loading (MW)	Loading percentage (%)	Change rate (%)
Base Case	442.89	171.000	0
With PV power at Bus 14	512.820	198.000	15.789
With PV power at Bus 10	505.05	195.000	14.035
With PV power at Bus 9	507.640	196.000	14.620
With PV power at Bus 5	466.200	180.000	5.236
With PV power at Bus 4	476.560	184.000	7.602

Chapter IV Simulation and Results Analysis

Table IV. 14: Maximum active power in each load bus with and without solar PV power

Bus No.	$P_{L\,acual}$ (MW)	$P_{L\,max}$ (MW) Without PV power	$P_{L\,max}$ (MW) With PV power
Bus 1	0	0.000	0.000
Bus 2	21.7	37.134	42.966
Bus 3	94.2	161.200	186.516
Bus 4	47.8	81.798	94.644
Bus 5	7.6	13.006	15.048
Bus 6	11.2	19.166	22.176
Bus 7	0	0.000	0.000
Bus 8	0	0.000	0.000
Bus 9	29.5	50.482	58.41
Bus 10	9	15.401	17.82
Bus 11	3.5	5.989	6.93
Bus 12	6.1	10.439	12.078
Bus 13	13.5	23.102	26.73
Bus 14	14.9	25.498	29.502
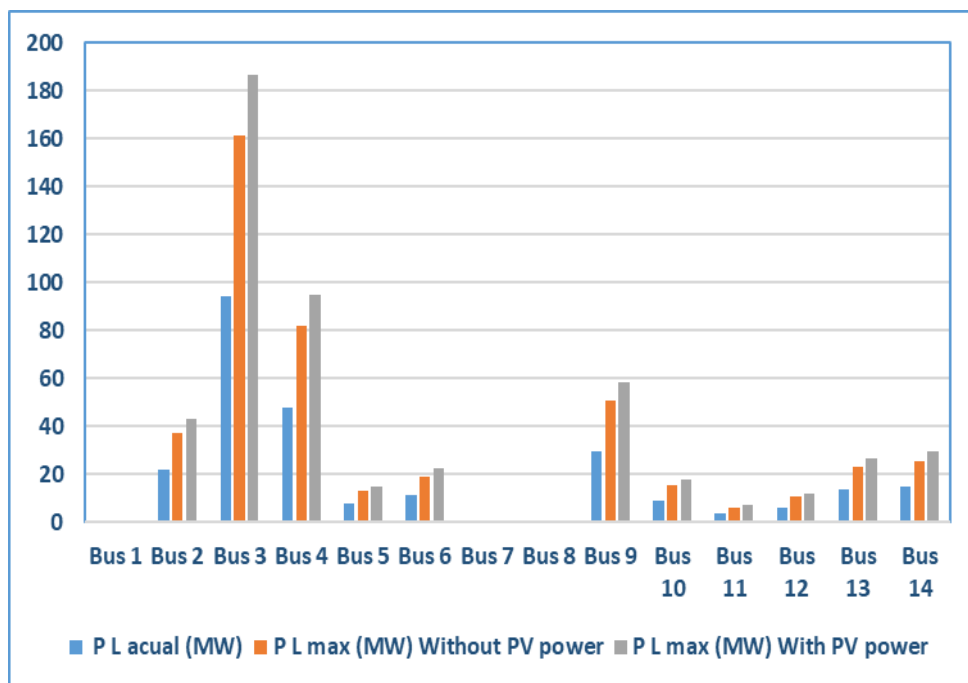
Figure IV. 14: Maximum active power at load buses with and without solar PV system unit

Chapter IV Simulation and Results Analysis

Table IV. 15: Maximum reactive power at each load bus with and without solar PV power

Bus no	$Q_{L\,acual}$ (Mvar)	Q_{Lmax} (Mvar) Without PV power	Q_{Lmax} (Mvar) With PV power
Bus 1	0	0.000	0.000
Bus 2	12.7	21.733	25.146
Bus 3	19	32.514	37.620
Bus 4	3.9	6.674	7.722
Bus 5	1.6	2.738	3.168
Bus 6	7.5	12.834	14.850
Bus 7	0	0.000	0.000
Bus 8	0	0.000	0.000
Bus 9	16.6	28.407	32.868
Bus 10	5.8	9.925	11.484
Bus 11	1.8	3.080	3.564
Bus 12	1.6	2.738	3.168
Bus 13	5.8	9.925	11.484
Bus 14	5	8.556	9.900

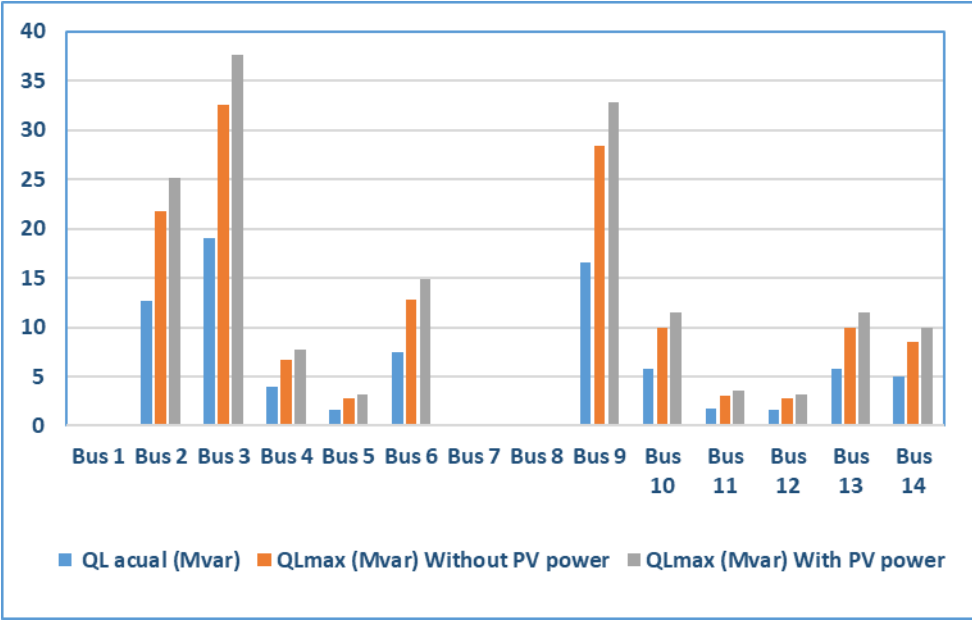**Figure IV. 15:** Maximum reactive power with and without solar PV system unit

IV.4 Transient Stability Analysis

The primary purpose of this study is to present an approximate dynamic analysis that examines the effect of incorporating the Zaouiet Kounta solar photovoltaic power plant into the

current distribution system. This is done in order to study the influence of its integration while the distribution network is experiencing transient conditions. The analysis of all the results is carried out in ETAP, which is software designed specifically for studies on power systems. With the use of transient analysis, we investigate the effect that the solar photovoltaic plant has on the fluctuations that occur in the distribution network. The ability of the power system to retain synchronism in the face of a significant perturbation, such as a fault, a loss on a transmission line, the loss of a large generating unit, or something similar, is what is meant by the term "transient stability."[95]. The duration of the perturbation that is being studied for transient stability is typically between three and five seconds. Utility engineers would be capable of assessing whether or not the addition of a PV system would affect the stability of the system if they analyzed the electrical network under a variety of different transient situations. As a consequence of this, the test distribution network is put through three distinct transient scenarios for the purpose of this investigation. These scenarios include: I a fault on the network main busbar; ii) an abrupt disconnection of load; and iii) an abrupt loss of PV power. The result shows the voltage and frequency at the main busbar, as well as the rotor angle of generator. In this analysis, the results for 3 MW, 6 MW, and the basic scenario with no PV power in the distribution network are analyzed in order to demonstrate the influence that increasing the PV power has on the performance of the network when it is through a transient. Since it is common knowledge that PV units do not contain any moving parts, there is no possibility of an inertia response being delivered when there are disruptions in the network. Once photovoltaic (PV) power begins to permeate the grid, the total system inertia will begin to decrease. When there is less inertia in the system, the oscillations of the system will be greater. The performance of the system is further impacted by high angle variations between the bus voltages, which are brought about by the injection of PV power. Three scenarios for feeding a distribution network are considered:

1- A grid source with a conventional power plant

2- A grid source alone

3- A conventional power plant (without and with control units; exciter and AVR system and turbine governor)

The three different transient circumstances are analyzed for each above scenario. Figure IV.16 illustrates the methodology used for the analysis.
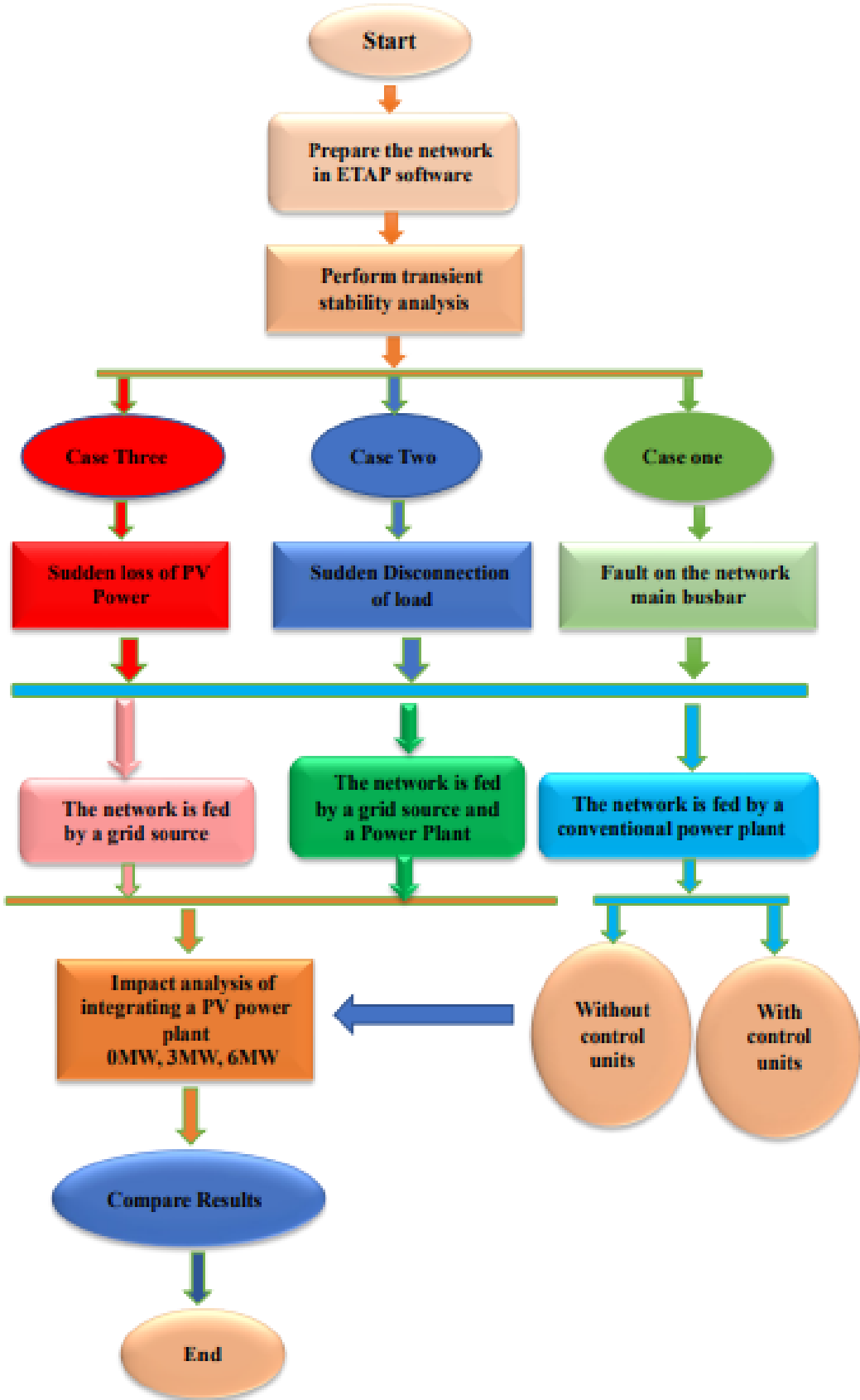
Figure IV. 16: Transient stability analysis methodology flow chart

Chapter IV Simulation and Results Analysis

IV.4.1 A description of a solar photovoltaic power plant and distribution network

Southwest Algeria is the location of the solar power plant that is being constructed in the Zaouiet Kounta region (wilaya Adrar). It has a surface area of 12 hectares and is formed of 24,552 panels. Moreover, it is linked to a main busbar of a 30 kV distribution network. This plant is made up of six (6) photovoltaic sub-fields, each of which has its own 1 MW output, and 93 arrays. Each array is made up of 44 panels that have been divided into two strings, and each string has 22 panels that are connected in series. Each sub-field is further subdivided into two connected fields, each of which is independently connected to a 1.25/0.630/0.630 MVA step-up three-winding transformer through the use of two 500 kW inverters. The generation voltage of 0.315 kV is increased by the transformer to 30 kV, and it is then injected into the distribution network that operates at 30 kV. The panels are of the YL245P-29b type and were manufactured by YINGLI SOLAR utilizing polycrystalline silicon. The inverters are of the SG 500MX type and were manufactured by Sun Grow.

The test network is a medium-voltage distribution network with nine (9) loads. These loads are designated as follows: CDRAS 1, CDRAS 2, CDRAS 3, CDRAS 4, REG N, REG S, ZK, MEKKKID, and AIN ELFETH. The values of these loads are as follows: 0.52 MVA, 1.559 MVA, 6.235 MVA, 5.196 MVA, 3.897 MVA, 5.196 MVA, 3.793 MVA, and 5. There is a 30-kilovolt load here. The network that is being analyzed here receives its electricity from one of three sources: either a grid source via a 220 KV transmission line, Adrar-Zaouiet Kounta, and a step-down transformer of 40 MVA at 220/30 kV; a traditional power station; or both a traditional power station and a grid source working together. If a grid source is not available, a traditional power station is the only option. The traditional power station is comprised of four gas turbine units, each with a capacity of 17 MW. Each of every two units is linked to a step-up transformer that has three windings. (11.5KV, 11.5KV, 220KV). The four units each use a step-down transformer with a capacity of 40 MVA to transmit their power to the same 30 kV busbar. Additionally, in order to boost the overall performance of the grid, this plant is wired to connect to the Adrar grid via the Adrar - Zaouiet Kounta transmission. The figure IV.17. presents an overview of the ETAP network as well as the PV plant's physical configuration.
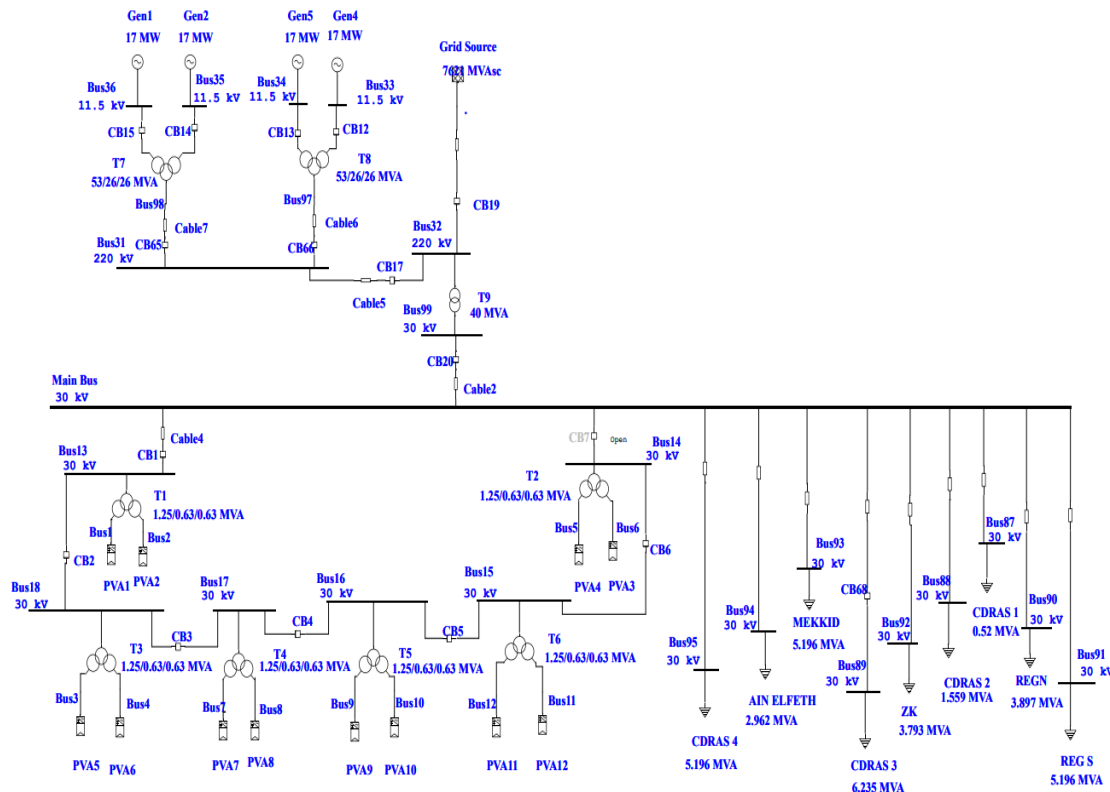
Figure IV. 17: The system network in ETAP as well as the PV plant's physical configuration

IV.4.2 Scenario one: A grid source and a conventional power plant together with distribution network

This scenario was done in the case that the distribution network is considered as a part of adrar public gid. . The distribution network performance under different transient condition is listed below.

1- Influence of fault on the system main bus

There are many other kinds of faults, but three-phase faults are particularly harmful because they can cause the entire system to become unstable. This defect generates extremely high-current short circuits. Because of this, significant thermal tensions are created, which in turn impact the electrical apparatus. Furthermore, instability issues are brought on by the fact that the three-phase voltage goes to zero for this type of fault. In this scenario, a three-phase-to-ground fault is applied to the main busbar of the network at a rate of one second for a duration of six cycles. Figure IV.18 displays the outcomes of the network when subjected to this scenario.

From the diagram of the frequency, figure IV.18(a), It is possible to observe that the frequency for the base case and after the fault is eliminated demonstrates minute oscillations, which gradually diminish until it stabilizes at its value in the stable condition. The frequency variations for the 3 MW and 6 MW PV powers are quite minor in compared to the base case,

and they quickly settle at the initial value of the frequency. In this case, photovoltaic (PV) electricity demonstrated a favorable reaction to the improvement of network frequency.

As can be seen in Figure IV.18(b), when a fault happens, the voltage for all of the various solar power outputs drops to almost zero before returning to its stable state.

Figure IV.18 (c) demonstrates the relative rotor angle. From figure IV.18(c), it can be noticed that the relative rotor angle for the base and for various PV powers after the fault is eliminated tends to oscillate, which gradually reduces until it returns to the value it had when it was in a condition of stable before the fault happened.
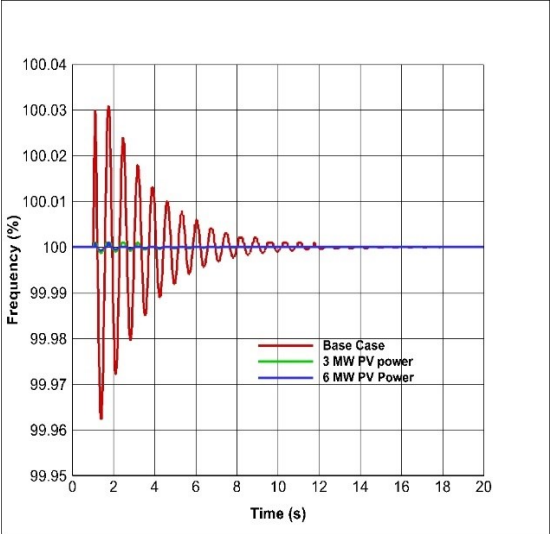
(a)
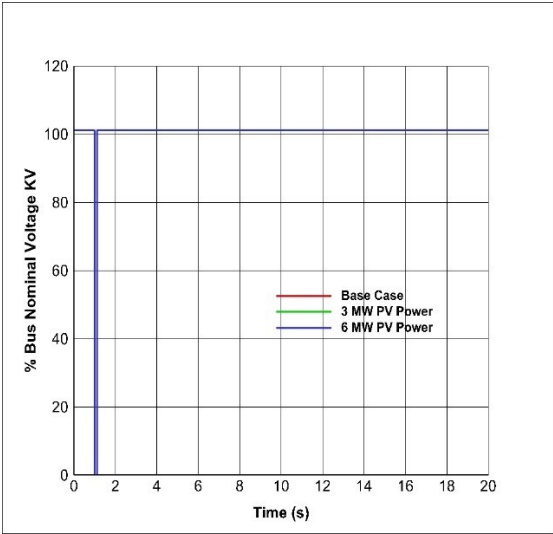
(b)
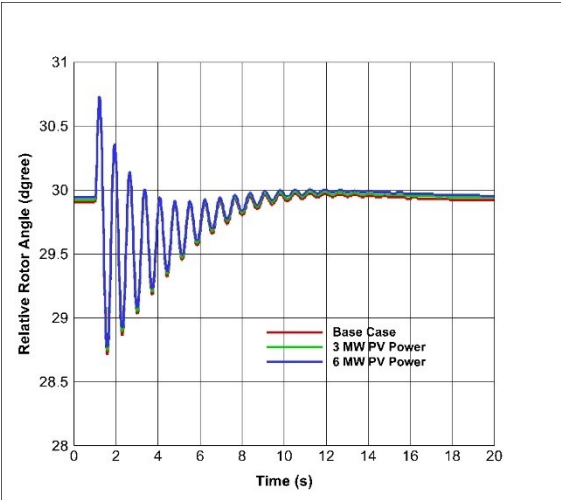
(c)

Figure IV. 18: Behavior of the system as a result of fault at main bus (a) Frequency at main busbar (b) Voltage a main bus (c) Relative rotor angle

2- Effect of the sudden removal of load

One sort of disturbance that might cause a system to become unstable is the unexpected disconnection of load that is present in the system. This scenario can only be carried out by disconnecting the load on CDRAS 3, which represents the biggest load in the test network (6.235 MVA), at the one-second. Figure IV.19 depicts the outcomes that occurred as a result of this scenario.

It is possible to deduce from the chart of the frequency that is presented in figure IV.19 (a) that the frequency did not change in response to the unexpected disconnection of the load and maintained its consistency across all of the various solar PV power levels. The voltage at the time of disconnecting the load reaches a higher value than it does when it is in a steady condition, as shown in figure IV.19 (b), which may be observed by referring to the diagram. The voltage increased from 101,094% to 101,832% while considering the base scenario. The voltage increased from 101.159% to 101.915% when 3 MW of PV power is utilized. The percentage of bus nominal voltage increased from 101.22% to 101.992% for 6 MW of PV power.. Figure IV.19 (c) depicted the performance of the relative rotor angle as a result of a sudden disconnect of the load. The relative rotor angle for the base case and different PV powers tends to oscillate with tiny oscillations, which gradually degrease and stabilize at a new value a little higher than its original value for the three cases, as shown in the figure.
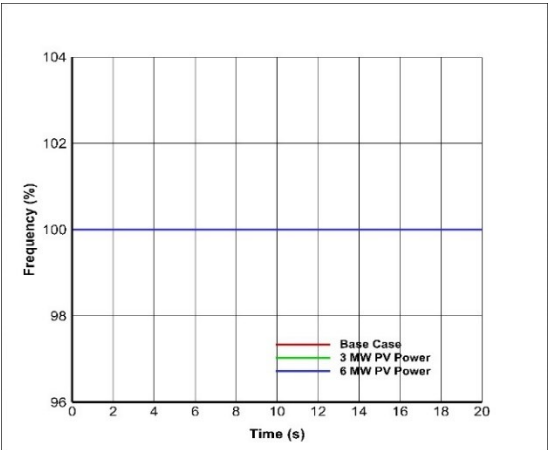
(a)
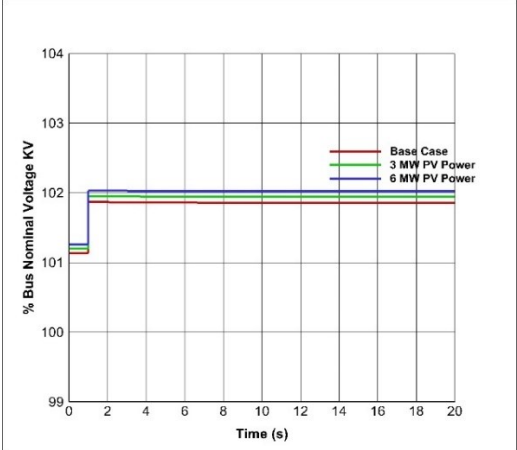
(b)
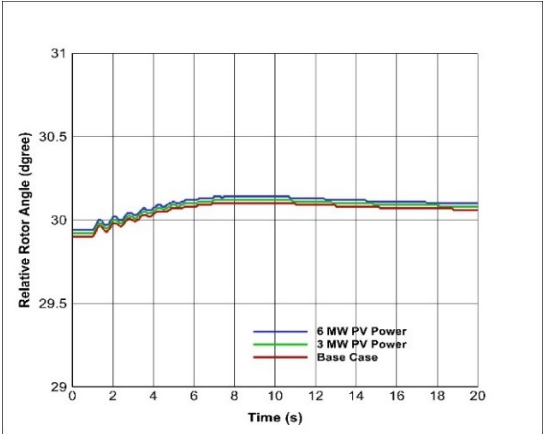
(c)

Figure IV. 19: System behavior due to sudden removal of load (a) Frequency at system main bus(b) Voltage at system main bus (c) Relative rotor angle

3- Impact of an abrupt loss of PV power

It is possible for the output of PV systems to fluctuate as a result of changes in the weather, which can result in the loss of a significant portion of the distributed power output of PV systems. Voltage drops might potentially result in the simultaneous shutdown of the connected PV system [130]. In the context of this scenario, PV power is expected to trip at a rate of 1 second for both the 3 MW and 6 MW PV power scenarios. Figure IV.20 illustrates the performance of the network when subjected to this situation.

Figure IV.20 (a) is an illustration of the frequency at the network main bus as a result of an abrupt loss of PV power. As may be seen in Figure IV.21 (a), the frequency does not change at all for two cases of PV power. When 3 MW of PV power is lost, the voltage on the bus reduces from 101.139% of the bus nominal voltage to 101.22% of the bus nominal voltage, as shown in figure IV.20 (b), which may be observed. In the case that a 6 MW PV power loss occurs, the bus voltage will drop from 101.22 % down to 101.08 % of its nominal value. The graph of the relative rotor angle that can be found in figure IV.20 (c) demonstrates that the relative rotor angle has a propensity to oscillate with little oscillations for two situations of PV power before beginning to gradually diminish until it stabilizes at its initial value.
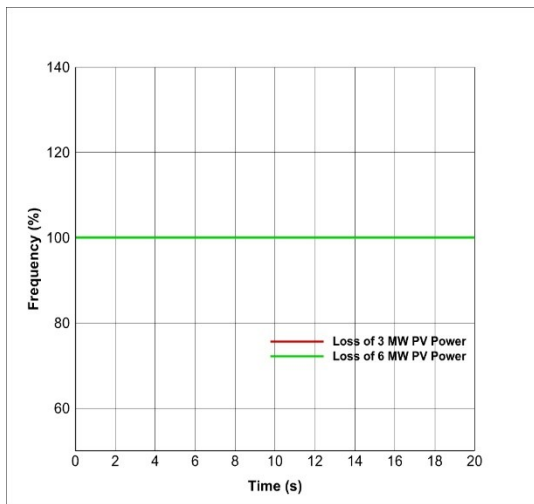
(a)
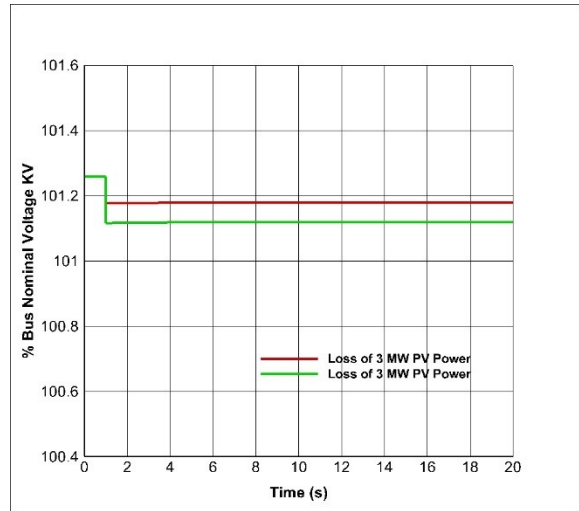
(b)
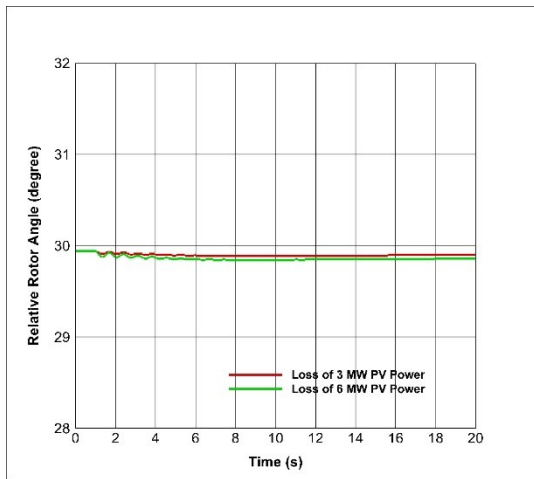
(c)

Figure IV. 20: System performance due to loss of PV power (a) Frequency at system main bus (b) Voltage at system main bus (c) Relative rotor angle

IV.4.3 Scenario two: A grid source is utilized to feed the system network

The planning for this scenario was done in preparation for the possibility that the generation station will be unavailable. As a result, the sole source that provides power to the distribution network in this scenario is the grid source. Figure IV.21 shows how the network works in a number of different "transient" situations.

Figure IV.21 (a) illustrate the frequency and the voltage at the network main bus due to fault in the main bus. When a fault happens, the voltage for all of the different powers of the solar power system drops to zero, and then it restores to its stable condition. This behavior viewed in figure IV.21(a). The frequency did not change regardless of the presence or absence of the malfunction, as evidenced by the chart of the frequency, which shows that the frequency maintained its consistency throughout all of the various solar PV powers.

111

The abrupt removal of the load is depicted in Figure IV.21 (b), along with its effect on the frequency and voltage at the main bus of the network. The voltage at the time of disconnecting the load reaches a higher value than it does when it is in a steady condition, as can be seen in figure IV.21 (b), which demonstrates this phenomenon. The voltage increased from 101,094% to 101,832% while considering the base scenario. The voltage increased from 101.159% to 101.915% when 3 MW of PV power was used. The increase for 6 MW of PV power was from 101.22 % to 101.992 % of the bus's nominal voltage. According to the frequency chart, it is possible to deduce that the frequency did not change at any point during the disturbance.

The unexpected loss of PV power is depicted in Figure IV.21 (c), along with its effects on the frequency and voltage at the main bus of the network. When 3 MW of PV power is lost, the voltage on the bus reduces from 101.139% to 101.22% of its nominal value, as shown in figure IV.21 (c), which may be observed by referring to this figure. In the event that 6 MW of PV power is lost, the bus nominal voltage falls from 101.22% to 101.08% of its original value. In addition, the frequency does not change in any way, as can be seen in the frequency chart.

the grid source operates as a buffer to absorb any fluctuations in power and maintain a consistent level of PV output. Yet, in order to accommodate the varying levels of power generated by PV systems, it is necessary to frequently modify the output of traditional power plants.

(a)

(b)

(c)
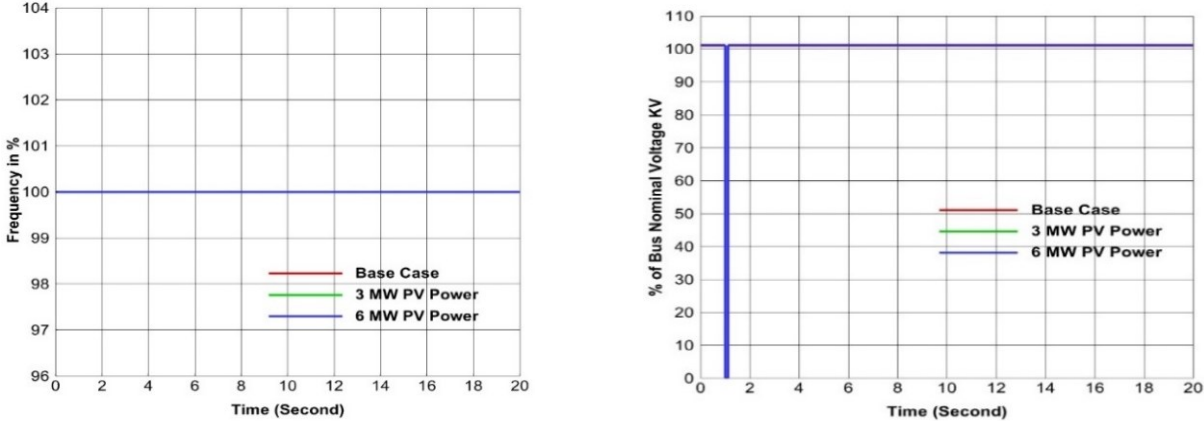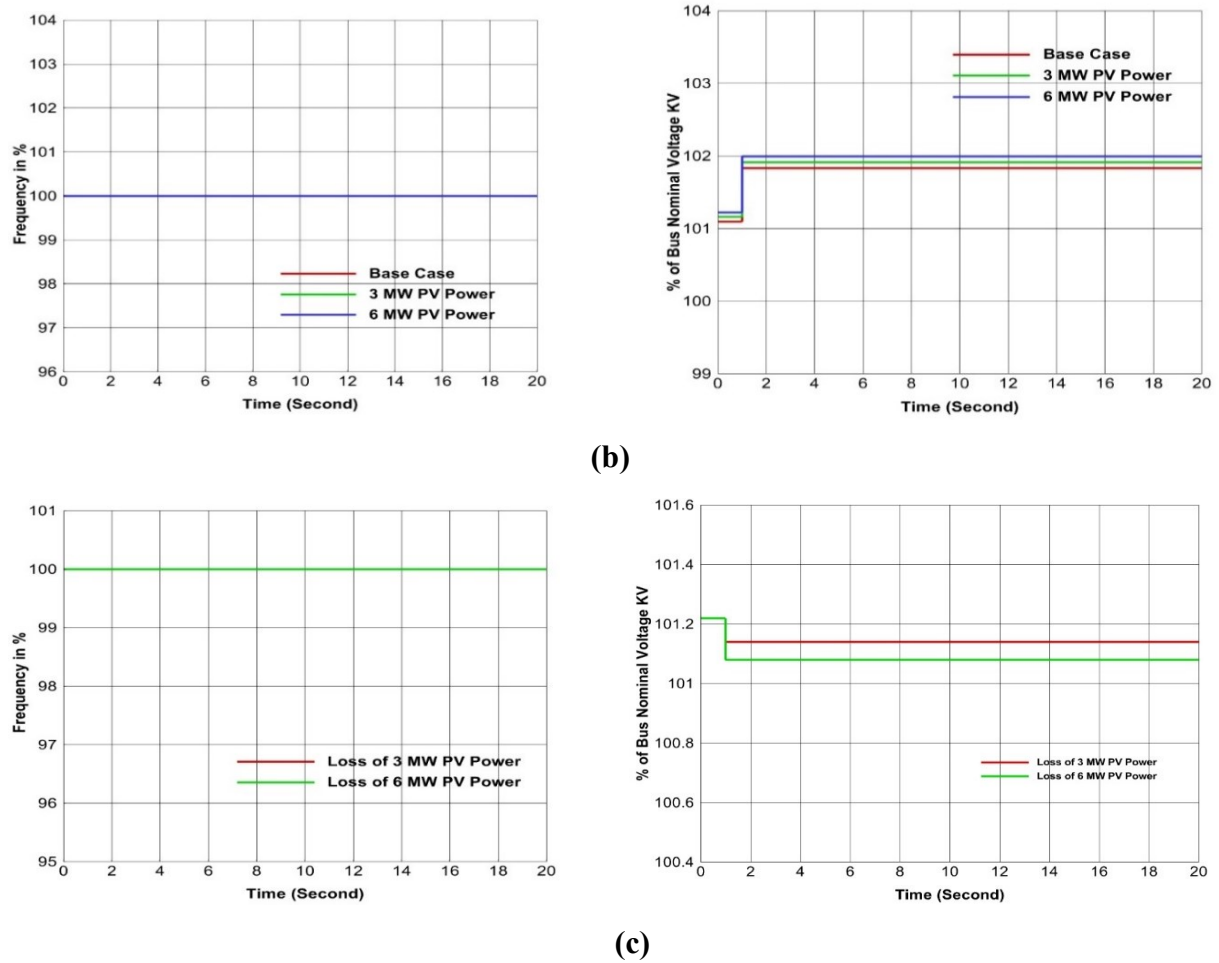
Figure IV. 21: System behavior once a grid source is utlized to feed the system

(a) Frequency and voltage at main bus due to fault at the network main busbar

(b) Frequency and voltage at main bus due to sudden removal of load

(c) Frequency and voltage at main bus due to sudden outing of PV power

IV.4.4 Scenario three: A generation station is used to feed network

This scenario was done to prepare for the possibility that the grid source might not be available. As a result, the only source that can supply power to the distribution network in this scenario is a power generation plant. The behavior of the network in a number of different temporary situations is described below. In each scenario, a comparison is shown between the performance of the network when the generation station is operated with control units and when it doesn't have them (turbine governor and exciter with AVR).

1- Influence of fault on the system main bus

In this scenario, a three-phase-to-ground fault is applied to the main busbar of the network at the rate of one second for a duration of six cycles. Figure IV.22 illustrates the outcomes of the network when subjected to this situation.

(a)

(a1)

(b)

(b1)

(c)

(c1)
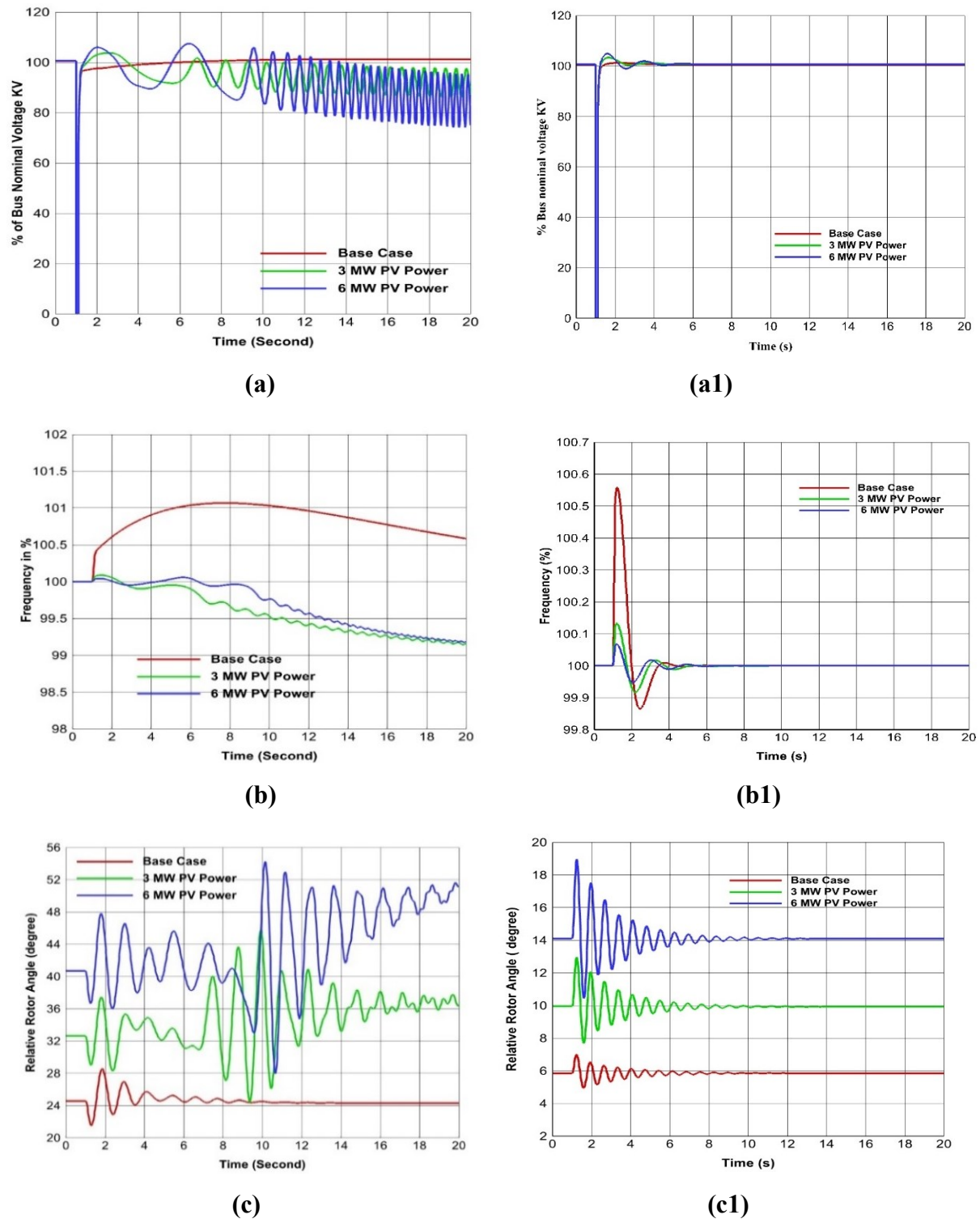
Figure IV. 22: System performance due to fault at the main bus

(a) Voltage at main bus without control units (**a1)** with control units

(b) Frequency at main bus without control units **(b1)** with control units

(c) Relative rotor angle without control units **(c1)** with control units

Figure IV.22 (a) shows the voltage at the network main bus in the case that the generation station operates without a control unit. In Figure IV.22 (a), it is possible to see that the voltage

in the base case drops to a value that is virtually zero at the time of the fault but that it thereafter recovers to its value in the steady state condition after the fault has been fixed. With 3 MW of PV power, it has been observed that once the fault has been eliminated, the voltage recovers with very slight oscillations for 7.8 seconds, after which the oscillations become more pronounced while maintaining an amplitude that is somewhat lower than its value when the system is in a steady condition. When the PV power is increased to 6 MW, similar oscillations take place; however, these oscillations are more severe and have a somewhat bigger amplitude than when the PV power is increased to 3 MW. On the other hand, when the control units are taken into account (the governor for the turbine as well as the exciter with AVR), the voltage at the main bus of the network shows as shown in figure IV.22 (a1). When looking at figure IV.22(a1), one can see that the existence of PV power has a beneficial effect on the performance of the network voltage. This can be inferred from the graph, where the presence of photovoltaic power leads to a more stable voltage in the network.

Figure IV.22 (b) depicts the frequency that would be present at the network main bus in the event that the generation station operated without a control unit. After the fault is cleaned up, the frequency of the base case continues to increase until it reaches 101.067% of the frequency of the network, which is 50 Hz. When the frequency reaches this point, it starts to slowly go down until it reaches a new value that is just a little bit higher than 100.5%. This can be seen in figure IV.22 (b). The frequency increases to 100.63% and 100.031%, respectively, for 3 MW and 6 MW of PV power before progressively falling with little oscillations until it settles down at a value marginally greater than 99% of the frequency in the stable state. This is the case when the frequency is at steady state (50 Hz). Keeping in mind that the drop in PV power of 3 MW takes place before the decline in PV power of 6 MW. On the other hand, when the control units are taken into consideration (turbine governor and exciter with AVR) the frequency at the network main bus is showing in figure IV.22 (b1). From figure IV.22 (b1), it can be noticed that the frequency of the bas case (system without PV power) after the fault is cleared rises until reaches somewhat more than 100.5%, and then begins to decline with very tiny oscillations before stable in its steady state value. For 3 MW and 6 MW PV powers, the oscillation amplitude of the frequency is tiny compared to the base case, decreasing with tiny oscillations until it quickly stabilizes at its original value. In terms of performance, the 6MW is superior to both the 3MW and the base case. Once again, the presence of photovoltaic (PV) power has a favorable impact on the performance of the network frequency when it is subjected to a three-phase-to-ground fault at the network main bus with control units at the generation station.

Figure IV.22 (c) illustrates the relative rotor angle in case that the generation station operates without control unit. In figure IV.22 (c), it is possible to see that after the fault has been fixed, the relative rotor angle of generator 2 for the base continues to show very small oscillations. But these changes get smaller and smaller until the value is back to what it was when it was stable before the fault happened. After the problem is fixed, the relative rotor angle tends to move more and more erratically, with a bigger swing at times. After this, the unsteady oscillation starts to slowly go down at a rate that is higher than its starting rate. This is the case for 3 MW of PV power. The steady-state value of the relative rotor angle is greater than the base case by approximately 8.02 degrees. In a similar vein, for 6 MW of PV power, where it can be observed that the difference in the relative rotor angle of the steady-state is approximately 16.3 degrees from the base case, and where its oscillations are comparable to those seen in the case of 3 MW of PV power, these oscillations begin to decline gradually at a higher value than they do for 3 MW of PV power. On the other hand, when the control units are taken into account (the governor of the turbine as well as the exciter with AVR), the relative rotor angle is displayed in figure IV.22 (c1). Figure IV.22 (c1) shows that the base's relative rotor angle still has very small oscillations after the fault has been removed, but these oscillations get smaller and smaller until the base's rotor angle is back to where it was before the problem. After the fault has been eliminated, the relative rotor angle tends to change more often and with a slightly larger range than in the base case. The oscillation then starts to slowly go down until it settles at its original value. This happens for 3 MW of PV power after the fault has been cleared. In a similar manner, the oscillations that occur with 6 MW of PV power are comparable to those that occur with 3 MW, with the exception that the amplitude of the oscillations at 6 MW is slightly higher than that of 3 MW; these oscillations progressively reduce until they reach their initial value.

2- Effect of the abrupt removal of a load

In order to simulate this scenario, the load on CDRAS 3, which represents the biggest load in the test network (6.235 MVA), is turned off at 1 s. The findings of this investigation are displayed in Figure IV.23 below.

The voltage at the network main bus is depicted in Figure IV.23 (a) and is shown in the event that the generation station operates without control units. As seen in Figure IV.23 (a), the voltage in the base case, at the moment the load is removed, goes to a value that is greater than 110% of the bus's nominal voltage. When the load is removed during the output of 3 MW of PV power, the voltage immediately begins to oscillate with an amplitude that is greater than the value that

is allowed. The same may be said with 6 MW of PV power, albeit with a greater degree of oscillation and a higher amplitude than 3 MW of PV power. On the other hand, when the control units are taken into consideration, the voltage at the network main bus is shown in figure IV.23 (a1). From figure 5.23 (a1), it can be seen that the voltage for the base case when the load is disconnected rises to a value slightly higher than 102.5 % and quickly decreases and stabilises at a value slightly lower than 101.5%. For 3 MW power, when the load is suddenly lost, the voltage rises to a value slightly higher than 104% and then decreases quickly to stabilise at a value slightly higher than 103%. For 6 MW power, the voltage rises to a value slightly higher than 105.5% and then begins to decrease gradually with tiny oscillations until it stabilizes at a new value slightly higher than 104%.

Figure IV.23 (b) illustrates the frequency at the network main bus in case the generation station operates without control unit. It is possible to see from figure IV.23 (b) that when the load is removed, the frequency begins to increase and continues to do so until it reaches a value that is greater than 103% of the system frequency. There is a little variation in frequency for 3 and 6 MW of PV power. In case the control units taken into consideration, the frequency chart is shown in figure IV.23(b1). Frome figure IV.23(b1), it can be noticed that the frequency for the base case at the moment of disconnection of the load raised to value slightly higher than 100.45% and then decrease to stabilized at a value somewhat higher than 100.4%. For 3 MW PV power, the frequency shows tiny oscillations, which gradually reduce until it stabilizes at its steady stat value. Similarly for 6 MW PV power, where it can be noticed that the frequency has a little oscillation compared to the 3 MW.

Figure IV.23 (c) illustrates the relative rotor angle in case that the generation station operates without control unit. Figure IV.23(c) depicts the relative rotor angle with time for the base case, revealing a small and quick oscillation that eventually stabilizes at a value 2.77 degrees below that of the steady state. The oscillation for 3 MW of PV power is completely random and does not approach a steady state. In comparison to 3 MW of PV power, the oscillation at 6 MW of PV power is indeed fully erratic and quite severe. In the situation where the power plant uses a control unit, the relative rotor angle is shown in Figure IV.23(c1). The graphic shows that the relative rotor angle for the base case goes through a brief period of oscillation before stabilizing. For 3 and 6 MW, there is minimal oscillation and they quickly reach steady state.

(a)

(a1)
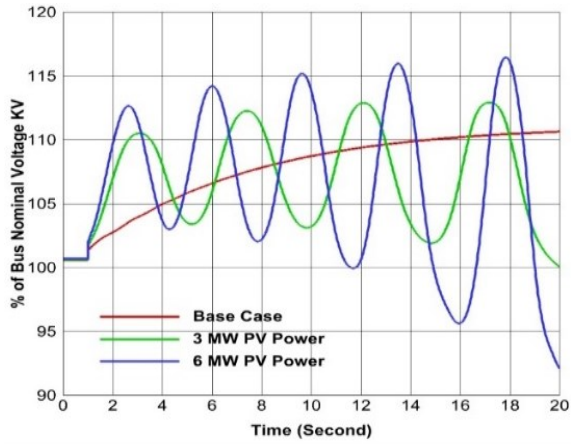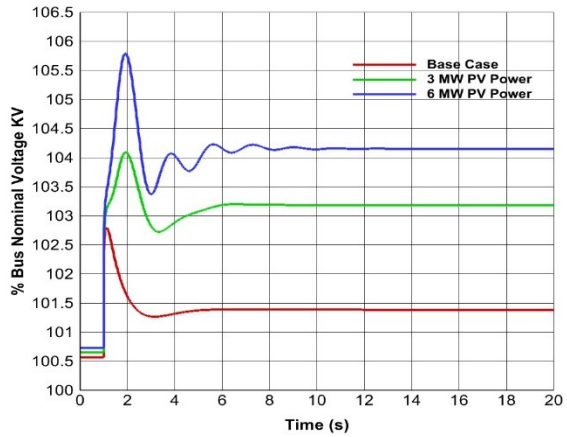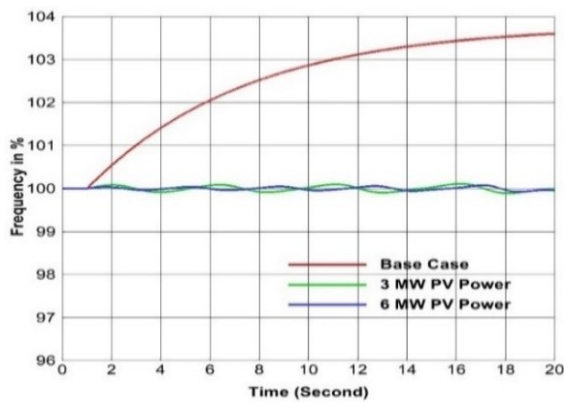
(b)
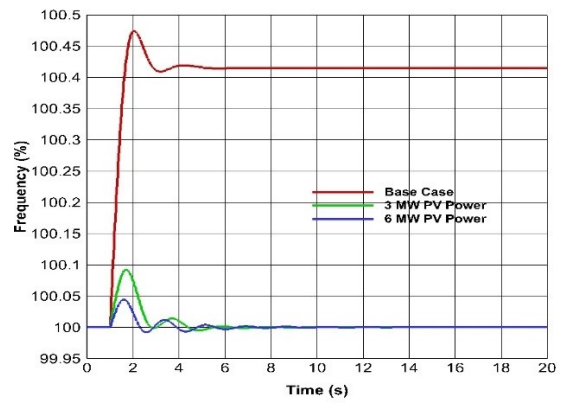
(b1)
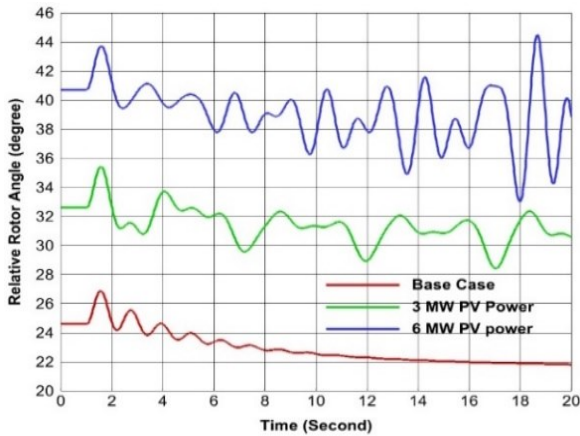
(c)
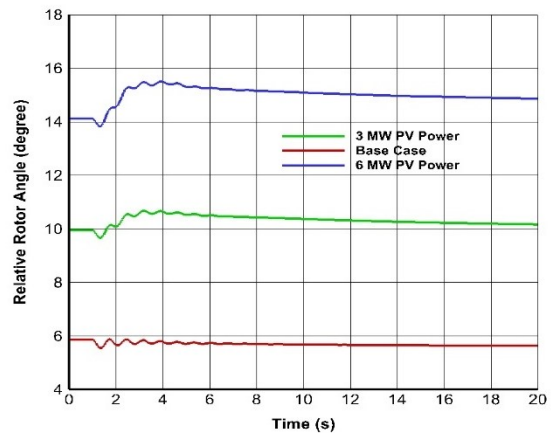
(c1)

Figure IV. 23: System behavior due to sudden removal of load

(a) Voltage at system main bus without control units **(a1)** with control units

(b) Frequency at system main bus without control units **(b1)** with control units

(c) Relative rotor angle without control units **(c1)** with control units

Chapter IV Simulation and Results Analysis

3- The influence of an unexpected loss of PV power

In the context of this scenario, a PV power outing at 1s for both the 3 MW and 6 MW PV power scenarios. The behavior of the network under these circumstances is shown in figure IV.24.

figure IV.24 (a), (b), (c), represents the network behavior in case that the generation station operates without control unit. When 3 MW of PV power is lost, the graph of voltage that is displayed in Figure IV.24 (a) demonstrates that the voltage has a significant oscillation that occurs on a consistent basis and lasts for a significant period of time. The voltage progressively drops to a new value that is only a little bit higher than 92% of the bus's normal voltage when a loss of 6 MW of PV power occurs. When looking at Figure IV.24 (b), one can see that the frequency drops from its original value when 3 and 6 MW of PV power are lost, with the drop in the case of a loss of 6 MW being substantially larger than the drop in the case of a loss of 3 MW. As can be seen in Figure IV.24 (c), which depicts the relative rotor angle, the relative rotor angle rises in the event of a loss of 6 MW of PV output, accompanied by a little oscillation that gradually diminishes until it stabilizes at a new value greater than the value at steady state. By comparing a loss of 6 MW of PV power to a loss of 3 MW of PV power, we see that the oscillation is more severe and has a higher amplitude in the former instance. At first, this oscillation goes up, and then it goes down, until it stabilizes at a value that's higher than the steady state value.

When there is a loss of 6 MW of PV power, the network is not penetrated with PV; as a result, the inertia of the traditional generators does not affect the improvement of the network performance, which results in reduced oscillation. In the event that 3 MW of PV power is lost, the network will still be penetrated by 3 MW of PV electricity. This will produce a drop in the system's inertia, which will result in oscillation.

Figure IV.24 (a1) (b1) (c1) illustrates the network performance when the control units are considered. From the graph of voltage illustrated in Figure IV.24 (a1), it can be noted that the voltage has an irregular, and persistent oscillation when 3 MW PV power is lost. When 6 MW PV power is lost, the voltage is not affected much and then very quickly stabilizes at its normal value. From figure IV.24 (b1), It can be noticed that the frequency declines a little from its initial value when 6 is lost and it stabilizes at a new stable value. When 3 MW PV power is lost the frequency has an irregular, and persistent oscillation. Figure IV.24 (c1) depicts the relative rotor angle, it can be noted that in the case of loss of 6 MW PV power, the relative rotor angle oscillates with a minor oscillation that quickly decreased and stabilized at a value little higher

than its the steady state value. In the case of loss 3 MW PV power, the oscillation is persistent with irregular amplitude.

(a) **(a1)**

(b) **(b1)**

(c) **(c1)**
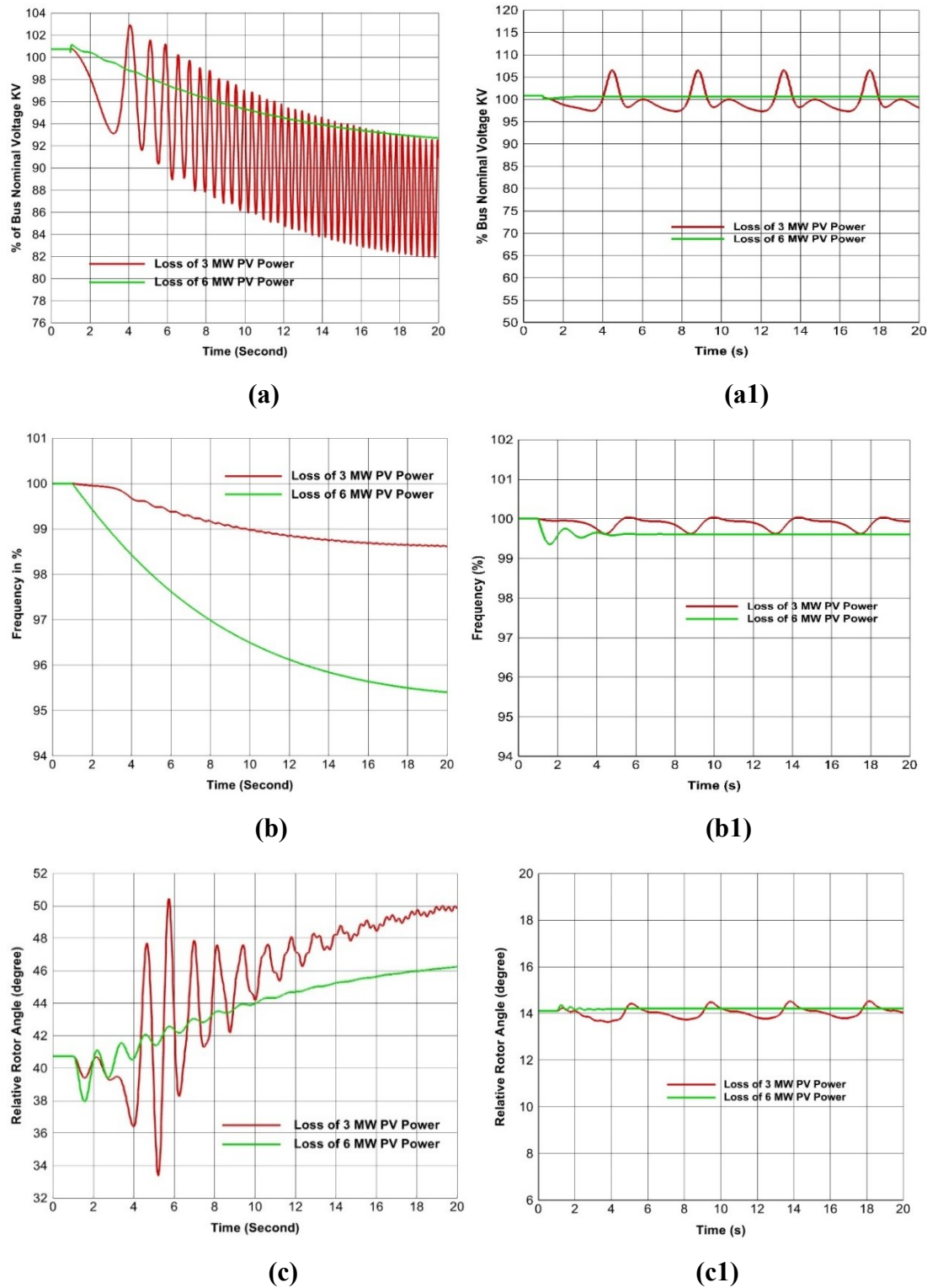
Figure IV. 24: The behavior of the system as a result of an unexpected loss of PV power

(a) Voltage at system main bus without control units **(a1)** with control units

120

(b) Frequency at system main bus without control units **(b1)** with control units

(c) Relative rotor angle without control units **(c1)** with control units

IV.5 Small Signal Stability Analysis of Power System

The ability of the power system to keep its synchronization intact in the face of relatively minor disturbances is referred to as its "small signal stability." This kind of disruption happens all the time on the system as a result of the tiny change in the loads and the generations[95] .There are two possible types of instability: a steady increase in rotor angle as a result of insufficient synchronizing torque, or rotor oscillations with rising amplitude as a result of insufficient damping torque. Several elements, such as system operating state at the outset, transmission system strength, and generation excitation controls, determine how the system reacts to minor disruptions. Inadequate damping of system oscillation causes modest signal instability in most real-world power systems. Hence, evaluating the power system under the given operating parameters via small-signal stability analysis is the primary objective of the analysis. [131].

So, utilizing the IEEE 14 bus test system, an investigation into the impact of solar PV power generation on the small signal stability of the power system was carried out. In order to study the impact that the solar PV power generation unit has on the stability of the system's small signal, the solar PV power generator operate in constant power -constant voltage mode is connected at several buses through a transformer and Bus 2. The simulations are performed with the assistance of PSAT simulation toolbox [132]. A single-line representation of the IEEE 14-Bus system on PSAT toolbox can be seen in Figure IV.25

Figure IV. 25: Layout of the IEEE 14-node system in PSAT

IV.5.1 Eigenvalue analysis of the base case (system without PV unit)

Eigenvalue analysis is utilized to check the small-signal stability of the test system in the baseline case (Initial system). Eigenvalue analysis of the base scenario is shown in Figure IV.26. The results reveal that every eigenvalue lies in the left half of the s-plane and contains only negative real parts. In this sense, the system can be described as primarily small-signal stable. After conducting an analysis, we find that out of a total of 55 eigenvalues, one is zero and the remaining 54 have negative real parts. This is the system's dynamic order. In nature, there are twelve decaying complex pairings.

Eigenvalues with complex imaginary parts of zero are filtered because the focus is on oscillatory components. Table IV.16 shows modes and the oscillatory mode, most associated states, damping ratio, and frequency.

122

Figure IV. 26: Eigenvalues for the IEEE-14 bus system (Base case) (S-domain Map)

Table IV. 16: Modes with most associated states (base case)

Most associated states Variables	Modes/ Eigen values (Real part ± Imag. Part)	Damped frequency (Pseudo-Freq) (Hz)	Damping Ratio %
vr1_Exc_1, e2q_Syn_1	-43.9628 ± 8.1602	1.2987	98.321%
e1q_Syn_1, vf_Exc_1	**-0.74447 ± 9.2646**	**1.4745**	**8.010 %**
omega_Syn_5, delta_Syn_5	-4.6461 ± 9.8113	1.5615	42.798 %
omega_Syn_4, delta_Syn_4	-3.4399 ± 9.1304	1.4531	35.256 %
omega_Syn_3, delta_Syn_3	-2.1973 ± 8.2383	1.3112	25.771 %
omega_Syn_2, delta_Syn_2	-3.0301± 7.0684	1.125	39.401 %
tg1_Tg_1, e2d_Syn_4	-10.2087 ± 0.19611	0.03121	99.982 %
e1q_Syn_4, vf_Exc_4	-1.0504 ± 1.4556	0.23167	58.517 %
tg2_Tg_1, omega_Syn_1	-1.0346 ±1.1015	0.17531	68.463 %
e1q_Syn_5, vf_Exc_5	-1.1943 ±0.99198	0.15788	76.926%
e1q_Syn_2, vf_Exc_3	-0.59836 ± 0.74499	0.11857	62.625%
e1q_Syn_3, vf_Exc_2	-0.59634 ± 0.35016	0.05573	86.233%
vm_Exc_1	-1000.0002	0	100 %
vm_Exc_4	-1000	0	100 %

vm_Exc_2	-1000	0	100 %
vm_Exc_3	-1000	0	100 %
vm_Exc_5	-1000	0	100 %
vr1_Exc_4	-49.926	0	100 %
vr1_Exc_5	-49.9418	0	100 %
vr1_Exc_2	-49.9818	0	100 %
vr1_Exc_3	-49.9698	0	100 %
e2d_Syn_1	-37.6632	0	100 %
e2q_Syn_3	-33.7893	0	100 %
e2q_Syn_2	-30.9765	0	100 %
e2q_Syn_5	-27.7022	0	100 %
e2q_Syn_4	-23.8947	0	100 %
e2d_Syn_3	-17.9082	0	100 %
e2d_Syn_2	-14.1335	0	100 %
e2d_Syn_4	-12.6537	0	100 %
tg1_Tg_2	-10.2037	0	100 %
e1d_Syn_3	-8.1634	0	100 %
e1d_Syn_2	-6.6349	0	100 %
tg2_Tg_2	-2.1182	0	100 %
delta_Syn_1	**0**	0	0
tg3_Tg_2	-0.01997	0	100 %
tg3_Tg_1	-0.07702	0	100 %
e1d_Syn_5	-0.85705	0	100 %
e1d_Syn_4	-0.86555	0	100 %
vr2_Exc_1	-1.0234	0	100 %
vr2_Exc_2	-1.0093	0	100 %
vr2_Exc_3	-1.0044	0	100 %
vr2_Exc_4	-1.0025	0	100 %
vr2_Exc_5	-1.0005	0	100 %

The eigenvalue (mode) that has the lowest damping ratio among those listed is the one that is taken into consideration for small signal stability analysis. The eigenvalue associated with

e1q Syn 1 and vf Exc 1 has a damping ratio of 8.010% is utilize as a metric for study the small signal stability. For this mode, an evaluation of the influence that the solar PV power generation system unit integration has on the small signal stability of the testing system is carried out.

IV.5.2 Influence of addition of the solar PV power system unit

A small signal stability analysis is performed in order to evaluate the impact that the integration of the solar PV power generation unit would have on the stability of the system using eigenvalue analysis. An eigenvalue analysis is performed on the system being tested for a variety of different locations of solar PV power units. Buses 4, 5, and 10, as we previously discussed, are chosen as the system's strongest buses, while buses 14, 10, and 9 are chosen as its weakest. The eigenvalue analysis of the IEEE-14 bus system with PV at various places is shown in Table IV.17. The real-part of the crucial eigenvalue was shown to migrate away from the imaginary axis, demonstrating that the test system's small-signal stability had improved. The increase in critical mode damping displayed in the table can also be used to examine the improvement in small signal stability. The critical mode's damping ratio increased from zero PV power, which increased system stability. The system becomes more stable as the damping ratio rises.

Table IV. 17: Critical eigenvalue with and without PV system unit

PV power system unit placement	Critical mode (Critical Eigen Value)	Damped frequency (Pseudo-Freq) (Hz)	Damping Ratio %	Improvement in damping
Base case	-0.74447 ± 9.2646	1.4745	8.010 %	-
PV power at bus 14	-1.0486± 9.3871	1.494	11.102 %	38.600%
PV power at bus 10	-1.0805 ± 9.3923	1.4948	11.429 %	42.684 %
PV power at bus 9	-1.1011± 9.397	1.4956	11.638%	45.296 %
PV power at bus 4	-1.1837± 9.4123	1.498	12.468 %	55.781 %
PV power at bus 5	-1.2147± 9.3948	1.4952	12.823 %	60.088 %

From the table IV.17, it can be seen that integrating the solar PV system unit at the stronger buses led to a better improvement in the damping ratio compared to integrating it at the weaker buses. Figure IV.27 displays the eigenvalues for the IEEE-14 node system in the S-domain map for various PV system unit placements in the test system. It can be seen that the open left half plane contains all of the eigenvalues for the test system.

(a)

(b)

(c)

(d)

(f)
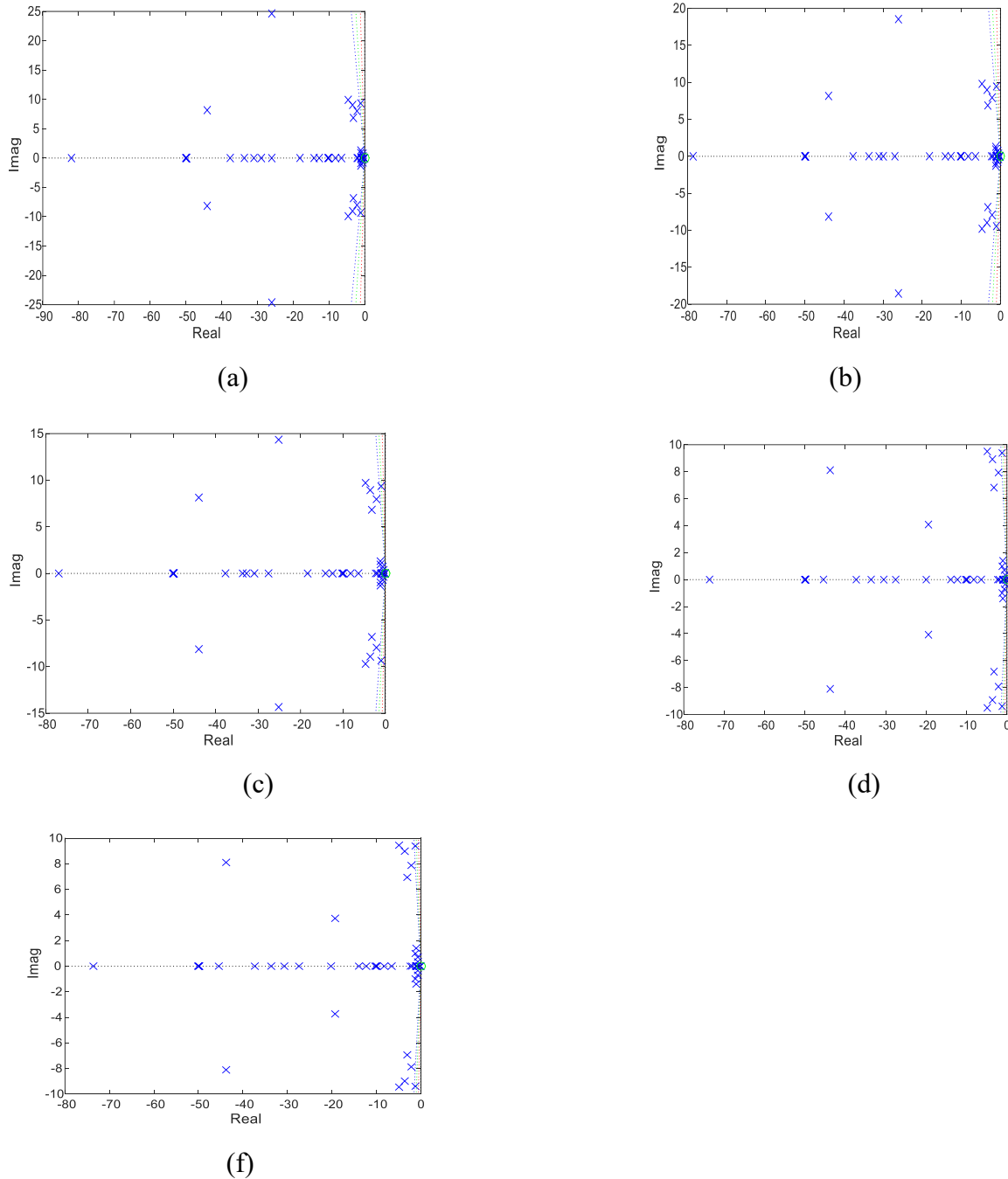
Figure IV. 27: Eigenvalues plots for the IEEE-14 bus system for various PV power placement options

(a) Solar PV power system at bus 14   (b) Solar PV power system at bus 10

(c) Solar PV power system at bus 9   (d) Solar PV power system at bus 4

(f) Solar PV power system at bus 5

IV.5.3 Impact of replacement of generator

In this scenario, a small signal stability study is conducted in the case that PV power generation replaces one of the generators. The system's total number of modes reduces as more conventional generators are replaced. For the base case analysis, the generator 2 is replaced by

126

equivalent size of PV power in order to assess the most associated state that is used to examine small signal stability of the system and then the power from the PV is gradually increase to investigate the impact of PV generation penetration on the test system's small signal stability. The power from PV generation increased from 40 MW to 70 MW in steps 10. For each step, the damping ratio, and frequency of oscillation of critical mode is obtained. The result of the simulation is shown in table IV.18 which is illustrate also in figure IV.28.

From the table, it can be seen that the damping ratio of the critical eigen value of base case improved when replaced generator 2 by equivalent size of PV power, where damping ratio rose from 8.010 **% to** 10.907 % indicating that improvement in small signal stability of the test system. Besides that, with increasing power from PV generation the damping ratio of critical eigen value showed improvement. For 40 MW is 10.907 % and it's increased to 11.261 %for 70 MW.

Eigenvalues plot for the case of replaced generator 2 by equivalent size of PV power is showed in figure IV.29.

Table IV. 18: Effect of solar PV power generation penetration on damping ratio

Solar PV power [MW]	Critical mode	(Pseudo-Freq) (Hz)	Damping Ratio %
40	-1.118 ± 10.1894	1.6217	10.907 %
50	-1.1301±10.187	1.6213	11.026 %
60	-1.1421± 10.1848	1.621	11.144 %
70	-1.154±10.1827	1.6206	11.261 %
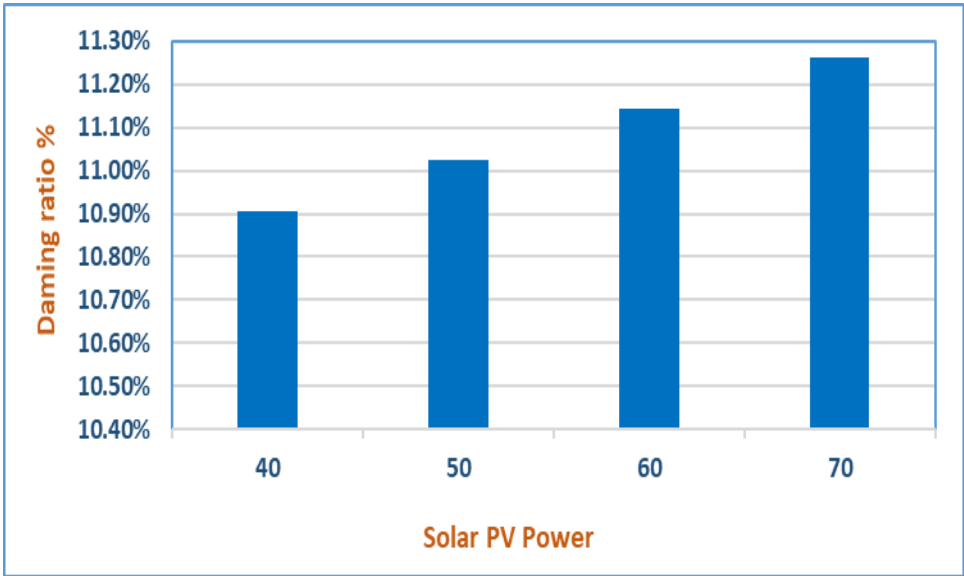
Figure IV. 28: Impact of PV power on small signal stability
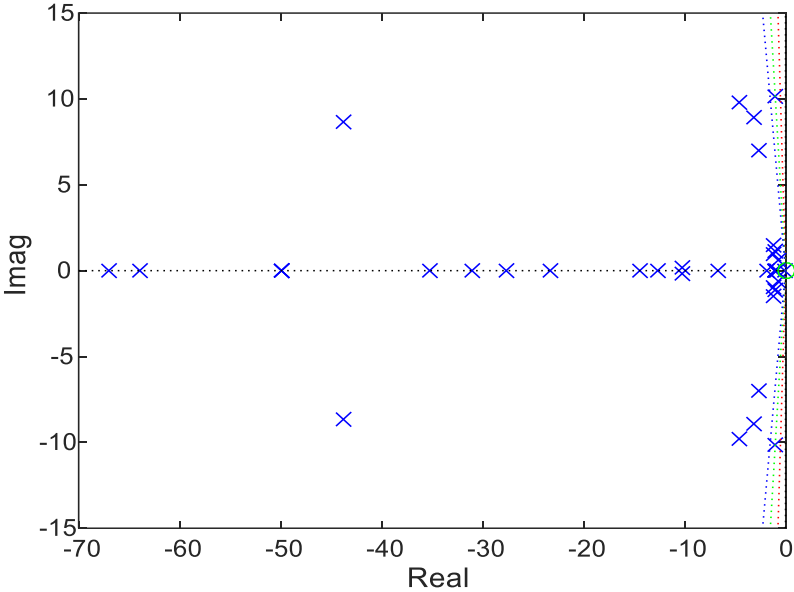
Figure IV. 29: Eigenvalues plot for the case where the generator is replaced

IV-6 Conclusion

This chapter examined the impact that installing a solar photovoltaic (PV) power generation system has on the stability of the grid by making use of three distinct software packages. Both steady-state analyses and voltage stability analyses involve use of the NEBLAN program. For the purpose of investigating transit stability, the ETAP software is utilized. In addition, the PSAT toolbox was put to use in order to investigate the effect that solar PV had on the small signal stability of the power system. A number of possible scenarios were explored for this analysis, and the results of those investigations are reported.

General Conclusion

General Conclusion

The primary objective of this thesis was to study and analysis the effect that the addition of solar systems would have on the stability of the power grid.. In order to accomplish this goal, various pieces of software were utilized in order to conduct an analysis of the effects that grid-integrated PV systems have on the stability of the electric network. In order to achieve the desired level of stability, various scenarios were considered.

The following results were drawn from the simulation of the power grid to ascertain the effects of solar PV power integration on grid stability:

According to an analysis of the network's steady-state stability, the addition of solar photovoltaic (PV) power to the grid has a beneficial effect on the network, which results in an increase in the voltage level and a decrease in the amount of electrical losses in the network. This is taken into account in accordance with optimal penetration, which is based on the smallest possible losses.

Studies of voltage stability in a grid with distributed photovoltaic systems are conducted using the NEPLAN software, which is used to provide a comprehensive examination of the voltage stability of a 14-bus system network utilizing four distinct analysis methods. For each method, an analysis and discussion of the impact of incorporating photovoltaic (PV) power into a system network are conducted. Modal analysis is used to evaluate the condition of the voltage stability of the testing system and to discover the reasons for the instability. In order to identify the buses in the testing system that have the highest levels of sensitivity, sensitivity analysis is carried out. In order to depict the voltage profile at the critical point and to compute the MW loading of the test system, PV curves that use CPF are generated. Following this step, QV curves are produced in order to calculate the reactive power margin of the IEEE 14-bus system network. The findings revealed that the integration of distributed solar PV power into the testing system resulted in a discernible enhancement in the system's voltage stability, a reduction in the sensitivity of buses, a significantly improved system MW loading, an improvement in the voltage profile, and a discernible enhancement in the reactive power margin of identified buses. In transient stability analysis, the possible dynamic effects of adding PV power plants to the distribution network under test are looked at. Analyses are done to compare how the test distribution network acts during sudden changes with and without the PV powers. In this analysis, we take into consideration three different probable transient circumstances. For each of the three potential scenarios, the displayed results show the voltage and frequency at the main busbar of the network, in addition to the rotor angle. According to the findings,

incorporating the Zaouiet Kounta PV plant into the distribution network has a negative effect on the operation of the network during transient situations. This is the case when a traditional power plant is utilized to feed the network in the absence of control units. This effect can manifest itself in a variety of ways, including changes in frequency, changes in the relative rotor angle of generators, and variations in voltage at the main busbar. On the other hand, the integration of a PV plant has been shown to have a favorable impact on the operation of the network when a conventional power plant is operating with control units. In addition to this, when a grid source is utilized to supply the network, it has very little impact on the voltage of the main busbar of the network.

In addition, the findings of a study that investigated the impact of solar photovoltaic (PV) integration on the impact of small signals on the stability of a power system revealed an improvement in the test system's level of stability. It has been observed that integrating the solar PV system unit at the stronger buses led to a better improvement in the damping ratio as compared to integrating it at the weaker buses. In addition to this, the replacement of the generator with a solar PV power system of comparable scale resulted in an increase in the small-signal stability of the grid.

The next analysis can be in the overall PIAT network

References

REFERENCES

[1]   M. Al Talaq and C. A. Belhaj, "Optimal PV penetration for power losses subject to transient stability and harmonics," *Procedia Computer Science,* vol. 175, pp. 508-516, 2020.

[2]   K. Nwaigwe, P. Mutabilwa, and E. Dintwa, "An overview of solar power (PV systems) integration into electricity grids," *Materials Science for Energy Technologies,* vol. 2, no. 3, pp. 629-633, 2019.

[3]   S. R. Paital, P. K. Ray, A. Mohanty, and S. Dash, "Stability improvement in solar PV integrated power system using quasi-differential search optimized SVC controller," *Optik,* vol. 170, pp. 420-430, 2018.

[4]   M. A. Eltawil and Z. Zhao, "Grid-connected photovoltaic power systems: Technical and potential problems—A review," *Renewable and sustainable energy reviews,* vol. 14, no. 1, pp. 112-129, 2010.

[5]   M. H. Rashid, *Power electronics handbook: devices, circuits, and applications handbook*. Butterworth-Heinemann, 2018.

[6]   M. A. Khan, N. Arbab, and Z. Huma, "Voltage profile and stability analysis for high penetration solar photovoltaics," *Int. J. Eng. Work,* vol. 5, no. 5, 2018.

[7]   W. Omran, "Performance analysis of grid-connected photovoltaic systems," 2010.

[8]   S. Al-Refai, "Design of a Large Scale Solar PV System and Impact Analysis of Its Integration into Libyan Power Grid," ed: Nicosia: near east university, 2016.

[9]   I.-T. Theologitis, "Comparison of existing PV models and possible integration under EU grid specifications," ed, 2011.

[10]   Y. Abou Jieb, E. Hossain, and E. Hossain, *Photovoltaic systems: fundamentals and applications*. Springer, 2022.

[11]   E. Mulenga, "Impacts of integrating solar PV power to an existing grid. Case Studies of Mölndal and Orust energy distribution (10/0.4 kV and 130/10 kV) grids," 2015.

[12]   P. Jayaprakash, "Impact of Solar Photovoltaic Penetration on Voltage Stability of Power Network," in *2021 International Conference on Communication, Control and Information Sciences (ICCISc)*, 2021, vol. 1: IEEE, pp. 1-6.

[13]   R. L. Boylestad, *Electronic devices and circuit theory*. Pearson Education India, 2009.

[14]   A. S. Al-Ezzi and M. N. M. Ansari, "Photovoltaic Solar Cells: A Review," *Applied System Innovation,* vol. 5, no. 4, p. 67, 2022.

[15]   D. M. Tobnaghi and R. Vafaei, "The impacts of grid-connected photovoltaic system on distribution networks-a review," *ARPN Journal of Engineering and Applied Sciences,* vol. 11, no. 5, pp. 3564-3570, 2016.

[16]   M. Azzouzi, D. Popescu, and M. Bouchahdane, "Modeling of electrical characteristics of photovoltaic cell considering single-diode model," *Journal of Clean Energy Technologies,* vol. 4, no. 6, pp. 414-420, 2016.

[17]   M. El-Ahmar, A. El-Sayed, and A. Hemeida, "Mathematical modeling of photovoltaic module and evaluation the effect of various parameters on its performance," in *Power Systems Conference-MEPCON, IEEE*, 2016.

[18]   P. Casado, J. Blanes, C. Torres, C. Orts, D. Marroquí, and A. Garrigós, "Raspberry Pi based photovoltaic IV curve tracer," *HardwareX,* vol. 11, p. e00262, 2022.

[19]   Y. T. Tan, "Impact on the power system with a large penetration of photovoltaic generation," *The University of Machester Institute of Science and Technology,* 2004.

[20]   N. Jenkins and J. Thornycroft, "Grid connection of photovoltaic systems: technical and regulatory issues," in *McEvoy's Handbook of Photovoltaics*: Elsevier, 2018, pp. 847-876.

[21] Z. Hyder, "Compared: Grid-tied, off-grid, and hybrid solar systems," in *https://www.solarreviews.com/blog/grid-tied-off-grid-and-hybrid-solar-systems*, ed. SolarReviews, 03/29/2022.

[22] Y. Yang, *Advanced control strategies to enable a more wide-scale adoption of single-phase photovoltaic systems*. Department of Energy Technology, Aalborg University, 2014.

[23] F. Rahman and W. Xu, *Advances in solar photovoltaic power plants*. Springer, 2016.

[24] L. Hassaine, E. OLias, J. Quintero, and V. Salas, "Overview of power inverter topologies and control structures for grid connected photovoltaic systems," *Renewable and Sustainable Energy Reviews,* vol. 30, pp. 796-807, 2014.

[25] M. Y. Ali Khan, H. Liu, Z. Yang, and X. Yuan, "A comprehensive review on grid connected photovoltaic inverters, their modulation techniques, and control strategies," *Energies,* vol. 13, no. 16, p. 4185, 2020.

[26] B. P. Singh, S. K. Goyal, and S. A. Siddiqui, "Grid connected-photovoltaic system (GC-PVS): Issues and challenges," in *IOP conference series: materials science and engineering*, 2019, vol. 594, no. 1: IOP Publishing, p. 012032.

[27] T. Adefarati and R. Bansal, "Integration of renewable distributed generators into the distribution system: a review," *IET Renewable Power Generation,* vol. 10, no. 7, pp. 873-884, 2016.

[28] P. Rani, V. Arora, and N. Sharma, "An overview of integration of PV system into electric grid," in *IOP Conference Series: Materials Science and Engineering*, 2022, vol. 1228, no. 1: IOP Publishing, p. 012017.

[29] K. Jha and A. G. Shaik, "A comprehensive review of power quality mitigation in the scenario of solar PV integration into utility grid," *e-Prime-Advances in Electrical Engineering, Electronics and Energy,* p. 100103, 2023.

[30] M. Shafiullah, S. D. Ahmed, and F. A. Al-Sulaiman, "Grid Integration Challenges and Solution Strategies for Solar PV Systems: A Review," *IEEE Access,* 2022.

[31] O. U. Rehman, "Impact of High Solar Photovoltaic Penetration on Power System Operations," 2021.

[32] M. ElNozahy and M. Salama, "Technical impacts of grid-connected photovoltaic systems on electrical networks—A review," *Journal of Renewable and Sustainable Energy,* vol. 5, no. 3, p. 032702, 2013.

[33] A. R. Alzyoud *et al.*, "The impact of integration of solar farms on the power losses, voltage profile and short circuit level in the distribution system," *Bulletin of Electrical Engineering and Informatics,* vol. 10, no. 3, pp. 1129-1141, 2021.

[34] R. Shah, N. Mithulananthan, R. Bansal, and V. Ramachandaramurthy, "A review of key power system stability challenges for large-scale PV integration," *Renewable and Sustainable Energy Reviews,* vol. 41, pp. 1423-1436, 2015.

[35] Z. H. Salih, G. T. Hasan, M. A. Mohammed, M. A. S. Klib, A. H. Ali, and R. A. Ibrahim, "Study the effect of integrating the solar energy source on stability of electrical distribution system," in *2019 22nd International Conference on Control Systems and Computer Science (CSCS)*, 2019: IEEE, pp. 443-447.

[36] R. R. a. D. B. M. Emmanuel, "Impact of large-scale integration of distributed photovoltaic with the distribution network," presented at the 2016 IEEE International Conference on Power System Technology (POWERCON), Wollongong, NSW, Australia, 2016.

[37] A. Tavakoli, S. Saha, M. T. Arif, M. E. Haque, N. Mendis, and A. M. Oo, "Impacts of grid integration of solar PV and electric vehicle on grid stability, power quality and energy economics: A review," *IET Energy Systems Integration,* vol. 2, no. 3, pp. 243-260, 2020.

[38] V. Cirjaleanu, "Investigation of Cloud-Effects on Voltage Stability of Distribution Grids with Large Amount of Solar Photovoltaics," *Chalmers University of Technology, Gothenburg,* 2017.

[39] D. S. Kumar, A. Sharma, D. Srinivasan, and T. Reindl, "Stability implications of bulk power networks with large scale PVs," *Energy,* vol. 187, p. 115927, 2019.

[40] Y. T. Tan and D. S. Kirschen, "Impact on the power system of a large penetration of photovoltaic generation," in *2007 IEEE power engineering society general meeting*, 2007: IEEE, pp. 1-8.

[41] S. Eftekharnejad, V. Vittal, G. T. Heydt, B. Keel, and J. Loehr, "Impact of increased penetration of photovoltaic generation on power systems," *IEEE transactions on power systems,* vol. 28, no. 2, pp. 893-901, 2012.

[42] H. M. Sultan, A. A. Z. Diab, O. N. Kuznetsov, Z. M. Ali, and O. Abdalla, "Evaluation of the impact of high penetration levels of PV power plants on the capacity, frequency and voltage stability of Egypt's unified grid," *Energies,* vol. 12, no. 3, p. 552, 2019.

[43] E. Munkhchuluun, L. Meegahapola, and A. Vahidnia, "Impact on rotor angle stability with high solar-PV generation in power networks," in *2017 IEEE PES Innovative Smart Grid Technologies Conference Europe (ISGT-Europe)*, 2017: IEEE, pp. 1-6.

[44] J. Thapa and S. Maharjan, "Impact of penetration of photovoltaic on rotor angle stability of power system," in *International Journal of Engineering and Applied Sciences (IJEAS)*, 2019, vol. 6, no. 4.

[45] H. Liu, L. Jin, D. Le, and A. Chowdhury, "Impact of high penetration of solar photovoltaic generation on power system small signal stability," in *2010 international conference on power system technology*, 2010: IEEE, pp. 1-7.

[46] R. Shah, N. Mithulananathan, R. Bansal, K. Y. Lee, and A. Lomi, "Influence of large-scale PV on voltage stability of sub-transmission system," *International Journal on Electrical Engineering and Informatics,* vol. 4, no. 1, pp. 148-161, 2012.

[47] Z. H. Al-Tameemi, K. M. Abuwaleda, H. M. Almukhtar, and M. K. Abbas, "Voltage stability enhancement based on DG units," *Electrical Engineering,* vol. 100, pp. 2707-2716, 2018.

[48] C. Dondariya and D. Sakravdia, "Voltage Stability Assessment and Improvement in Power Systems with Solar Photovoltaic Penetration," in *2021 IEEE 2nd International Conference On Electrical Power and Energy Systems (ICEPES)*, 2021: IEEE, pp. 1-4.

[49] R. Shah, N. Mithulananthan, R. C. Bansal, K. Y. Lee, and A. Lomi, "Power system voltage stability as affected by large-scale PV penetration," in *Proceedings of the 2011 International Conference on Electrical Engineering and Informatics*, 2011: IEEE, pp. 1-6.

[50] S. Qazi, "Photovoltaics for Disaster Relief and Remote Areas," *Standalone Photovoltaic (PV) Systems for Disaster Relief and Remote Areas,* no. 1, pp. 1-30, 2017.

[51] K. Debnath and L. Goel, "Power system planning—a reliability perspective," *Electric Power Systems Research,* vol. 34, no. 3, pp. 179-185, 1995.

[52] A. Chakrabarti and S. Halder, *Power system analysis: operation and control*. PHI Learning Pvt. Ltd., 2022.

[53] F. Gonzalez Longatt, "Chapter 1 Introduction to Power Systems," *Univ. South-Eastern Norway,* vol. 1, pp. 2-6, 2019.

[54] c. globe. "Electrical Load." circuitglobe.com. https://circuitglobe.com/electrical-load.html (accessed 2023).

[55] R. Shankar and P. Kundur, "Power system stability and control II," *New York, McGraw-Hill Books pp581,* 1994.

[56] T. A. Short, *Electric power distribution equipment and systems*. CRC press, 2018.

[57] R. E. Stein, *Electric power system components: Transformers and rotating machines*.

Springer Science & Business Media, 2013.

[58] H. Saadat, *Power system analysis*. McGraw Hill, 1999.

[59] A. R. Al-Roomi and M. E. El-Hawary, "M-Model: a new precise medium-length transmission line model," in *2020 IEEE Canadian Conference on Electrical and Computer Engineering (CCECE)*, 2020: IEEE, pp. 1-6.

[60] B. Theraja and A. Theraja, "A Textbook of Electrical Technology, Volume III Transmission," *Distribution, and Utilization, S. Chand & Co,* pp. 1567-1116, 2001.

[61] T. Gonen, *Modern power system analysis*. CRC Press, 2013.

[62] M. A. Salam, *Fundamentals of electrical power systems analysis*. Springer, 2020.

[63] S. Krishna, *An introduction to modelling of power system components*. Springer, 2014.

[64] A. Von Meier, *Electric power systems: a conceptual introduction*. John Wiley & Sons, 2006.

[65] M. Čepin and M. Čepin, "Methods for Power Flow Analysis," *Assessment of Power System Reliability: Methods and Applications,* pp. 141-168, 2011.

[66] I. Adebayo, D. Aborisade, and K. Oyesina, "Steady state voltage stability enhancement using static synchronous series compensator (SSSC); A case study of Nigerian 330 kV grid system," *Research Journal in Engineering and Applied Sciences,* vol. 2, no. 1, pp. 54-61, 2013.

[67] O. A. Afolabi, W. H. Ali, P. Cofie, J. Fuller, P. Obiomon, and E. S. Kolawole, "Analysis of the load flow problem in power system planning studies," *Energy and Power Engineering,* vol. 7, no. 10, p. 509, 2015.

[68] S. Wiguna, A. Aripriharta, and I. Fadlika, "Analysis of power loss on the addition of new networks in Malang transmission system," in *Journal of Physics: Conference Series*, 2020, vol. 1595, no. 1: IOP Publishing, p. 012019.

[69] O. Eseosa and E. Promise, "Economic Effects of Technical and Non Technical Losses in Nigeria Power Transmission System," *IOSR Journal of Electrical and Electronics Engineering Ver. I,* vol. 10, no. 2, pp. 2278-1676, 2015.

[70] D. Idoniboyeobu and C. Ibeni, "Analysisfor Electical Load Flow Studies in Port Harcourt, Nigeria, Using Newton Raphson Fast Decoupled Techniques," *American Journal of Engineering Research,* vol. 6, no. 12, pp. 230-240, 2017.

[71] A. Vijayvargia, S. Jain, S. Meena, V. Gupta, and M. Lalwani, "Comparison between different load flow methodologies by analyzing various bus systems," *Int. J. Electr. Eng,* vol. 9, no. 2, pp. 127-138, 2016.

[72] X.-F. Wang, Y. Song, and M. Irving, "Load flow analysis," *Modern power systems analysis,* pp. 71-128, 2008.

[73] A. F. H. AL-GBURI, "IMPACT OF HIGH PENETRATION OF SOLAR PV DISTRIBUTED GENERATION ON KARABUK UNIVERSITY LOW VOLTAGE NETWORK," 2022.

[74] C. Balu and D. Maratukulam, *Power system voltage stability*. McGraw-Hill New York, NY, USA, 1994.

[75] Y. Tang, *Voltage stability analysis of power system*. Springer, 2021.

[76] L. A.Salinas, "The Impact of Electrical Losses on a Customers Service Bill," in *acclaimenergy, strategic energy management*, ed. acclaimenergy.com, 2022.

[77] G. Aburn and M. Hough, "Implementing EPA's Clean Power Plan: A Menu of Options," Technical report, National Association of Clean Air Agencies (NACAA), 2015.

[78] I. Pavičić, N. Holjevac, I. Ivanković, and D. Brnobić, "Model for 400 kV Transmission Line Power Loss Assessment Using the PMU Measurements," *Energies,* vol. 14, no. 17, p. 5562, 2021.

[79] F. C. d. Member. "Grid Loss " European Union. https://europa.eu/capacity4dev/public-energy/wiki/sustainable-energy-handbook (accessed 2023).

[80] A. Otcenasova, A. Bolf, J. Altus, and M. Regula, "The influence of power quality indices on active power losses in a local distribution grid," *energies,* vol. 12, no. 7, p. 1389, 2019.

[81] A. Jimoh, M. Siti, and I. Davidson, "Analysis of Domestic feeder technical loss reduction option using both engineering and economic models," in *Ninth UIE conference*, 2000.

[82] A. Mehebub, S. Yasin, and G. Mandela, "Analysis of losses in power system and its economic consequences in power sector," *International Journal Of Enhance Research in Science Technology and Engineering,* pp. 90-93, 2014.

[83] O. I. Boakye, "An analysis of distribution losses in electric power system in Ghana, a case study of the Brong Ahafo Region," University of Education, Winneba, 2018.

[84] D. Carr and M. Thomson, "Non-Technical Electricity Losses," *Energies,* vol. 15, no. 6, p. 2218, 2022.

[85] A. Chauhan and S. Rajvanshi, "Non-technical losses in power system: A review," in *2013 International Conference on Power, Energy and Control (ICPEC)*, 2013: IEEE, pp. 558-561.

[86] T. B. Smith, "Electricity theft: a comparative analysis," *Energy policy,* vol. 32, no. 18, pp. 2067-2076, 2004.

[87] N. E. S. Corporation, "Energy Theft and Fraud Reduction," ed. www.smart-energy.com: Smart Energy International, 2020.

[88] A. H. Nizar, Z. Y. Dong, and P. Zhang, "Detection rules for non technical losses analysis in power utilities," in *2008 IEEE Power and Energy Society General Meeting-Conversion and Delivery of Electrical Energy in the 21st Century*, 2008: IEEE, pp. 1-8.

[89] M. Mahmood, O. Shivam, P. Kumar, and G. Krishnan, "Real time study on technical losses in distribution system," *International journal of advanced research in electrical, electronics and instrumentation engineering,* vol. 3, no. 1, pp. 131-137, 2014.

[90] J. R. Agüero, "Improving the efficiency of power distribution systems through technical and non-technical losses reduction," in *PES T&D 2012*, 2012: IEEE, pp. 1-8.

[91] H. Wanniarachchi and W. Wijayapala, "Modelling of distribution losses in an urban environment and strategies for distribution loss reduction," 2012.

[92] A. Alshahrani, S. Omer, Y. Su, E. Mohamed, and S. Alotaibi, "The technical challenges facing the integration of small-scale and large-scale PV systems into the grid: A critical review," *Electronics,* vol. 8, no. 12, p. 1443, 2019.

[93] R. G. Farmer, "Power system dynamics and stability," *The Electric Power Engineering Handbook,* vol. 2, 2001.

[94] J. Kumar, P. P. Kumar, A. Mahesh, and A. Shrivastava, "Power system stabilizer based on artificial neural network," in *2011 International Conference on Power and Energy Systems*, 2011: IEEE, pp. 1-6.

[95] P. Kundur *et al.*, "Definition and classification of power system stability IEEE/CIGRE joint task force on stability terms and definitions," *IEEE transactions on Power Systems,* vol. 19, no. 3, pp. 1387-1401, 2004.

[96] P. S. Kundur and O. P. Malik, *Power system stability and control*. McGraw-Hill Education, 2022.

[97] A. L. Shenkman, "Static and Dynamic Stability of Power Systems," *Transient Analysis of Electric Power Circuits Handbook,* pp. 517-543, 2005.

[98] S. S. Refaat, H. Abu-Rub, and A. Mohamed, "Transient analysis and simulation of a grid-integrated large-scale photovoltaic (PV) energy system," *QScience Connect,* vol. 2017, no. 2, p. 8, 2017.

[99] G. Lammert, *Modelling, control and stability analysis of photovoltaic systems in power system dynamic studies*. kassel university press GmbH, 2019.

[100] L. L. Grigsby, *Power system stability and control*. CRC press, 2007.

[101] G. Morison, B. Gao, and P. Kundur, "Voltage stability analysis using static and dynamic approaches," *IEEE transactions on Power Systems,* vol. 8, no. 3, pp. 1159-1171, 1993.

[102] P. Tielens and D. Van Hertem, "The relevance of inertia in power systems," *Renewable and Sustainable Energy Reviews,* vol. 55, pp. 999-1009, 2016.

[103] G. M. Giannuzzi, V. Mostova, C. Pisani, S. Tessitore, and A. Vaccaro, "Enabling Technologies for Enhancing Power System Stability in the Presence of Converter-Interfaced Generators," *Energies,* vol. 15, no. 21, p. 8064, 2022.

[104] M. J. Basler and R. C. Schaefer, "Understanding power system stability," in *58th Annual Conference for Protective Relay Engineers, 2005.*, 2005: IEEE, pp. 46-67.

[105] P. S. Kundur, N. J. Balu, and M. G. Lauby, "Power system dynamics and stability," *Power system stability and control,* vol. 3, pp. 827-950, 2017.

[106] U. Annakkage and A. Mehrizi-Sani, "Transient Stability in Power Systems," *Encyclopedia of Life Support Systems, s interneta* http://www. *eolss. net/samplechapters/c05/E6-39-59-03. pdf,* vol. 20, 2022.

[107] O. Mogaka, R. Orenge, and J. Ndirangu, "Static voltage stability assessment of the Kenyan power network," *Journal of Electrical and Computer Engineering,* vol. 2021, pp. 1-16, 2021.

[108] T. T. Wondie and T. G. Tella, "Voltage Stability Assessments and Their Improvement Using Optimal Placed Static Synchronous Compensator (STATCOM)," *Journal of Electrical and Computer Engineering,* vol. 2022, 2022.

[109] K. Z. Heetun, S. H. Abdel Aleem, and A. F. Zobaa, "Voltage stability analysis of grid-connected wind farms with FACTS: Static and dynamic analysis," *Energy and Policy Research,* vol. 3, no. 1, pp. 1-12, 2016.

[110] N. Serem, L. K. Letting, and J. Munda, "Voltage Profile and Sensitivity Analysis for a Grid Connected Solar, Wind and Small Hydro Hybrid System," *Energies,* vol. 14, no. 12, p. 3555, 2021.

[111] M. Pai and A. M. Stankovic, *Power Electronics and Power Systems*. Springer, 2013.

[112] T. Van Cutsem and C. Vournas, *Voltage stability of electric power systems*. Springer Science & Business Media, 2007.

[113] O. Skoglund, "Dynamic voltage regulation using SVCs: A simulation study on the Swedish national grid," ed, 2013.

[114] N. Hosseinzadeh, A. Aziz, A. Mahmud, A. Gargoom, and M. Rabbani, "Voltage stability of power systems with renewable-energy inverter-based generators: A review," *Electronics,* vol. 10, no. 2, p. 115, 2021.

[115] B. Gao, G. Morison, and P. Kundur, "Voltage stability evaluation using modal analysis," *IEEE transactions on power systems,* vol. 7, no. 4, pp. 1529-1542, 1992.

[116] S. S. Manjani and S. Tambay, "Voltage stability improvement using modal analysis based compensationf," in *National Power Systems Conference, NPSC*, 2004.

[117] R. K. Jaganathan and T. K. Saha, "Voltage stability analysis of grid connected embedded generators," in *Proceedings of the Australasian Universities Power Engineering Conference–AUPEC*, 2004, pp. 1-6.

[118] N. Manjul and M. S. Rawat, "Pv/qv curve based optimal placement of static var system in power network using digsilent power factory," in *2018 IEEE 8th Power India International Conference (PIICON)*, 2018: IEEE, pp. 1-6.

[119] A.-F. Ali, A. Eid, and M. Abdel-Akher, "Online voltage instability detection of distribution systems for smart-grid applications," *International Journal of Automation and Power Engineering,* vol. 1, no. 2, pp. 67-72, 2012.

[120] P. Chawla and B. Singh, "Voltage Stability Assessment and Enhancement Using STATCOM-A Case Study," *International Journal of Electrical and Computer*

Engineering, vol. 7, no. 12, pp. 1759-1764, 2014.

[121] N. K. Roy, H. Pota, and A. Anwar, "A new approach for wind and solar type DG placement in power distribution networks to enhance systems stability," in *2012 IEEE International Power Engineering and Optimization Conference Melaka, Malaysia*, 2012: IEEE, pp. 296-301.

[122] J. D. Glover, M. S. Sarma, and T. Overbye, *Power system analysis & design, SI version*. Cengage Learning, 2012.

[123] P. Murthy, *Power system analysis*. BS Publications, 2007.

[124] B. Khaki, "Optimizing controller's parameters for exciters and different wind turbines to enhance small signal and transient stability of power system," in *2016 18th Mediterranean Electrotechnical Conference (MELECON)*, 2016: IEEE, pp. 1-7.

[125] A. Pathak and R. Gupta, "Small Signal Stability of a Power System," *Int. J. Recent Technol. Eng,* vol. 8, no. 3, pp. 2277-3878, 2019.

[126] D. Lin, "Methods for analyzing power system small signal stability," Memorial University of Newfoundland, 2015.

[127] C. Chennakesavan and P. Nalandha, "Multi-machine small signal stability analysis for large scale power system," *Indian Journal of Science and Technology,* vol. 7, no. S6, pp. 40-47, 2014.

[128] T. He, S. Li, S. Wu, and K. Li, "Small-signal stability analysis for power system frequency regulation with renewable energy participation," *Mathematical Problems in Engineering,* vol. 2021, pp. 1-13, 2021.

[129] F. Milano, *Power system modelling and scripting*. Springer Science & Business Media, 2010.

[130] N. R. E. L. GE Corporate Research and Development, NREL/SR-560-34634, Golden, Colorado, "Reliable, Low Cost Distributed Generator/Utility System Interconnect: 2001 Annual Report," UNT Digital Library, 2003. Accessed: July 2021. [Online]. Available: https://digital.library.unt.edu/ark:/67531/metadc1410727/

[131] Y. Sun, L. Wang, G. Li, and J. Lin, "A review on analysis and control of small signal stability of power systems with large scale integration of wind power," in *2010 International Conference on Power System Technology*, 2010: IEEE, pp. 1-6.

[132] F. Milano, "An open source power system analysis toolbox," *IEEE Transactions on Power systems,* vol. 20, no. 3, pp. 1199-1206, 2005.